

The University of Maine

DigitalCommons@UMaine

Electronic Theses and Dissertations

Fogler Library

Summer 8-18-2023

Designing and Modeling a Fail-Safe Mechanism to Be Used in Attachment of a Transcutaneous Femoral Implant to a Prosthetic Device

Emma Sperry
emma.sperry@maine.edu

Follow this and additional works at: <https://digitalcommons.library.umaine.edu/etd>



Part of the [Biological Engineering Commons](#), [Biomechanics and Biotransport Commons](#), and the [Biomedical Devices and Instrumentation Commons](#)

Recommended Citation

Sperry, Emma, "Designing and Modeling a Fail-Safe Mechanism to Be Used in Attachment of a Transcutaneous Femoral Implant to a Prosthetic Device" (2023). *Electronic Theses and Dissertations*. 3844.

<https://digitalcommons.library.umaine.edu/etd/3844>

This Open-Access Thesis is brought to you for free and open access by DigitalCommons@UMaine. It has been accepted for inclusion in Electronic Theses and Dissertations by an authorized administrator of DigitalCommons@UMaine. For more information, please contact um.library.technical.services@maine.edu.

**DESIGNING AND MODELING A FAIL-SAFE MECHANISM TO BE USED IN
ATTACHMENT OF A TRANSCUTANEOUS FEMORAL IMPLANT TO A
PROSTHETIC DEVICE**

By

Emma F. Sperry

B.S. University of Maine, 2022

A THESIS

Submitted in Partial Fulfillment of the

Requirements for the Degree of

Master of Science

(in Biomedical Engineering)

The Graduate School

The University of Maine

August 2023

Advisory Committee:

David J. Neivandt, Professor of Chemical and Biomedical Engineering, Advisor

Senthil Vel, Professor of Mechanical Engineering

Michael Mason, Professor of Chemical and Biomedical Engineering

THESIS ACCEPTANCE STATEMENT

On behalf of the Graduate Committee for Emma F. Sperry, I affirm this manuscript is the final and accepted thesis. Signatures of all committee members are on file with the Graduate School at the University of Maine, 5775 Stodder Hall, Orono, Maine.

David Neivandt

Dr. David J. Neivandt, Professor of Chemical and Biological Engineering

Date 08/11/2023

LIBRARY RIGHTS STATEMENT

In presenting this thesis in partial fulfillment of the requirements for an advanced degree at The University of Maine, I agree that the Library shall make it freely available for inspection. I further agree that permission for “fair use” copying of this thesis for scholarly purposes may be granted by the Librarian. It is understood that any copying or publication of this thesis for financial gain shall not be allowed without my written permission.

Signature: *Emma Sperry*

Date: 08/28/2023

**DESIGNING AND MODELING A FAIL-SAFE MECHANISM TO BE USED IN
ATTACHMENT OF A TRANSCUTANEOUS FEMORAL IMPLANT TO A
PROSTHETIC DEVICE**

By Emma F. Sperry

Thesis Advisor: Dr. David J. Neivandt

An Abstract of the Thesis Presented
in Partial Fulfillment of the Requirements for the
Degree of Master of Science
(in Biomedical Engineering)
August 2023

Amputations are quite common and even modern prosthetic devices are plagued by problems. There are approximately 2 million people living with limb loss in the U.S. and on average 185,000 amputations occur yearly. Common attachment mechanisms for external prosthetic components to a residual limb, that is, sockets, pose numerous challenges. Issues include skin irritation, discomfort, socket fit issues, and immobility. Issues include skin irritation, discomfort, socket fit issues, and immobility. Transcutaneous implants have great potential as a connection method for external prosthetic components to a residual limb but because the implants are typically solid, they correlate to extremely high infection rates at the skin interface. Only one such system is FDA-approved but is inadequate due to its corresponding high infection rates and suboptimal fail-safe mechanism. Highly porous transcutaneous technology potentially offers a solution to this problem via providing a permanent mounting point that bridges the skin and soft tissues while being anchored in the bone. However, a porous metal transcutaneous implant cannot be properly employed until a highly effective safety mechanism is engineered that prevents damage to the residual bone of the user when accidental loads are applied. Existing products on the market lack optimized fail-safe devices. A fail-safe mechanism is essential to release the

prosthesis in both falls and more extreme circumstances, such as the device becoming caught, to prevent injury to the prosthetic device and the user's residual skeleton and surrounding tissues. Hence, the present work, including manual calculations, finite element analysis, and mechanical testing, was undertaken to develop an optimized fail-safe mechanism to be incorporated into a porous metal transcutaneous implant system.

ACKNOWLEDGEMENTS

The author would like to thank her advisor, Dr. David J. Neivandt, for his guidance throughout the author's time at the University of Maine, and for his substantial feedback and edits on the presented manuscript. The author would also like to thank her committee member, Dr. Senthil Vel, for his invested time into the review of the present thesis, as well as his extensive feedback and mechanical engineering expertise on the related work, and her committee member, Dr. Michael Mason, for his willingness to provide extensive feedback on the presented manuscript. The author would also like to extend gratitude to her family and friends for their constant support.

The author would also like to thank the University of Maine Center for Undergraduate Research and BioME for previous funding, Bradley Denholm and John Belding of the University of Maine Advanced Manufacturing Center for performing mechanical testing, Justin Willis of the University of Maine Advanced Structures and Composites Center for designing testing components and performing mechanical testing, Damon Williams for undergraduate research assistance, and Thomas Narciso of Southern Maine Community College for machining test samples. Finally, the author would like to thank her employers at ARCH Additive for their support as the author worked while completing the presented work.

TABLE OF CONTENTS

ACKNOWLEDGEMENTS.....	iv
LIST OF TABLES.....	viii
LIST OF FIGURES.....	x
1 INTRODUCTION.....	1
1.1 History of Prosthetics.....	1
1.2 Challenges with Current Prosthetics.....	5
1.3 Current Prosthetic Mounting Mechanisms.....	7
1.4 Transcutaneous Implant Systems.....	12
1.5 Foam Metals as Hosts for Tissue Growth.....	23
1.6 Safety Mechanisms in Bone-Anchored Transcutaneous Implants.....	26
1.7 Overall Need for Further Work.....	27
1.8 Summary of Present Work.....	28
2 MATERIALS AND METHODS	
2.1 Introduction.....	30
2.2 Methods of Analysis.....	32
2.2.1 Manual Stress Calculations.....	32
2.2.1.1 Bending Manual Calculations.....	33
2.2.1.2 Torsion Manual Calculations.....	35
2.2.2 Finite Element Modeling.....	38
2.2.3 Mechanical Testing.....	49
2.2.3.1 Bending Test Systems.....	51

2.2.3.2 Torsion Test Systems.....	55
3 INITIAL DESIGN CONSIDERATIONS.....	57
3.1 Introduction.....	57
3.2 Material of Construction.....	58
3.3 Size and Geometry.....	59
3.4 Commercial Availability.....	60
3.5 Critical Applied Forces.....	62
3.6 Initial Manual Stress Calculations.....	63
3.7 FEA Modeling Material Property Setup.....	69
4 DETERMINATION OF THE EFFECT OF BOLT GEOMETRY ON FAILURE FORCES UNDER APPLICATION OF A BENDING FORCE.....	71
4.1 Introduction.....	71
4.2 Materials and Methods.....	71
4.3 Results and Discussions.....	74
4.4 Conclusions Regarding Shear Bolt Failure Under Bending Conditions.....	99
5 DETERMINATION OF THE EFFECT OF BOLT GEOMETRY ON FAILURE FORCES UNDER APPLICATION OF A TORSIONAL FORCE.....	101
5.1 Introduction.....	101
5.2 Materials and Methods.....	101
5.3 Results and Discussions.....	103
5.4 Conclusions Regarding Shear Bolt Failure Under Torsion Conditions.....	107
6 CONCLUSIONS AND FUTURE WORK.....	109
6.1 Conclusions.....	109

6.2 Future Work.....	111
7 BIBLIOGRAPHY.....	112
8 BIOGRAPHY OF THE AUTHOR.....	120

LIST OF TABLES

Table 1. Bending Stress Functions Employed in Manual Calculations.....	33
Table 2. Bending Stress Parameters.....	33
Table 3. Torsion Stress Functions Employed in Manual Calculations.....	36
Table 4. Torsional Stress Parameters.....	36
Table 5. Parameters Relevant to Equation 2.....	37
Table 6. Simplified von Mises Criterion Functions.....	38
Table 7. Simplified von Mises Criterion Parameters.....	38
Table 8. Units Employed in Abaqus FEA Model.....	40
Table 9. Material Properties.....	59
Table 10. Commercially Available Bolts Explored and Their Respective Material, Size, Cost, Threading, System of Measurement, and McMaster-Carr Part Number.....	60
Table 11. Input Titanium Material Properties in Abaqus.....	69
Table 12. Linear Strain-Hardening Parameters.....	70
Table 13. Input Values for Abaqus Linear Strain-Hardening Parameters.....	70
Table 14. Bending Test Titanium Bolt Geometries.....	73
Table 15. Bending Test Stainless Steel Bolt Geometries.....	73
Table 16. Peak Forces and Locations at Which Bolts A-D Failed.....	79
Table 17. Reported Failure Force Values for Bolts F1, H1, I1, and J1 and Their Respective Averages.....	87
Table 18. Reported Failure Force Values for Bolts E1, F1, and G1 and Their Respective Averages.....	92
Table 19. Bending Test Stainless Steel Bolt Geometries.....	95

Table 20. High Strength Steel Results with Varied Notch Width.....	96
Table 21. Force Values when Notch Minor Diameter was Varied.....	98
Table 22. Titanium Bolt Modifications for Torsion Tests.....	102

LIST OF FIGURES

Figure 1. Artificial big toe thought to be the first functional prosthetic.....	1
Figure 2. The oldest known prosthetic leg.....	2
Figure 3. J.E. Hanger’s first artificial leg.....	3
Figure 4. Endo-skeletal prosthesis (socket, suspension system, foot & knee unit) finalized by U.S. Veteran’s Administration.....	4
Figure 5. Highly specialized lightweight running blades.....	5
Figure 6. Locking pin liner mechanism for attachment to a prosthetic device.....	10
Figure 7. Gel suspension sleeve for prosthetic attachment.....	11
Figure 8. Neoprene suspension sleeve.....	12
Figure 9. OPRA Implant System – first surgery.....	14
Figure 10. Fixture coated with BioHelix™.....	14
Figure 11. OPRA Implant System – second surgery.....	15
Figure 12. OPRA Rotasafe attachment mechanism.....	16
Figure 13. OPRA Implant System.....	17
Figure 14. OPRA Axor II standard mounting mechanism, including (1) jaws for abutment connection, (2) rotatable grip for attachment and detachment, (3) alignment nuts, (4) plug for adjustable screw access, and (5) standardized prosthetic attachment area.....	17
Figure 15. OPRA Axor II bending release mechanism.....	18
Figure 16. OPRA Axor II rotational release mechanism.....	19
Figure 17. OPL Implant System.....	21
Figure 18. ILP Implant System.....	22
Figure 19. Components of the IPL system, including (1) ESKA endostem, (2) ESKA	

bridge module in double cone design with cone protection, (3) silicone cap as stoma protection, (4) ESKA bridge connection, and (5) ESKA connection adapter in cylindrical design.....	22
Figure 20. Histological stain of a transcutaneous implant, showing successful soft tissue ingrowth.....	24
Figure 21. A diagram displaying an applied bending force.....	30
Figure 22. Diagrams displaying applied torsional forces (two different views).....	31
Figure 23. An example of a bending stress concentration factor curve for $D/d=2.00$ using the corresponding table values for A and b.....	35
Figure 24. Torsional stress concentration factor.....	37
Figure 25. Main window in Abaqus.....	40
Figure 26. Creating a new material in Abaqus.....	42
Figure 27. (a) Course mesh and (b) fine mesh applied to a notched bolt.....	43
Figure 28. Plot of element size/minor diameter (mm) versus stress (MPa) as a mesh Convergence study.....	44
Figure 29. Creation of a set.....	45
Figure 30. Editing an applied load.....	46
Figure 31. Defining a coupling constraint for torsional loads.....	47
Figure 32. Fixed boundary condition.....	48
Figure 33. An example of a bolt displaying von Mises stress (MPa) results after an applied force had been modeled. “Avg: 75%” indicates the contour plot displays the average value of the output parameter over the specified region, and the value depicted	

corresponds to the average value at 75% of the simulation duration.....49

Figure 34. M8 Hex Bolt drawing.....50

Figure 35. Instron 8872 servo hydraulic machine.....52

Figure 36. Custom bending fixture for use with an Instron 8872.....53

Figure 37. MTS 810 servo-hydraulic machine with a 22kip load cell at the University of
Maine Advanced Manufacturing Center.....54

Figure 38. Bolt in the custom fixture with a nut threaded on for additional stability, with a
braided steel cable clamped to the bolt via a shackle.....54

Figure 39. Breaker bar, 13mm socket, and a half-inch drive socket attached to a digital
torque wrench.....56

Figure 40. Custom torsion set up at the University of Maine Advanced Structures and
Composites Center. On the bottom of the image the custom fixture is shown with a bolt
threaded in and secured in place. On the top of the image, custom tooling is shown
attached to the loading nose, which was employed to apply torsional loads to the hex head
of the bolts.....56

Figure 41. Example of a modified bolt, with labeled regions (threads not shown).....57

Figure 42. One potential overall coupling device, in which the partially threaded fail-safe
bolt would thread directly into the transcutaneous bone-anchored implant.....58

Figure 43. Example of a standard bolt customized to have a notch (threads omitted).....62

Figure 44. Stress (MPa) at the notched region of a shear bolt as a function of the minor diameter (mm) of the notch (solid curve) as a result of a bending load of 432N. Yield strength of various materials added to aid comparison (dotted lines).....65

Figure 45. Resultant stress (MPa) at the notch under an applied bending force of 1780N as a function of notch minor diameter (mm) over a range of 8 to 21mm length and 4 to 7.9mm minor diameter, plotted as individual curves at 1mm increments of distance of the notch from the bottom of the bolt head are presented (solid lines). Grade 5 titanium ultimate tensile strength to aid comparison (red dotted line).....66

Figure 46. Resultant stress (MPa) at the notch as a function of the notch minor diameter (mm) over a range of 5-5.7mm (solid orange line) as a result of an applied torque moment of 102Nm. Yield strength to aid comparison (dotted gray line).....68

Figure 47. General modified bolt (threads not depicted).....74

Figure 48. Unmodified steel bolt (left) and unmodified titanium bolt (right) after testing.....75

Figure 49. Bolt 1A (left) and Bolt 1B (right) after testing (both titanium bolts).....75

Figure 50. Plot of displacement (mm) versus load (N) of titanium bolts 1A and 1B.....76

Figure 51. Plot of stress (MPa) versus applied force (N). Manually calculated, FEA modeled, and experimental failure points of the modified titanium bolt geometry are

labeled for comparison.....	77
Figure 52. An example of a bolt that sheared at its notch region.....	79
Figure 53. Plot of displacement (mm) versus force (N) of bolts A1 (green line), C1 (blue line), and D1 (red line). As seen in Table 15 above, the results were consistent among bolts of the same geometry for bolts A, C, and D. To maintain simplicity, only one of each bolt geometry is depicted.....	80
Figure 54. Display of plastic yielding in bolt during testing.....	81
Figure 55. Resulting plot of the cable elongation and slack test displayed as displacement (mm) versus applied load (N) (solid line). Curve fit polynomial (dashed line).....	83
Figure 56. An example plot of displacement (mm) versus load (N) before and after cable displacement adjustment. G1 raw experimental data (orange line) versus Bolt G1 data with cable slack and elongation data subtracted (blue line).....	85
Figure 57. Plot of displacement versus load for bolts F1, I1, H1, and J1. F1 (notch width of 5mm) shown in red, H1 (notch width of 6mm) shown in green, I1 (notch width of 7mm) shown in yellow, and J1 (notch width of 8mm) shown in blue.....	87
Figure 58. FEA plot of displacement (mm) versus load (N) for bolt F (notch width of 5mm).....	88
Figure 59. FEA plot of displacement (mm) versus load (N) for bolt H (notch width of 6mm).....	89
Figure 60. FEA plot of displacement (mm) versus load (N) for bolt I (notch width of 7mm).....	89
Figure 61. FEA plot of displacement (mm) versus load (N) for bolt J (notch width of 8mm).....	90

Figure 62. Plot of displacement (mm) versus force (N) for bolts E1, F1, and G1. E1 (minor diameter of 2mm) shown in green, F1 (minor diameter of 3mm) shown in red, and G1 (minor diameter of 4mm) shown in blue.....91

Figure 63. Plot of displacement (mm) versus load (N) as a result of bending force on bolt E (minor diameter of 2mm). Experimental data is shown in blue, whereas FEA data is shown in red.....93

Figure 64. Plot of displacement (mm) versus load (N) as a result of bending force on bolt G (minor diameter of 4mm). Experimental data is shown in blue, whereas FEA data is shown in red.....94

Figure 65. Plot of displacement (mm) versus load (N) for bolts M1, P1, Q1, and R1. M1 (notch width of 5mm) shown in purple, P1 (notch width of 6mm) shown in green, Q1 (notch width of 7mm) shown in blue, and R1 (notch width of 8mm) shown in red.....96

Figure 66. Plot of displacement (mm) versus load (N) for bolts L1, M1, N1, and O1. L1 (minor diameter of 2mm) shown in purple, M1 (minor diameter of 3mm) shown in green, N1 (minor diameter of 4mm) shown in blue, and O1 (minor diameter of 5mm) shown in red.....98

Figure 67. Plot of rotation versus torque for bolts S1 and S2 (minor diameters of 2mm). S1 is shown in blue and S2 is shown in orange.....103

Figure 68. Plot of rotation versus torque for bolts T1 and T2 (minor diameters of 3mm). T1 is shown in orange and T2 is shown in blue.....104

Figure 69. Plot of rotation versus torque for bolts U1 and U2 (minor diameters of 4mm). U1 is shown in blue and U2 is shown in orange.....104

Figure 70. FEA plot as rotation versus torque for bolt S (minor diameter of 2mm).....105

Figure 71. FEA plot as rotation versus torque for bolt T (minor diameter of 3mm).....106

Figure 72. FEA plot as rotation versus torque for bolt U (minor diameter of 4mm).....106

1 INTRODUCTION

1.1 History of Prosthetics

Prosthetics – devices, such as an artificial leg, that replace a part of the body – are often used after amputations due to causes such as traumatic injuries, diseases, circulation problems, and birth defects.¹ Limb amputations date back more than 2500 years and are one of the most ancient surgical procedures.² Though survival rates for amputations and related diseases would have likely been low before modern medicine, artifacts such as artificial toes have been uncovered from as early as 710 BC (**Figure 1**).³



Figure 1. Artificial big toe thought to be the first functional prosthetic. Ref[4].

Other early prostheses have been discovered in the ruins of Pompeii and date back to 300 BC.⁵ The oldest known prosthetic leg – the Capua leg – was created by Romans with wood, bronze, and iron (**Figure 2**).



Figure 2. The oldest known prosthetic leg (Capua Leg). Ref [5]

Initially, wood and leather had been the most common materials used for prosthetic devices. However, wood and leather devices were often heavy for the user and difficult to clean, especially since leather absorbs perspiration. Heavy prosthetic devices are not ideal as they require increased energy consumption and lead to the development of sub-optimal gait habits. Through the Middle Ages (476-1000), peg legs and hand hooks were common. Between 1509 and 1590, technical standards for surgical amputations were established.⁵ In 1690, the first transtibial – below the knee – prosthesis was designed.⁵ The prosthesis comprised a copper socket, leather thigh corset, and a wooden foot. By 1865 an articulated prosthetic leg was created by J.E. Hanger, after he became the first amputee of the American Civil War (**Figure 3**).^{5,6} Hanger later went on to patent the prosthetic in 1871.

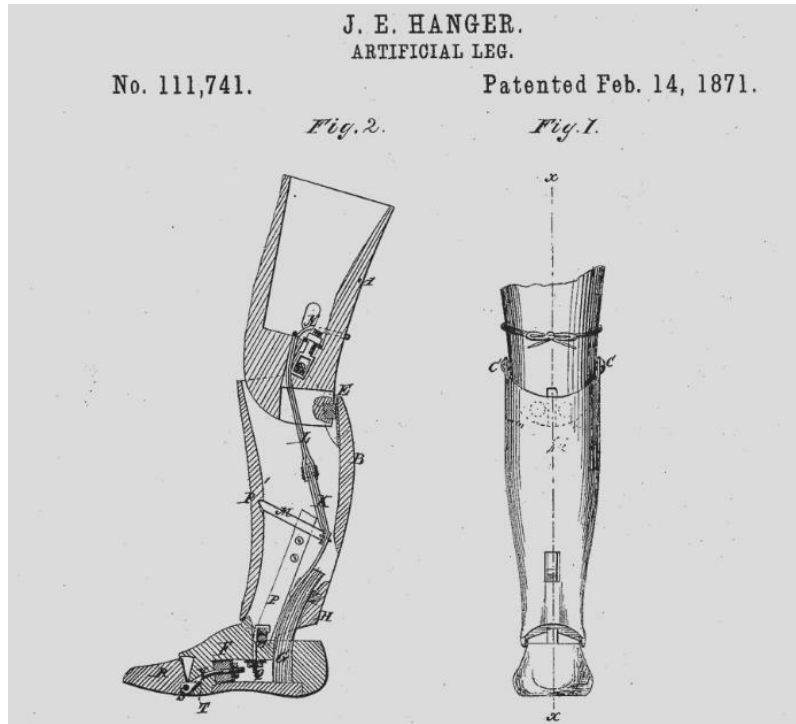


Figure 3. J.E. Hanger’s first artificial leg. Ref[6].

Throughout the next eighty years the development of patellar tendon-bearing sockets and quadrilateral sockets occurred. Patellar tendon-bearing sockets were designed to place the load of the user’s weight on the patellar tendon, which attaches the bottom of the patella to the top of the tibia.⁷ Quadrilateral sockets are rectangular shaped sockets that use opposing forces to keep the ischial tuberosity – a rounded bone extending from the ischium – on a weight-bearing ledge built into the socket.⁸ In 1970, the endoskeletal prosthesis was completed by the U.S. Veterans Administration, which comprised a socket, suspension system, foot, and knee unit (**Figure 4**).^{5,9}

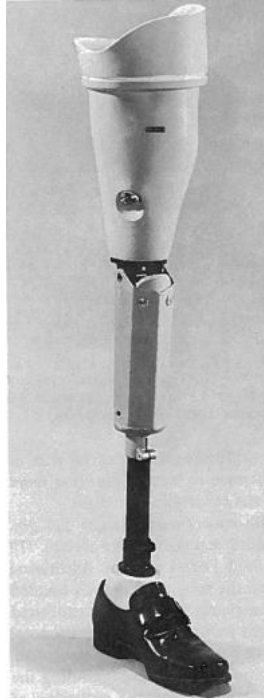


Figure 4. Endo-skeletal prosthesis (socket, suspension system, foot & knee unit)

finalized by U.S. Veteran's Administration. Ref[10].

Commencing in the 1970s, plastics, polycarbonates, resins, and laminates were introduced as prosthetic device materials. Carbon-fiber has also been utilized as a lightweight material. In the present day, highly specialized prosthetics are used, such as lightweight running blades (**Figure 5**), responsive legs and feet, and motorized devices controlled by microprocessors. However, despite the numerous advancements made in the field of prosthetics, amputees still face challenges with current devices.



Figure 5. Highly specialized lightweight running blades. Ref[11].

1.2 Challenges with Current Prosthetic Devices

Amputations are quite common and even modern prosthetic devices are plagued by problems. There are approximately 2 million people living with limb loss in the U.S. and on average 185,000 amputations occur yearly.^{12,13} The main causes of limb loss include vascular diseases, trauma, and cancer.^{12,14,15} For lower-limb amputations, prosthesis use has been found to vary from 49 to 95%, but it has been reported that 11 to 22% of patients abandon their prosthesis within the first year.^{16,17} Prosthesis abandonment leads to both physical and mental health problems, including reduced activity, reduced social participation, psychosocial problems, and further health effects due to inactivity.¹⁸ Limited literature is available to explain the likelihood of amputees to wear prosthetics and the inconsistent use rates. In addition, the existing studies are ambiguous.

Research has shown the overall performance satisfaction of individuals with lower-limb prosthetics to be approximately 75%.¹⁹ However, about a third of these amputees expressed dissatisfaction with prosthesis comfort. Typically, lower-limb prosthetics are attached through

means of a socket mechanism, which is an interface between the residual limb and the prosthetic device.²⁰ A successful socket design must maximize range of motion, provide stability throughout daily activities, and comfortably distribute forces exerted on the residual limb during movement and suspension. Unfortunately, amputees frequently report negative experiences with regard to prosthetics due to issues with the socket. The most common problems include discomfort, low stability, and reduced functionality.²⁰ Amputees experience 65% more dermatological complaints than the general population.²¹ To add to this, skin lesions have been found to occur in up to 82% of lower limb amputees.²² The contact between the skin and components of a socket mechanism and resulting interfacial stress often causes tissue trauma due to excessive heat, friction, and tension.

One challenge many amputees face is residual limb volume fluctuation. During the 12 to 18 months following amputation, oedema reabsorption and muscle atrophy can significantly affect residual limb volume. Oedema is the buildup of fluid in the body which causes swollen tissue, whereas muscle atrophy is the decrease in size and wasting of muscle tissue.²³⁻²⁶ Even beyond the 18 month mark, volume changes occur. Vascular compromise, or reduction in blood flow, can affect the movement of bodily fluids to the residual limb and lead to volume fluctuation. Vascular compromise is caused by vascular disease, which is any abnormal condition of the blood vessels.^{25,27} Body weight fluctuation can also affect residual limb volume.²⁸ Frequently a liner, socks, or both are applied to the residual limb before the socket and suspension sleeve.²⁹ The suspension sleeve assists in holding the prosthetic device on the residual limb and works by wrapping over the socket and onto the residual limb to provide friction.³⁰ The liner acts as a second skin and rolls beyond the socks so it can provide a seal when the suspension sleeve overlaps it, while also being a barrier between the sleeve and skin of the residual limb. The socks

come in varying thickness, also known as plies, and can be worn over the liner to keep the socket fitting consistently, as it is common for the limb volume to change throughout the day. Using socks for an optimal socket fit is easy to implement and inexpensive, however inconvenient for the user as it requires removing the prosthesis, socket, and any outer clothing to remove or add socks to the residual limb.³¹ Additionally, though the liner and socks are intended to increase stability, rubbing frequently occurs which produces sweating, ingrown hairs, irritation, and smell.²⁰ Another way to address residual limb volume fluctuation is through removing the socket periodically to help relieve socket pressures and facilitate limb volume recovery. Similar to using socks, the doffing method is inconvenient for the user as it requires removing the prosthesis and temporarily prevents mobility.³¹ Vacuum assistance, also referred to as vacuum assist or elevated vacuum, can be implemented into the socket to improve fit. The vacuum pulls the residual limb soft tissue outwards and helps to draw fluid into the residual limb.³² However, vacuum assistance requires a specifically designed socket. Additionally, even a small tear in the liner or sleeve material can cause a loss of vacuum pressure and therefore loss of socket fit.

Another challenge lower limb amputees face is a pistoning effect – a vertical movement of the stump relative to the socket – which can cause abrasiveness. Pistoning occurs as a result of poor socket fit and inadequate suspension. Overall, one of the biggest challenges within lower limb prosthetics are interfacial stresses, which cause skin problems, ingrown hairs, and pain for the amputee.

1.3 Current Prosthetic Mounting Mechanisms

The most common means of attachment of a lower limb prosthetic is through a socket. A socket is tailored to the user and is often created through a casting process.³³ First, measurements and a negative cast are taken of the residual limb. The cast is subsequently filled with plaster to create a

positive mold, which is then modified to optimize the socket fit by adding or removing plaster on the mold. The socket mold is then laminated with carbon fiber and a lamination resin to create a custom socket. Sockets can also be constructed employing fiberglass or nylon materials. It can take multiple attempts to achieve a well-fitting socket. Though the length of the residual bone varies from person to person, there is a section of soft tissue at the distal end of the residual limb between the bone and skin, which can contribute to the challenges of adjusting to a socket. Over time, muscle atrophy and subdermal damage at the distal end of the residual limb from prosthetic loading can lead to fluctuation in residual limb soft tissue composition and therefore limb size.³⁴ Even after obtaining the right fit, it may take time for the amputee to adjust to the feeling of taking weight through the residual limb.

Other socket-fabrication methods include computer-aided design (CAD) and additive manufacturing – a computer-controlled process that produces three dimensional objects by adding material in layers. Polypropylene is commonly employed in additive manufacturing for socket production due to its exceptional flex fatigue resistance, making it well suited to socket manufacture.³⁵ However, polypropylene can be problematic due to its chemical inertness and resultant challenges in bonding to other materials. Polylactic acid (PLA) is another commonly used material for additive manufacturing and has been employed for socket production.³⁶ The Modular Socket System (MSS) is one example of CAD and additive manufacturing of sockets and entails creating the socket directly on the user's residual limb.³⁷ The MSS differs from traditional socket fabrication methods in that it is created through direct lamination on the residual limb of the patient. Lamination is a manufacturing method that uses multiple layers, typically bonded together by cohesion or adhesion.³⁸ First, a casting liner is placed on the residual limb followed by the addition of dressings of silicon insulation sheets. Next, carbon fiber is layered, and then more

silicon insulation sheets. Finally, an injection gun is used to inject a material such as a carbon-fiber resin. The cast is left on the residual limb for 10 minutes before being removed to be assembled with other components. Compared to the more common casting process the MSS is significantly less time consuming, but unfortunately much more expensive.³⁹

Utilizing CAD and additive manufacturing for sockets is beneficial for customization, but issues can arise over time such as delamination and deformation due to long-term wear and heat. Adjustable-volume sockets are an alternative to casting and additive manufacturing as they are produced in common sizes and allow for fit alterations without having to remove the socket from the limb.⁴⁰ Several adjustable technologies are available, including ones with air-inflatable inserts, liquid-filled bladders, and magneto-rheological liquid systems. Air-inflatable inserts are placed at the interface between the residual limb and prosthetic socket and are managed by the user to replace lost volume in the residual limb. The inserts are controlled by an air pump commonly placed within the socket wall; as such the user has access from the outside to inflate or deflate the device. Air-inflatable inserts are typically only effective over a narrow volume range due to the fact that air is compressible.²⁷ Because water-based solutions are incompressible, liquid-filled bladders do not present the same challenges as air-inflatable inserts. Liquid-filled bladder systems utilize a passive mechanical control system to adjust the fluid volume which is regulated dynamically by the intrasocket pressure.⁴¹ However, there is risk with ineffectively filling the bladders.²⁷ When the fluid volume is too low, the user risks instability and falling. When the fluid volume is too high, the user risks tissue dehydration and soft-tissue injury. Magneto-rheological liquid systems employ smart materials which can transform the rigidity of the socket to accommodate movement and alignment changes.⁴² The smart materials' viscosity and yield stress is controlled and changed by the presence of an externally applied magnetic field. Unfortunately,

magneto-rheological liquids are challenging to prepare and store, and may change viscosity when subjected to stress over time.^{43,44} Adjustable sockets are appealing because they account for the prevalent issue of residual limb size changes, however they are still relatively new and require reimbursement reform. Overall, the casting process remains the most common for the creation of sockets.

Attachment of a socket to a residual limb can include additional components for improved stability and fit. Additional components may include a locking pin liner or a suspension sleeve. A locking pin liner mechanism comprises a liner that slides onto the residual limb and a pin on its distal end that attaches to the prosthetic device (**Figure 6**). Liners may be employed for replacement of, or in combination with, socks. Liners are often made from thermoplastic elastomer, polyurethane, or silicone.⁴⁵ Liners are intended to minimize friction between the residual limb and prosthesis but can still lead to sweating and rubbing.



Figure 6. Locking pin liner mechanism for attachment to a prosthetic device. Ref[46].

A suspension sleeve is attached to a prosthetic and rolled onto the residual limb, creating a seal to hold the prosthetic and limb together (**Figure 7**). The suspension method may be used as the primary attachment method, or in combination with other methods. Sleeves may be made from neoprene (synthetic rubber), a gel (such as silicone), or other fabrics (**Figure 8**).⁴⁷



Figure 7. Gel suspension sleeve for prosthetic attachment. Ref[48].



Figure 8. Neoprene suspension sleeve. Ref[49].

An alternate form of the suspension mechanism is through suction achieved via a one-way valve. The system works by releasing air from the socket due to the pistoning force of the residual limb; a one-way valve prevents the return of expelled air, essentially creating a vacuum seal. It may be seen therefore that while a variety of mounting mechanisms exist, the methods are problematic as they cause pain, skin issues, and mobility challenges.

1.4 Transcutaneous Implant Systems

Recently, scientists and engineers have investigated the concept of transcutaneous – existing across the depth of the skin – implants and their potential in the field of prosthetics, specifically as a bone-anchored mounting point for an artificial limb.⁵⁰ Transcutaneous bone-anchored implants as a connection for a prosthesis to a residual limb eliminate the need for sockets and their respective challenges, such as skin irritation and mobility issues. Typically, such implants are solid and do not encourage soft tissue ingrowth or attachment, which is problematic as external pathogens may enter the body via the open wound surrounding the implant, leading to high infection rates and the need for antibiotics.

The first long-term, bone-anchored surgical procedure occurred in Sweden in 1990 on a transfemoral amputee.⁵¹ The surgery was performed by Rickard Brånemark on a young woman who lost both legs in an automobile accident. Since then, a variety of solid transcutaneous implants have been tested for use as skeletal attachment points for external prosthetic devices. An attachment mechanism is required at the interface of the transcutaneous implant and the prosthetic device. Some forms of attachment of external prosthetic components to a bone-anchored implant are spring systems with jaw configurations, spring systems with a ball and socket, shear pins, latches, and threaded bolts.⁵²⁻⁵⁴ Each system contains a fail-safe mechanism to protect the residual limb and implant by releasing the prosthetic under dangerously high loads.

The only bone-anchored transcutaneous implant for amputees approved by the U.S. Food and Drug Administration (FDA) is the OPRA Implant System, manufactured by Integrum AB, based in Mölndal, Sweden.⁵⁵ The system was initially used as a Humanitarian Use Device, a type of Pre-Market Approval that allows FDA to grant exemption from the effectiveness requirements of Pre-Market Approval regulations.^{56,57} The OPRA Implant System was FDA approved on December 18, 2020.⁵⁵ The implant system is intended for use with transfemoral amputations and is comprised of parts that allow a prosthesis to attach directly to the femur.⁵⁶ The overall implant system includes seven components that are implanted during two surgeries: a fixture, central screw, healing cylinder, graft screw, washer, abutment, and abutment screw.

During the first surgery (**Figure 9**), the fixture, essentially an internally and externally threaded titanium screw meant to anchor the prosthesis to the bone, is implanted in the medullary canal of the residual femur and a central screw is inserted into the fixture, which allows access to the bone without removing the fixture.

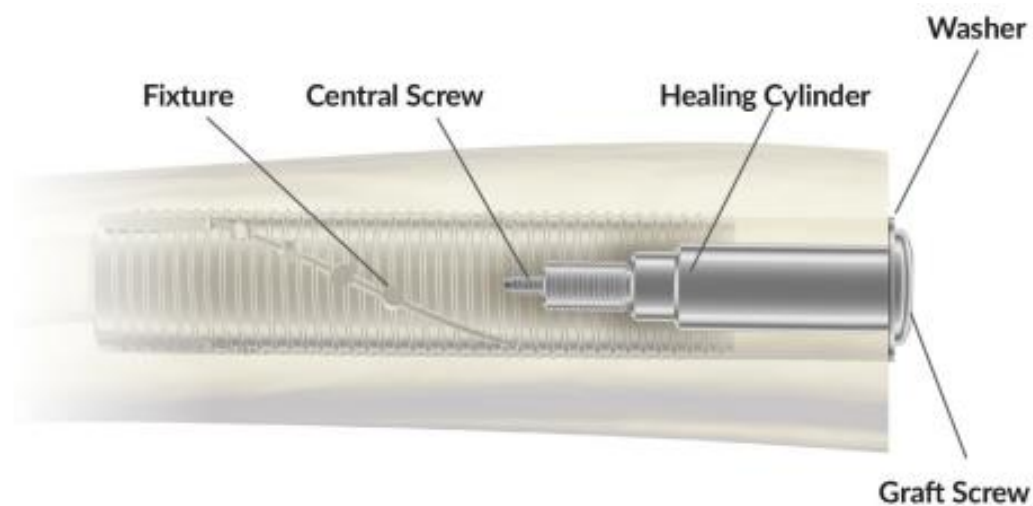


Figure 9. OPRA Implant System – first surgery. Ref[56].

The fixture is coated in Integrum's unique surface technology, BioHelix™ (**Figure 10**).⁵⁸ The coating has been shown to increase the strength of the bone-to-implant interface and to decrease the time to healing. The fixture is the only component of the implant system with the BioHelix™ coating.

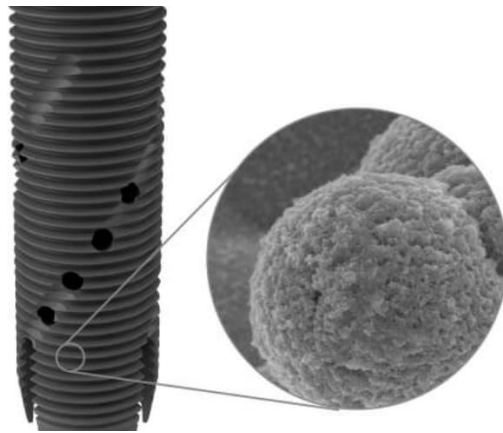


Figure 10. Fixture coated with BioHelix™. Ref[61].

A healing cylinder is attached to the fixture and prevents bone from growing into the fixture opening where the abutment is meant to later be placed. Transplanted bone, commonly referred to as a bone graft, is inserted and held in place by a graft screw. During a six-month healing period following the first surgery, the bone of the residual femur grows onto the fixture to anchor it to the femur. During the second surgery (**Figure 11**), the healing cylinder and graft screw are removed. An abutment is then attached to the fixture which extends partially outside the distal end of the residual limb to allow for attachment of a prosthetic device. It is important to note that the abutment is solid titanium and does not have any coating or porous structure on its surface. An abutment screw is used to lock the abutment and fixture together.

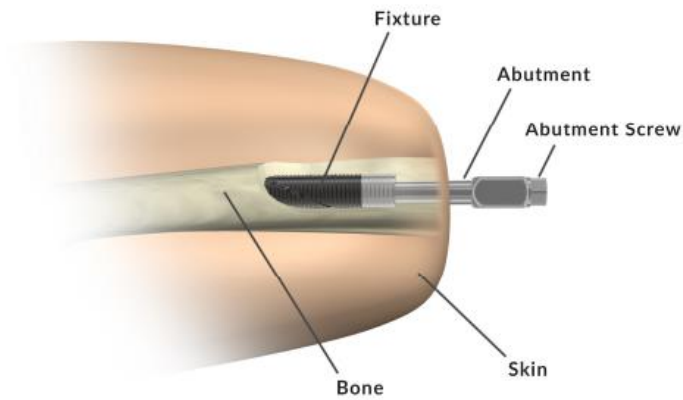


Figure 11. OPRA Implant System – second surgery. Ref[59].

Initially, the OPRA Implant System was used jointly with the OPRA Rotasafe (**Figure 12**), which connected the abutment to the prosthetic and was designed to protect the OPRA Implant System from damage caused by overloads.⁵⁶ The OPRA Rotasafe was designed to twist the prosthesis in the event of a torque overload to protect the fixture and prevent bone fractures. The torque limitation was manually adjusted by a prosthetist to suit the user. If an overload occurred, the OPRA Rotasafe released by twisting between 15° and 360° to relieve stress on the fixture and bone. A disadvantage of the OPRA Rotasafe is that it only failed under rotational loads, not under other loads such as bending. Additionally, the OPRA Rotasafe could only be used with specific prosthetic components, manufactured by Ottobock.

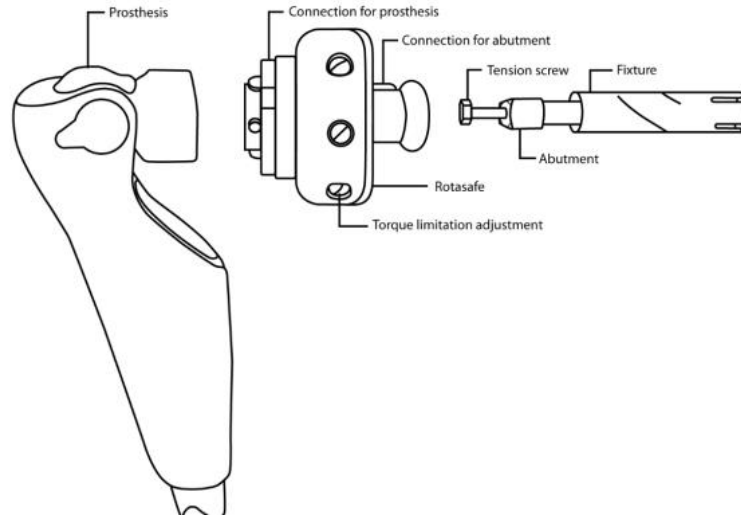


Figure 12. OPRA Rotasafe attachment mechanism. Ref[60].

Current OPRA Implant Systems are used with the OPRA Axor II fail-safe system (hereafter referred to as the Axor), which connects external prosthetic components to the bone-anchored fixture (**Figures 13 and 14**).⁵⁹ The Axor includes a standard European 4 hole mounting system, allowing connection to all prosthetic devices that use the standardized mounting mechanism. The Axor connects to the abutment through four conical jaws which are tightened with a screw mechanism around the abutment. A spring mechanism allows for the connection to close automatically, but tightening must be done manually.



Figure 13. OPRA Implant system. Ref[61]



Figure 14. OPRA Axor II standard mounting mechanism, including (1) jaws for abutment connection, (2) rotatable grip for attachment and detachment, (3) alignment nuts, (4) plug for adjustable screw access, and (5) standardized prosthetic attachment area. Ref[59].

In addition to the Axor's connection role, it acts as a protection mechanism from excessive loads. The Axor employs a release mechanism in both bending and rotation to limit rotational forces along the center of the implant and bending forces when the prosthetic knee is flexed to its maximum position (see Section 1.6 for additional detail). There are two main challenges with the Axor. First, the fail-safe mechanism is an incomplete release when an overload occurs. That is, during bending release, the prosthetic component bends backwards and releases from the anterior side but remains attached on the posterior side (**Figure 15**). During rotational release, the prosthetic device twists to reallocate the torsional load, but remains attached to the abutment (**Figure 16**). The prevention of a complete release from the bone-anchored fixture could be problematic in extreme cases, such as the prosthesis being caught or in an automobile accident. The other challenge is the unidirectional bending release. Bending release will only occur if the dangerous load is applied normal to the anterior side of the prosthetic device, which does not protect the user and his or her residual limb in all scenarios.



Figure 15. OPRA Axor II bending release mechanism. Ref[59].



Figure 16. OPRA Axor II rotational release mechanism. Ref[59].

A major complication with the FDA-approved OPRA Implant System is infection occurring at the interface of the skin and the prosthetic connection component.^{62,63} In 1999, an OPRA Implant System Study was executed. The study included a group of fifty-one test subjects, which at the time was about one third of all patients with an OPRA Implant System. Of those participating in the study, there were forty-four reported infection events and nine abutment mechanical complication events.^{62,63} The abutment was designed to be solid titanium in an attempt to prevent biofilm adhesion, but the interface of the skin and abutment was then unable to form a biological seal, leading to high infection rates.

There are alternative implant systems to the OPRA Implant System which attempt to address some of the shortcomings. The OPRA Implant System is a screw-type implant, whereas systems such as the Osseointegrated Prosthetic Limb (OPL) and Integral Leg Prosthetic (ILP) implants are press-fit.⁶⁴ The OPL is manufactured by Permedica, based in Merate LC, Italy and the ILP is

manufactured by ESKA Orthopaedic, based in Lübeck, Germany. Neither system is FDA-approved.

The OPL is composed of several components, which can be divided into an endo-module and exo-module (**Figure 17**).⁶⁵ The surgery was initially performed in two stages, spaced six to eight weeks apart. However, the current model is surgically completed in one stage. A titanium stem, which has a rough surface created by plasma spray, is first implanted in the bone of the residual limb. A dual cone adaptor is utilized to connect the implant to the external prosthetic components. The adaptor's highly polished surface and titanium niobium coating aims to minimize soft tissue friction. All remaining components are attached externally. The dual adapter connects to a torque control safety device, the connector. The connector allows for easy attachment and detachment of the prosthesis, while acting as a fail-safe mechanism under high torsional loads through breakage of shear pins incorporated into the bushing-taper sleeve connection (refer to Section 1.6 for additional detail).

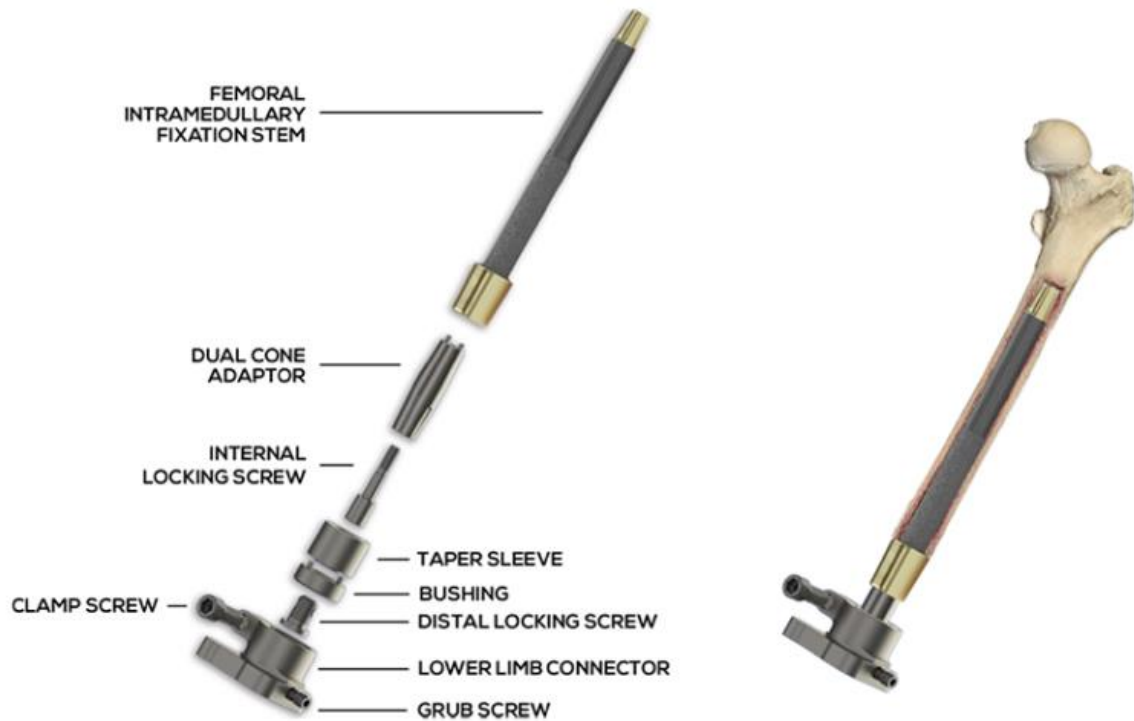


Figure 17. OPL Implant System. Ref[65].

The ILP components are implanted in two surgeries, spaced six to eight weeks apart (**Figures 18 and 19**). The ILP stem is made of a cobalt-chrome-molybdenum alloy and is implanted into the residual femoral bone during the initial surgery. The stem's proximal end has a microporous surface to mimic a spongiosa – the combined tissues of the bone trabeculae and marrow tissues located beneath cortical bone – structure.⁶⁶ The stem's distal end is solid and has a nonabrasive titanium niobium oxynitride alloy coating to limit biofilm adhesion. The second surgery occurs about 4 to 8 weeks post-initial surgery to allow for osseointegration. During the second surgery, a bridge module component is attached to the stem and acts as a connection to external prosthetic components. The bridge module is fastened on the inside but extends out of the distal end of the residual limb and attaches to a bridge connection. The bridge connection is a metal cylinder with an inner cone, toothed disk coupling, torsion adjustment disk, and locking body elements. A safety mechanism resides in the bridge connection (see Section 1.6 for additional information).



Figure 18. ILP Implant System. Ref[67].



Figure 19. Components of the IPL system, including (1) ESKA endostem, (2) ESKA bridge module in double cone design with cone protection, (3) silicone cap as stoma protection, (4) ESK bridge connection, and (5) ESKA connection adapter in cylindrical design. Ref[67].

Both the OPL and ILP have resulted in infections at the interface of the skin and implant. Additionally, studies with longer follow-up have shown that the risk of deep infection continues over time.⁶⁴ Although the products described above attempt to address the need for bone-anchored prosthetics, their transcutaneous components which attach the femoral implant to the external prosthesis are smooth and solid. A smooth surface prevents soft tissue ingrowth or attachment and is therefore problematic as external pathogens may enter the body via the open wound surrounding the implant component, leading to high infection rates.

1.5 Foam Metals as Hosts for Tissue Growth

In order to accomplish bone-anchored prosthetics, a mounting system is required that penetrates from the bone through all layers out to the skin. However, existing implants with transcutaneous systems such as the prosthetic mounting systems outlined above, are prone to high infection rates due to non-adherence of tissues to the implant and hence the creation of an open wound.^{62,63} Another example of transcutaneous systems are external fixator pins, which are employed to stabilize bone fractures via external fixation. The pins typically are comprised of stainless steel or titanium and have smooth surfaces. The most common problem reported with external fixation pins is infection at the pin-site.⁴⁴

One prospective solution to the challenges with solid transcutaneous implants is porous structures that encourage bone and tissue ingrowth, thereby creating a biological tissue seal, and integration of the implant into the host. Highly porous metals, titanium and tantalum in particular, have been observed to be biocompatible – not harmful to living tissue – and promote bone ingrowth, also known as osseointegration.⁶⁸⁻⁷¹ The vast majority of porous implants have only been used for internal bone growth, with few studies analyzing porous transcutaneous implants which cross multiple tissues such as skin, fascia, and muscle. Studies performed by Alexander Caddell,

David J. Neivandt, Ian D. Dickey, James A. Weber, and Anne Lichtenwalner with titanium and biocompatible polymer porous materials in various animals models have given promising results in regard to non-bone anchored transcutaneous implants. Preliminary work has shown that incorporating three-dimensional porous structures into a transcutaneous implant anchored in the bone of the residual limb and extending beyond the skin is capable of serving as a mounting point for a prosthetic, and to have very low infection outcomes. Studies were conducted by Kyle Spivack et al. to analyze soft tissue ingrowth into highly porous implants. Various parameters were tested, including implant material, pore size, implantation time, and implant location. It was found that soft tissue ingrowth was successful and highly vascularized.⁷² Additionally, the ingrowth occurred within one week post-surgery and in many cases reached nearly 100% void filling status (**Figure 20**). Another important note is that with antibiotics only administered on the first day of implantation, there were zero infections reported.⁷²



Figure 20. Histological stain of a transcutaneous implant, showing successful soft tissue ingrowth. Ref[72].

Two human trials were also performed with bone-anchored transcutaneous implants and showed healthy tissue ingrowth in subcutaneous tissue, fascia, skeletal muscle, and dermal tissue.^{72,73} In addition, the tissue ingrowth was highly vascularized. A biological seal was successfully formed around the transcutaneous implants, preventing bacteria external to the body

from causing infection. The biological seal formation is important to note as it potentially solves the common issue of infection and post-surgical failure in orthopedic and prosthetic transcutaneous surgeries.

Porous metals have been used in an attempt to imitate porous biomaterials such as trabecular bone in recent years, however the history of non-biomedical foam metals dates back to 1925.⁷⁴ Maurie De Meller is known to be the earliest scientist to introduce and patent the process of metal foaming.⁷⁴ The method entailed either injecting gas into a molten metal or adding a blowing agent to a molten metal coupled with stirring. Foam metals were initially used in the oil industry as filters. In addition to the research done by De Meller, there is documentation that foaming of aluminum, lead, and zinc also occurred in the 1950s for use in light-weight sandwich constructions.⁷⁵

Metal foams may be formed from materials such as aluminum, titanium, and tantalum.⁷⁶ The key properties of metal foams are that they have high strength and high volumetric porosity and are therefore lightweight (in some cases more than 90% void volume).^{77,78} Metal foams have a variety of potential applications in the medical field, automotive industry, and for other functional utilizations such as filtration. Specifically, the medical community has looked into the potential use of porous metals for orthopedic applications in recent years. In fact, highly porous biomaterials have been shown to promote bone in growth with low rates of infection, making them desirable for orthopedic applications.^{68-71,79}

There are various methods used for manufacturing orthopedic implants, but porous lattice structures designed to mimic bone cannot be fabricated with traditional subtractive manufacturing methods. Previously, solid metal implants were machined or forged. Metal porous structures can be fabricated in the form of titanium plasma spray coatings and cobalt-chromium-alloy fiber metal

meshes.⁸⁰ Both structures have proven capable of facilitating bone ingrowth. However, both titanium plasma spray coatings and cobalt-chromium-alloy fiber metal meshes have low porosities (20-30% and 40-50%, respectively) and therefore do not mimic cancellous bone in the way a fully porous implant may.⁸⁰ Implants with trabecular structures and therefore greater porosities demonstrate greater biocompatibility than those with porous coatings. Trabecular structures can be designed utilizing lattice generation software (for example, nTopology) and physically fabricated via additive manufacturing. Currently, additive manufacturing is the primary method of porous metal implant production. Benefits of additive manufacturing for medical devices include the ability to create complex geometries, faster and easier pathways to manufacturing products compared to traditional subtractive manufacturing, creation of patient specific products, reduced waste, and rapid prototyping.

1.6 Safety Mechanisms in Bone-Anchored Transcutaneous Implants

Transcutaneous implants have great potential as a connection method for external prosthetic components to a residual limb, especially with the porous metal developments of the UMaine foam metals research group which address the major issue of infection control. However, a porous metal transcutaneous implant cannot be properly employed until a highly effective safety mechanism is engineered that prevents damage to the residual bone of the user when accidental loads are applied. Existing products on the market lack optimized fail-safe devices.

The OPRA Implant System employs the Axor II as a safety device. The device has two forms of failure, however neither completely releases the prosthetic from the residual limb. The device twists when a factory-set torque value is applied to the prosthetic and flexes backwards when a factory-set bending moment is applied to the prosthetic. The torque and bending moment release values are typically set to $15\pm 2\text{Nm}$ and $70\pm 5\text{Nm}$, respectively. In addition to the device's

incomplete release, the bending release is unidirectional and therefore is only effective when a bending moment is applied normal to the anterior side of the prosthesis.

The OPL and IPL Implant systems make use of a bushing within their respective coupling mechanisms as a safety component. However, neither system is FDA-approved. Additionally, the safety-mechanisms only fail under torsion, and therefore fails to address dangerous bending forces on the external prosthesis.

Overall, there is limited data available on the existing safety mechanisms and their effectiveness. For the industry to move forward with employing bone-anchored implants as an attachment mechanism of an external prosthesis to a residual limb, the lack of optimized fail-safe mechanisms must be addressed. A reliable and effective method to protect the residual femoral bone and its surrounding tissues from accidental loads is essential and must be developed in depth before moving to the remainder of the overall implant system design.

1.7 Overall Need for Further Work

The current predominant attachment solution for lower limb prosthetics is sockets, however they are associated with numerous downsides. Amputees frequently experience discomfort, low stability, and reduced functionality. Limb volume fluctuation is common, making maintenance of a snug and comfortable socket fit a challenge. When the fit of a socket is inadequate, rubbing occurs resulting in skin lesions and sores. An alternate mounting technology, such as employing a bone anchored transcutaneous implant to mount a prosthetic to, has been shown to be prone to post-surgical infection due to the lack of creation of a biological tissue seal, which is a prominent issue surrounding recovery after orthopedic surgeries involving transcutaneous implants. Critically however, recent work has demonstrated that highly porous metal implants promote

bone and soft tissue ingrowth, including all tissues from the skin down to the bone. The research findings lead to the conclusion that porous metal devices can be implanted without the previous high risk of infection.

Porous metal transcutaneous implants have great potential as a connection method for external prosthetic components to a residual limb. What is required prior to further animal model or human implants however, is the development of a functional mounting and pivoting device for attachment of a prosthesis to a transcutaneous implant that includes a fail-safe mechanism. Existing transcutaneous implant systems lack optimized fail-safe devices. A safety mechanism to protect the residual femoral bone and its surrounding tissues from high applied loads is essential and must be engineered prior to moving to the remainder of the overall implant system design. The need for a fail-safe mechanism is exemplified by the fact that approximately 53% of lower limb amputees have reported falling accidents, with 40% resulting in injury.⁸¹ A fail-safe mechanism is crucial to release the prosthesis in both falls and more extreme circumstances, such as the device becoming caught, to prevent injury to the prosthetic device and the user's residual skeleton and surrounding tissues.

1.8 Summary of Present Work

It is known that transcutaneous implants with three-dimensional porous structures promote soft-tissue ingrowth and successfully form a biological seal around the implant, preventing external bacteria from causing infection.⁷² Furthermore, porous metal implants in bone have been proven to promote osseointegration, so it is assumed that porous metal transcutaneous implants have the potential to be used for bone-anchored prosthetic devices. Various solid transcutaneous implants have been tested as a bone-anchored mounting point for a prosthesis. However, the existing methods present challenges such as high infection rates and inadequate safety

mechanisms. Previous work on porous metal implants can be applied to develop a transcutaneous implant that incorporates porous structures for both bone and soft tissue ingrowth. However, a safety mechanism is needed to release the prosthetic under dangerously high loads to protect the user. The current work aims to develop a fail-safe mechanism to be used in attachment of a transcutaneous femoral implant to a prosthetic device. The device would provide complete release of a prosthetic under both bending and torsion events of dangerous magnitudes. Finite element analysis was utilized to model and analyze stress concentration distribution. Mechanical testing has been performed to validate the finite element analysis model and thereby lay the foundation for the further development of an osseointegrated transcutaneous implant to act as a direct mount for a prosthetic to the residual skeleton.

2 MATERIALS AND METHODS

2.1 Introduction

Several methods were employed in the present work to test the feasibility of a potential fail-safe component for the anchoring of a prosthetic device to a residual limb. Methods included manual calculations, finite element analysis (FEA), and various mechanical testing techniques. The current work proposes a notched bolt as a fail-safe mechanism, which entails a partially threaded bolt modified to have a notched region along its shaft. The notched region is intended to act as a stress riser and fail under controlled applied loads. Additionally, a notched bolt has the potential to fail under multiple modes of failure, such as failure in bending or torsional failure. **Figure 21** depicts a representation of applied bending force to a notched shear bolt, while **Figure 22** depicts a representation of applied torsional force to a notched shear bolt.

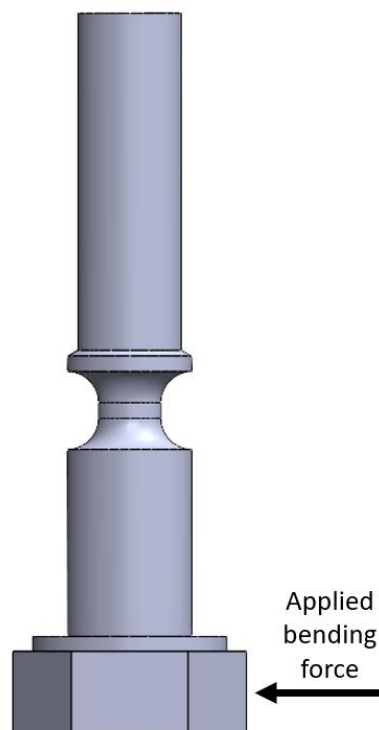


Figure 21. A diagram displaying an applied bending force.

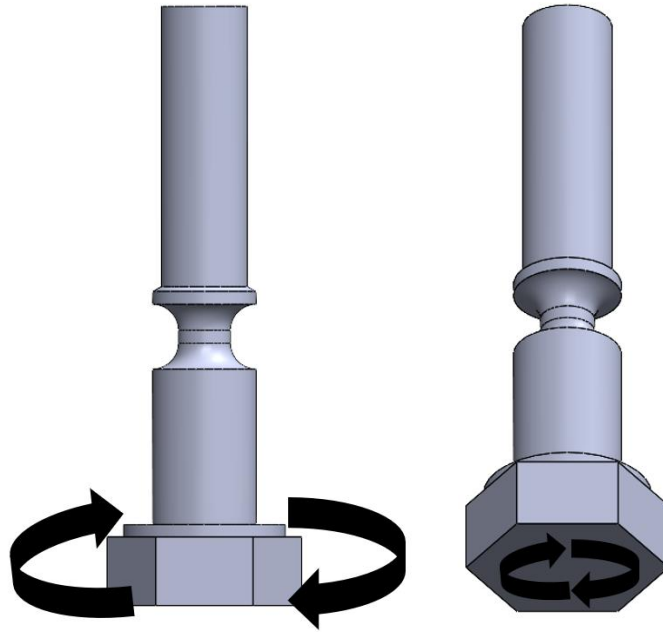


Figure 22. Diagrams displaying applied torsional forces (two different views) to a notched shear bolt.

Essential considerations when designing the notched bolt were material of construction, the commercial availability of components, applied loads, size and geometry, and suitability for manual calculations, FEA modeling, and experimental testing.

Transfemoral amputation was selected as the focus for the present work due to its comparative prevalence for the present modeling.⁶¹ However, it is noted that the work has the potential to be applicable to other surgical procedures, such as transtibial amputation. Critical forces on a residual limb are dependent on body weight, size of the residual limb, and other factors, such as gender.⁸² It is essential to determine the value at which the fail-safe component should fail. Existing devices may also be referenced for safety release levels. The user's lifestyle and typical activity levels should also be considered, giving rise to the possibility of customized mechanisms to meet individual needs.

Yield strength and ultimate tensile strength were used as reference values in manual calculations. Yield strength is the maximum tensile stress a material can withstand prior to permanent deformation.⁸³ Ultimate tensile strength is the maximum stress reached before failure occurs, while fracture strength is the value that corresponds to the stress at which total failure occurs.⁸³ Though the ultimate tensile strength value of a given material may be reached in an experimental test, it is not necessarily the point at which failure occurs. From the author's understanding, fracture strength (i.e., failure) typically occurs relatively soon after the material reaches its ultimate strength. However, it is important to note that the failure point/fracture strength is less consistent and therefore more difficult to predict than ultimate tensile strength, especially when testing unique geometries such as a notched bolt. Therefore, ultimate tensile strength values were employed in manual calculations, whereas fracture strength values were reported from experimental data.

2.2 Methods of Analysis

2.2.1 Manual Stress Calculations

Manual calculations were completed to understand and estimate bending stress and torsional stress at the notched region of the partially threaded bolt. The calculated values were intended to be used as a comparison to material property thresholds, notch geometry stress values, and to gauge the approximate accuracy of the finite element model. The bending stress and torsional stress formulae used were based on those of a solid rod. To obtain values that more accurately represent the unique geometry of a notched bolt, a stress concentration factor was implemented (**Figures 23 and 24**). To the author's knowledge, due to the unique nature of the notched bolt geometry, information regarding the bending and torsional stress concentration factors does not exist which completely represents the notch geometry under the tested forces. Hence, the bending stress

concentration and torsional stress concentration used was the closest to an accurate representation the author could obtain. A stress concentration factor is a dimensionless value used to quantify the stress concentration in a mechanical part.⁸⁴ Based on the geometry of the notched bolt, the stress concentration factor was determined and then multiplied with the nominal stress value to obtain the maximum stress, presumably concentrated at the notched region. The nominal stress value is the stress at the unmodified portion of the bolt (i.e., shaft with the original major diameter). The calculated maximum stress values were compared to material properties to predict failure of the bolts modified in the notched region.

2.2.1.1 Bending Manual Calculations

The formulae listed in **Table 1** were employed to manually calculate bending stress at the notch region of various modified bolts. Refer to **Table 2** for parameters relevant to the functions in **Table 1**.

Table 1. Bending Stress Functions Employed in Manual Calculations.

Function	Formula	Units
Moment	$M = F * l$	N-mm
Moment of inertia	$I = \frac{\pi * d^4}{64}$	mm ⁴
Bending stress	$\sigma = \frac{M * d}{2I}$	MPa

Table 2. Bending Stress Parameters.

Parameter Symbol	Parameter	Units
F	Applied force	N

Table 2 continued.

l	Distance from the applied force to the end of the notch furthest from the applied force	mm
d	Diameter of the residual shaft of the modified bolt (i.e., the minor diameter)	mm
D	Major diameter	mm
r	Radius (half of the diameter)	mm
$\sigma_{nominal}$	Nominal stress	MPa
k_t	Stress concentration factor	-

Figure 23 presents stress concentration factor information relevant to an applied bending moment on both sides of a notched bolt, including an example of a stress concentration curve for the D/d ratio of 2.00. Although the bolt geometry tested in the present work was only placed under bending forces on one side and held fixed on the other, the detail in **Figure 23** was the closest representation of the unique bolt geometry that the author could obtain. Based on a given notch's minor diameter and radii, and the major diameter of the bolt, the stress concentration factor was determined employing **Equation 1**.

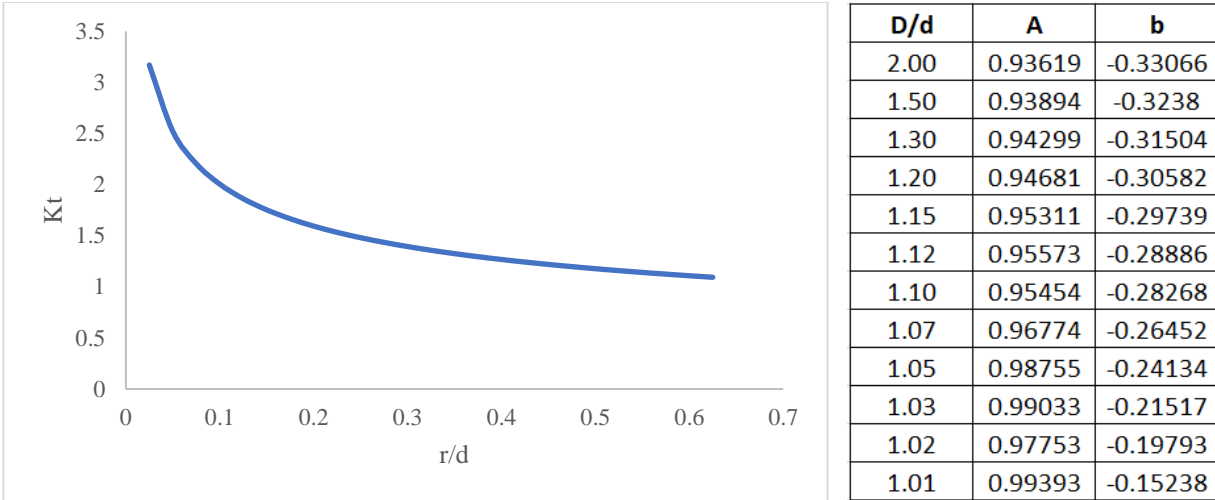


Figure 23. An example of a bending stress concentration factor curve for D/d=2.00 using the corresponding table values for A and b. Ref[85].

$$k_t = A\left(\frac{r}{d}\right)^b$$

Equation 1. Bending stress concentration factor. Ref[85]. Refer to Figure 23 for A and b values.

2.2.1.2 Torsion Manual Calculations

The functions listed in **Table 3** were employed to manually calculate bending stress at the notch region of various modified bolts. Refer to **Table 4** for parameters relevant to the functions in **Table 3**. Regarding the torsion stress calculations, von Mises criterion, which states that failure occurs when the energy of distortion reaches the same energy for yielding in uniaxial tension, was applied in addition to initial manual calculations for evaluation of the unique notch geometry.⁸⁶

Equation 2 presents the general form of the von Mises criterion. The left-hand side of the equation is equivalent to von Mises stress. Refer to **Table 5** for the von Mises criterion formulas simplified for application with the notched bolts and **Table 6** for their respective parameters. When the von Mises stress equals the tensile yield strength, yielding occurs. As an example, with regard to the

notched bolts, for a material with a yield strength of 900 MPa, the von Mises criterion predicts the part would fail at approximately 520 MPa (i.e., $\frac{900}{\sqrt{3}} = 519.62$).

Table 3. Torsion Stress Functions Employed in Manual Calculations.

Function	Formula	Units
Polar moment of inertia	$J = \frac{\pi * d^4}{32}$	mm ⁴
Torsional stress	$\sigma = \frac{T * d}{2J}$	MPa
Maximum stress	$\sigma_{max} = k_t * \sigma_{nominal}$	MPa

Table 4. Torsional Stress Parameters.

Parameter Symbol	Parameter	Units
D	Major diameter	mm
d	Diameter of the residual shaft of the modified bolt (i.e., the minor diameter)	mm
r	Radius (half of the diameter)	mm
T	Torsion moment	N-m
$\sigma_{nominal}$	Nominal stress	MPa
k_t	Stress concentration factor	-

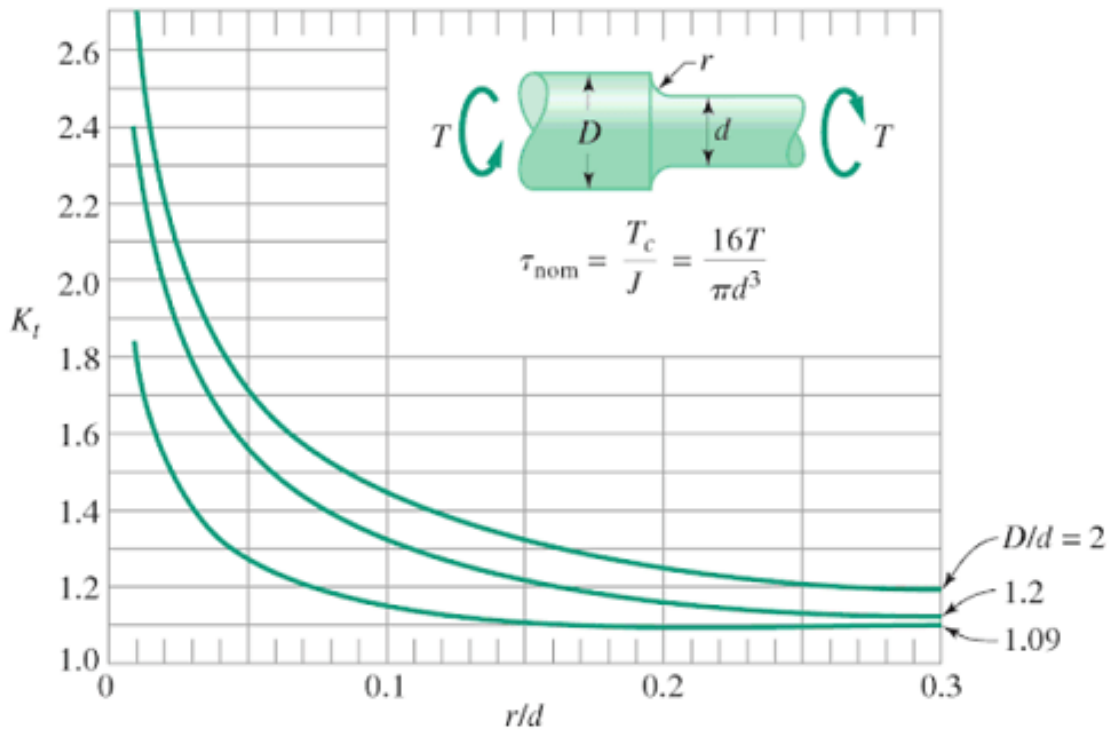


Figure 24. Torsional stress concentration factor. Ref[88].

$$\frac{1}{\sqrt{2}} [(\sigma_{xx} - \sigma_{yy})^2 + (\sigma_{yy} - \sigma_{zz})^2 + (\sigma_{zz} - \sigma_{xx})^2 + 6(\tau_{xy}^2 + \tau_{yz}^2 + \tau_{zx}^2)]^{1/2} = \sigma_y$$

Equation 2. General form of Von Mises criterion. Ref[87].

Table 5. Parameters Relevant to **Equation 2**.

Symbol	Parameter	Units
σ_y	Yield stress	MPa

Table 5 continued.

σ_{xx}	Normal stress in the x-direction	MPa
σ_{yy}	Normal stress in the y-direction	MPa
σ_{zz}	Normal stress in the z-direction	MPa
τ_{xy}	Shear stress in the xy-plane	MPa
τ_{yz}	Shear stress in the yz-plane	MPa
τ_{zx}	Shear stress in the zx-plane	MPa

Table 6. Simplified von Mises Criterion Functions.

Function	Formula	Units
Maximum stress	$\sigma_{max} = k_t * \sigma_{nominal}$	MPa
von Mises stress	$\sigma_{vm} = \sqrt{3} * \sigma_{max}$	MPa

Table 7. Simplified von Mises Criterion Parameters.

Parameter Symbol	Parameter	Units
σ_{max}	Maximum stress	MPa
$\sigma_{nominal}$	Nominal stress	MPa
k_t	Stress concentration factor	-

2.2.2 Finite Element Modeling

Finite element analysis (FEA) is the simulation of a given physical phenomenon using the numerical technique termed the finite element method (FEM).⁸⁹ FEA is often used to minimize physical prototype testing and to optimize design components by *in silico* predictions of physical performance. It is a method of numerically solving differential equations and is commonly used

for structural analysis. FEA was utilized in the present work to analyze stress concentration throughout models of the notched bolts, as well as to analyze displacement resulting from an applied load. The FEA results were compared with manual calculations, material thresholds, and to predict physical experimental outcomes. The software used for FEA was Abaqus, originally released in 1978. Abaqus can model a wide range of geometries, materials, and stress types. To design three-dimensional models of the bolts modified to have notches (hereafter referred to as modified bolts), SolidWorks was used. SolidWorks is a solid modeling computer-aided design and computer-aided engineering application published by Dassault Systemes, originally released in 1995.

Manual calculations are useful to predict trends in how shear bolts of a range of notch geometries may act under various loads, but an FEA model can provide more accurate results for analysis prior to spending time and money on physical testing. Manual calculations often require simplifications, which may decrease accuracy of the results. Additionally, for complex structures, such as a partially threaded bolt modified to have a notch region, fully appropriate manual calculation methods are seldom available. Manual calculations will only output stress values for certain sections determined by the operator, whereas FEA has the capability to consider the entire structure. Abaqus was employed to simulate bending and torsional forces on a variety of bolts. A standard/explicit model was used as an initial model database, which comprised various linear and nonlinear modeling options. Selecting an initial model database brings the user to the main window within the software (**Figure 25**). Abaqus is broken into different modules, each containing various tasks (such as sketching, creation of materials, mesh generation, etc.). An important note when setting up a model is that Abaqus does not have a default system of units, so the user must ensure

that the units used are consistent across all modules and features. Refer to **Table 7** for the units that were employed. The SI (mm) system was used for the present work.

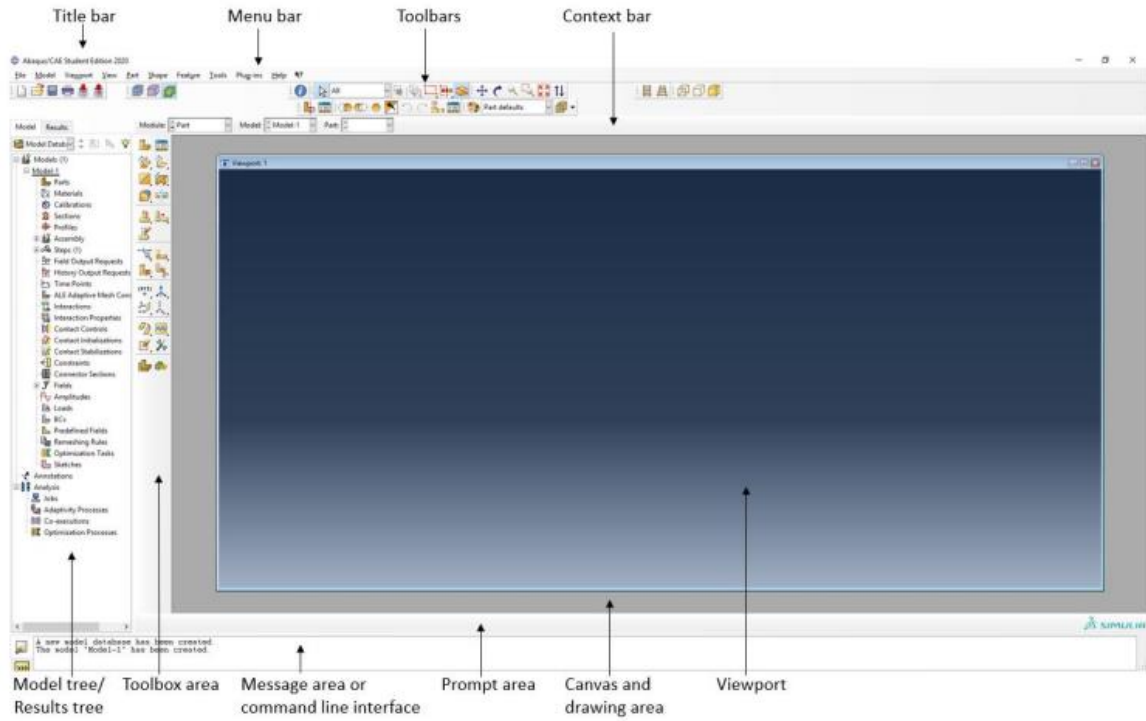


Figure 25. Main window in Abaqus. Ref[90].

Table 8. Units Employed in Abaqus FEA Model.

Quantity	Units
Length	mm
Force	N
Mass	tonne (10^3 kg)
Time	s
Stress	MPa (N/mm^2)
Energy	mJ (10^{-3} J)

Table 8 Continued.

Density	tonne/mm ³
---------	-----------------------

The module list includes part, property, assembly, step, interaction, load, mesh, optimization, job, visualization, and sketch. The part module contains details regarding the part and its geometry. Parts can be created as a CAD drawing in the module if desired, or may be imported from other software packages. In the present work, SolidWorks part files of the modified bolts were imported into Abaqus. The property module is where the material properties, cross sections, and other material related parameters are defined. To add a material, the “create material” tool was selected. An edit material popup appeared, where general, mechanical, thermal, electrical, and magnetic properties were input, as well as a material name (**Figure 26**). Density (termed mass density in Abaqus), Young’s modulus and Poisson’s ratio values were all input here based on the material of choice (see Section 3.2 for additional detail). A material’s Young’s modulus value describes its ability to withstand changes in length when under lengthwise bending or compression. A higher Young’s modulus value correlates with a stiffer material, whereas a lower Young’s modulus corresponds with a more elastic material. Poisson’s ratio is a value between zero and one that describes the elastic deformation of a material related to strain. It is the ratio of the proportional decrease in a lateral measurement to the proportional increase in length in a sample of material that is elastically stretched. A higher Poisson’s ratio correlates with a larger elastic deformation, no matter the amount of stain. Density is a materials mass per unit volume.⁹¹

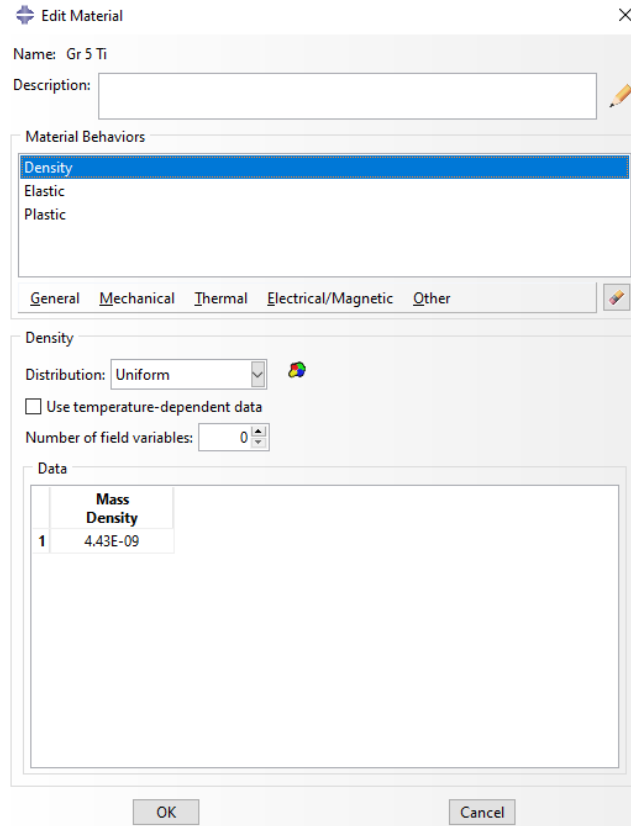


Figure 26. Creating a new material in Abaqus.

If the user were to not explicitly include the elastoplastic aspect of modified bolts, the model would be purely elastic, which only represents a portion of the bolt’s response to the applied load. To simulate plastic deformation, plastic material property information was added under the plastic module. Three plastic models in order of increasing complexity and accuracy are the elastic-perfectly plastic model, the linear strain-hardening model, and the Johnson-Cook model. While the Johnson-Cook method is the most accurate method, there are various parameters that would need to be experimentally determined to accurately represent the material and geometry. Therefore, the linear strain-hardening model was employed for the present work (see Section 3.7 for additional detail). The assembly module is where multiple parts can be formed into one assembly. A “part instance” is essentially a reference to the original part geometry and can be used

for assembly purposes. Since there was only one part being simulated at a time in the present work, one “part instance” was created to form an assembly by itself. The step module is where the static analysis components can be edited, such as the incrementation, equation solver method, and solution techniques. The incrementation corresponds to the computation step size and can be modified in terms of quantity and size. In the mesh module, the part is discretized into elements and nodes and the FEA mesh is created. The elements and nodes that comprise a mesh correlate with locations in space that represent the shape of the modeled geometry. To create a mesh, the element type was first selected by opening the “assign element type” tool. 3D stress was the default family of elements and was employed for the present work. The mesh controls tool contains options for the element shape. Tetrahedral (“tet”) element shapes can approximate surface contours effectively, and were therefore selected for the present work. Next, the “seed part” tool was selected to seed the model, which essentially means to assign the node positions on the part to specified regions of the geometry. The entire part was seeded at once to create a uniform mesh. The approximate global size was filled out, which equals the length of each mesh element. The smaller the approximate global size is, the finer the resulting mesh is. A finer mesh with a greater quantity of elements and nodes results in a more accurate representation of the modeled geometry. However, finer meshes typically require greater computational power and time. **Figure 27** displays a comparison of a fine mesh versus a course mesh.

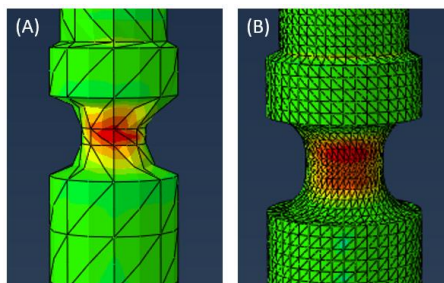


Figure 27. (a) Course mesh and (b) fine mesh applied to a notched bolt.

To generate the final mesh, the “mesh part instance” tool was selected. To determine the optimal mesh element size, a mesh convergence study was performed. A mesh convergence study is useful in terms of validating the model and determining an appropriate mesh element size. Briefly, a nominal notched bolt was generated and an arbitrary load of 800 N was applied. The mesh element size was varied and the stress at the notch was calculated at each element size. The mesh element size test range was from 0.6 to 10 mm. The bolt’s notch location from under the head of the bolt and notch minor diameter were modeled as 10mm and 4mm, respectively. **Figure 28** presents a plot of the mesh convergence study. It is important to note that only the relevant region of 0.6 to 2mm (corresponds an element size/minor diameter range of 0.12 to 0.36 on **Figure 28**) is shown on the plot.

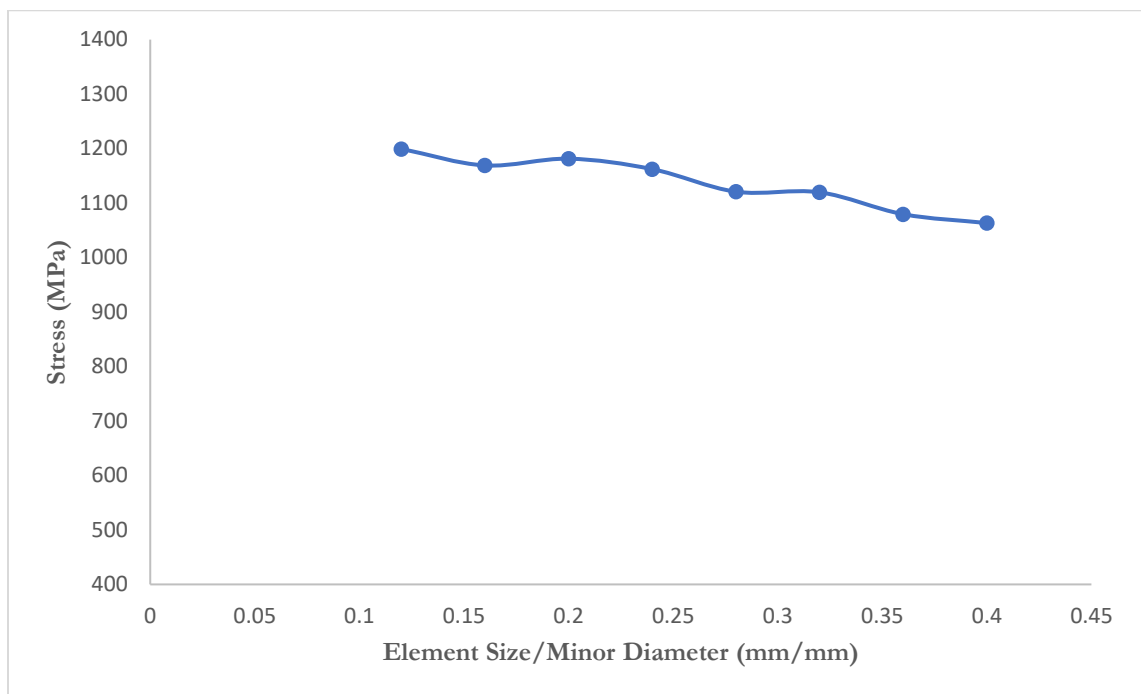


Figure 28. Plot of element size/minor diameter (mm) versus stress (MPa) as a mesh convergence study.

The mesh convergence study resulted in an optimal mesh element size of 0.8, which was ultimately determined by the plateau observed in the region of a stress value of 1200 MPa in a plot of stress versus mesh element size (**Figure 28**). A plateau on a convergence study plot indicates a solution value has been determined that is independent of the mesh size.

The load module contains detail regarding applied loads and boundary conditions. To add a load, the “create load” tool was selected. Types of loads available include concentrated force, moment, pressure, line load, and more. The load type to be applied depends upon the geometry of the part being processed and the simulated force of interest. To mimic a bending force, a concentrated force was applied via a set of nodes in a line along the edge of the unmodified shaft between the head of the bolt and the start of the notch region. To create a set of nodes, “create set” was selected under the tools drop down list (**Figure 29**). In the present work, a set was created in a line along the shaft of the bolt, where the load was to be applied.

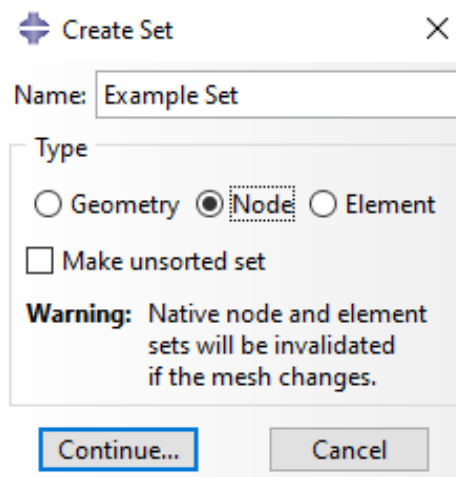


Figure 29. Creation of a set.

As depicted in **Figure 30**, the force was applied per node in the direction specified, where CF1 is the x-direction, CF2 is the y-direction, and CF3 is the z-direction.

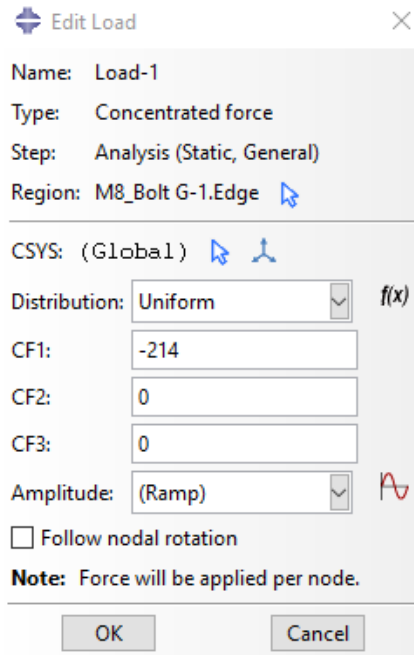


Figure 30. Editing an applied load.

To mimic a torsional force, a coupling constraint was employed. First, a reference point was established at the center of the bolt's hex head surface. A coupling constraint was then defined, employing the reference point as the constraint control point. The six outer surfaces of the hex head were selected for the reference point to control. The coupling type selected was kinematic, and U2 and UR2 were selected as degrees of freedom to prevent movement in the y-direction (**Figure 31**). A torsional moment was to be applied onto the reference point and therefore the head of the bolt.

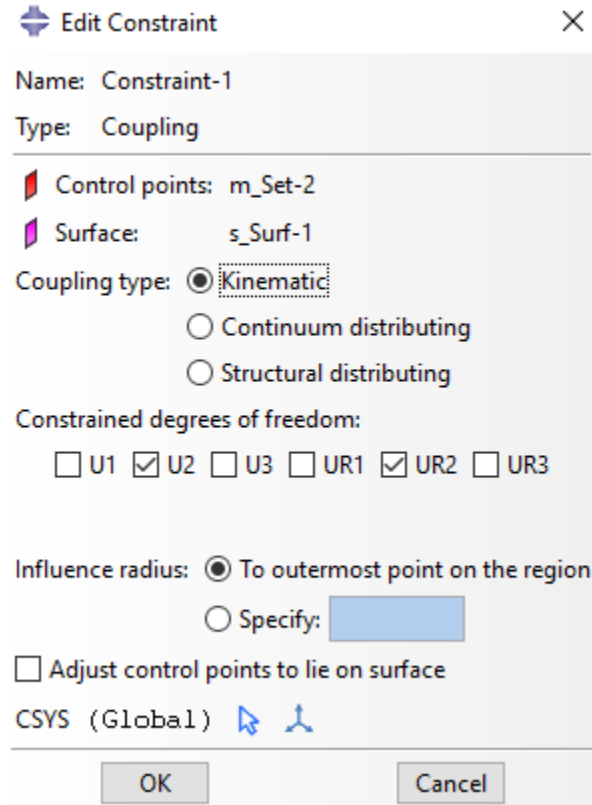


Figure 31. Defining a coupling constraint for torsional loads.

In addition, boundary conditions were added employing the load module. To create a boundary condition, the “create boundary condition” tool was selected. A fixed boundary condition on the section representing the threads of the bolt was needed for the present modeling to mimic the bolt being fully threaded and fixed into another component. The section where the threading would reside was selected and an “encastre” boundary condition type was selected, which essentially prevents movement of the selected region in any direction (**Figure 32**).

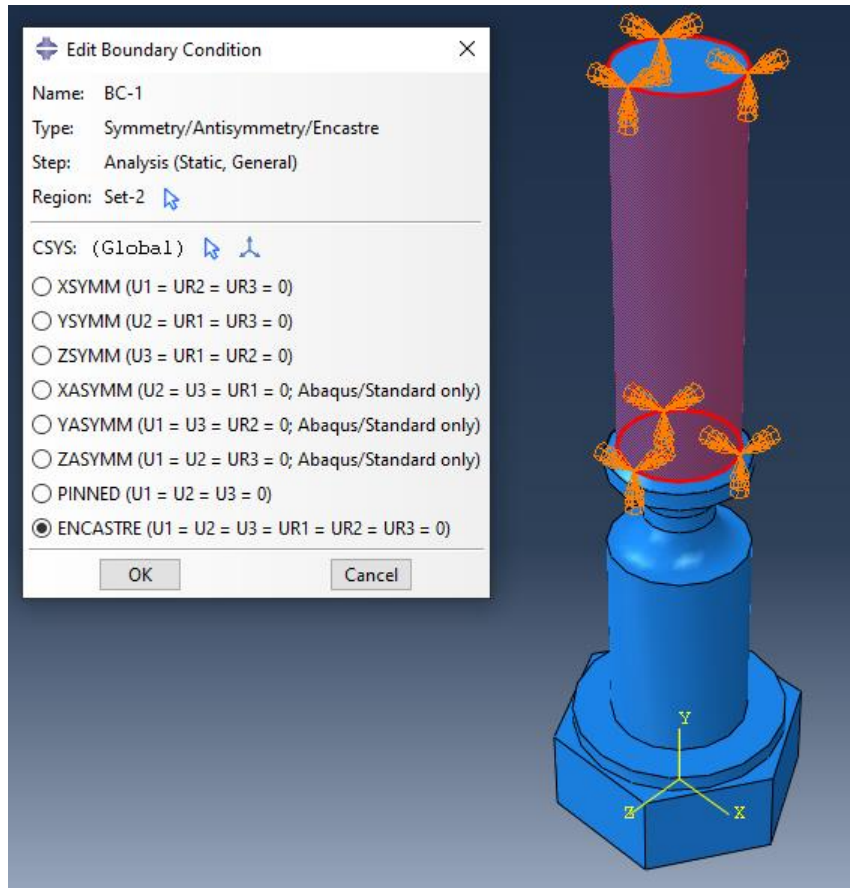


Figure 32. Fixed boundary condition.

Analysis was submitted to run via the job module. A job was created within the job manager tool. To run the job, the only step required was to select “submit”. While the job was running and computing, progress could be monitored by selecting the monitor tab, which displayed errors, warnings, and the status of the job being processed. The visualization module enabled post-processing. Analysis of the results was performed in the visualization module. Results could be viewed comparing the elements of the part’s mesh to the respective color gradient, an example of which is shown in **Figure 33**. To extract stress values at specific locations, the “probe values” tool was used, found within the tools drop down menu. With the “probe values” tool, exact nodes could be selected on the part to assess their respective stress value. To generate a plot displaying

displacement as a result of a gradually applied load, the “XY data” tool was selected within the tools drop down menu. The ODB output module provides options for creation of various plots, such as step time versus displacement. For the present work, displacement versus load plots were created.

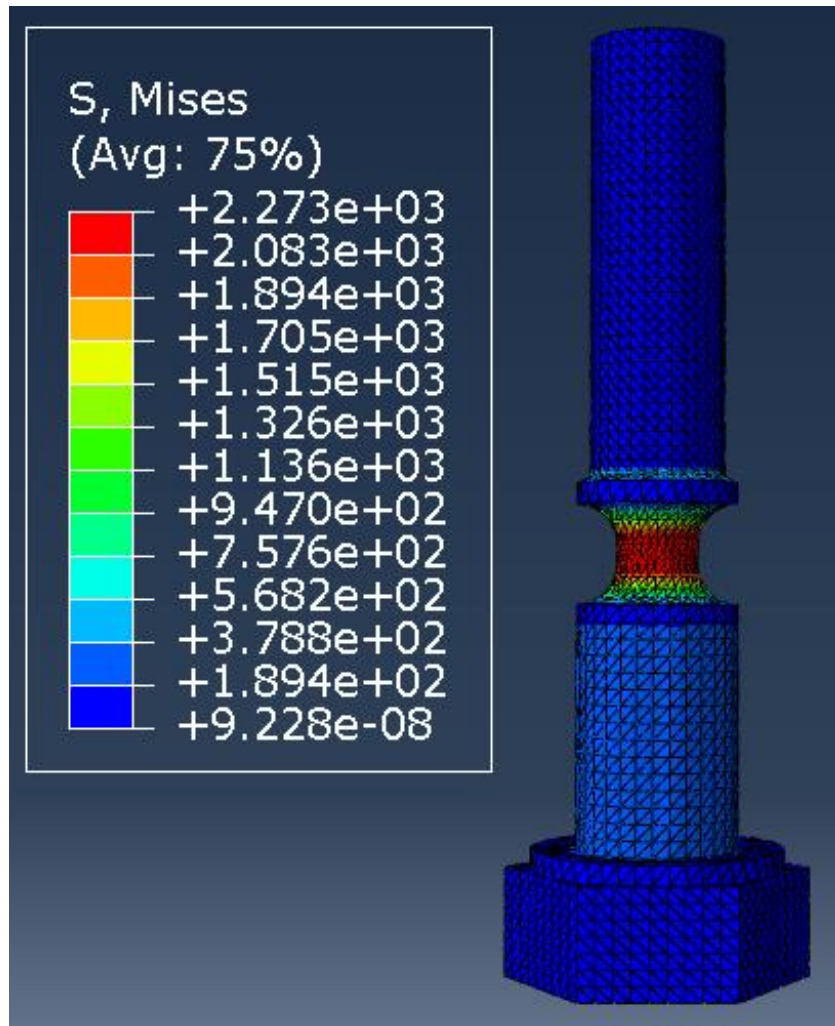


Figure 33. An example of a bolt displaying von Mises stress (MPa) results after an applied force had been modeled. “Avg: 75%” indicates the contour plot displays the average value of the output parameter over the specified region, and the value depicted corresponds to the average value at 75% of the simulation duration.

2.2.3 Mechanical Testing

Mechanical testing was performed to validate the FEA model and to compare physical results to both FEA and manual calculations. Commercially available metric partially threaded bolts were purchased and manually modified by the incorporation of a specified notch. Standard bolts were purchased for experimental tests rather than custom-fabricating bolts for the sake of cost savings and lead time. M8 grade 5 titanium bolts and M8 18-8 stainless steel bolts were obtained from McMaster-Carr (**Figure 34**). The part numbers were 94081A972 and 91287A156, respectively. Both were hex head partially threaded bolts, with a 1.25 mm thread pitch and 40mm unthreaded shaft. The titanium bolts had a reported tensile strength of 130,000 psi, equivalent to approximately 896 MPa. The stainless steel bolts had a reported tensile strength of 100,000 psi, equivalent to approximately 689 MPa.

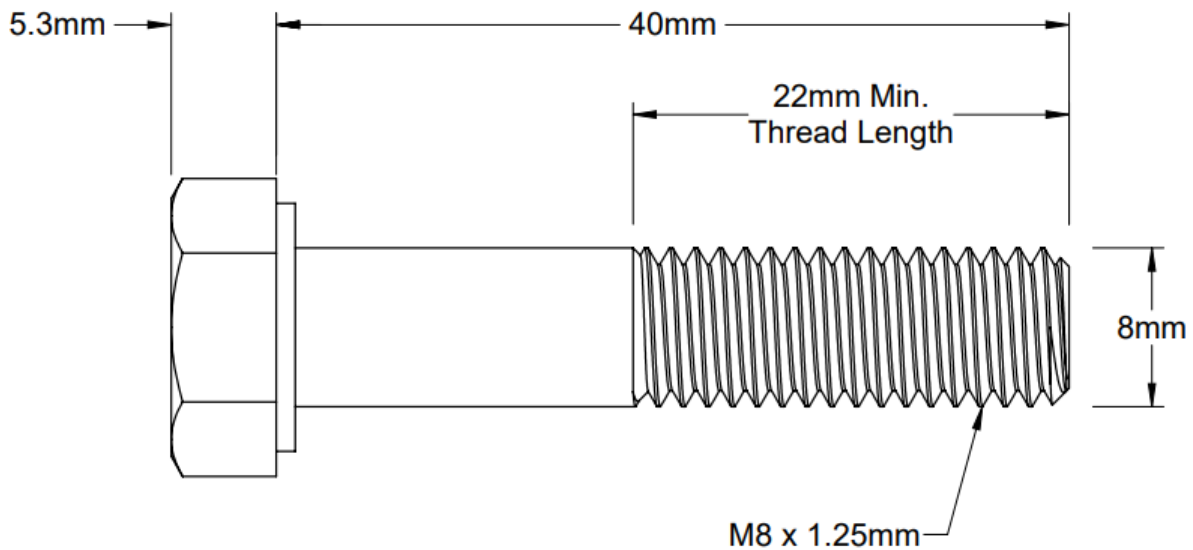


Figure 34. M8 Hex Bolt drawing. Ref[92].

Initial bolts for ranging studies were machined by Mr. Amos Cline, a prototype engineer at the University of Maine. Subsequently, bolts were precision-machined at Southern Maine Community College with a Kent 1440 lathe. The lathe process employed an oil sulfur based cutting fluid. To modify the bolts to have a specific notch geometry, custom tooling was required. The tooling was fabricated from cemented carbide on a George Fisher Cut 20P wire electrical discharge machine (EDM). The wire EDM utilized deionized water and 0.01-inch wire. The resultant tool was a custom cutting tool with a defined geometry of width 5mm and a radius of 2mm.

2.2.3.1 Bending Test Systems

Various experimental test setups for bending were explored. An initial bending test setup was employed at the University of Maine Advanced Structures and Composites Center. The test system included an Instron 8872 servo hydraulic machine, and a custom steel fixture for the bolts (**Figures 35 and 36**). The Instron 8872 machine was a tabletop servo hydraulic testing system employed for various static and dynamic tests. To run the test, a bolt was fully threaded 22mm into the custom fixture and an appropriate loading nose was selected, which was attached to the moving crosshead of the Instron such that it made contact with the bolt to apply a given load. The Instron 8872 was run using a preloaded methods program to collect relevant data while the load was applied at a rate of 1.27 mm/min. The nose moved vertically and applied force in a downward direction on the head of the bolt. Load, displacement, and time data were collected in the form of an Excel file to be analyzed.



Figure 35. Instron 8872 servo hydraulic machine.



Figure 36. Custom bending fixture for use with an Instron 8872.

The initial bending test setup was determined inadequate for the purposes of the present work due to yielding of the steel fixture and movement of the Instron loading nose throughout experimental testing, so a new experimental method was developed. The second setup for bending tests was at the University of Maine Advanced Manufacturing Center and included a material testing setup (MTS) 810 servo-hydraulic machine with a 22kip load cell (**Figure 37**). A custom fixture to mount a bolt was fabricated to be compatible with the MTS (**Figure 38**). A nut was fully threaded onto the bolt when in the fixture to improve stability. To apply a load, a braided cable was clamped onto the bolt via a shackle and pulled upwards until bolt failure occurred. The braided cable was made of galvanized steel and had a vinyl coating. The cable was 4mm in diameter and 635mm in length, with the top shackle measuring an additional 70mm and the bottom shackle measuring an additional 108mm. To understand the elongation occurring in the cable alone, a test was run in which the cable was attached directly to the base and a force was applied. Displacement data was produced based on the displacement of the top clamp relative to the bolt. For all MTS runs, load, displacement, and time data were collected in the form of an Excel file to be analyzed.



Figure 37. MTS 810 servo-hydraulic machine with a 22kip load cell at the University of Maine Advanced Manufacturing Center.



Figure 38. Bolt in the custom fixture with a nut threaded on for additional stability, with a braided steel cable clamped to the bolt via a shackle.

2.2.3.2 Torsion Test Systems

Various experimental test setups for torsion were explored. An initial torsion test set up was implemented at the University of Maine Advanced Structures and Composites Center. Equipment comprised a Durofix ½” Digital Angle Torque Adapter, a 13mm socket, a half-inch drive ratchet, a breaker bar, a clamp, and a custom fixture. The Durofix digital torque wrench had a part number of RM604-4A and could withstand 25-250 ft-lbs at a maximum rotation of 720 degrees. The digital torque wrench included audible and LED alerts as an option to alert the operator if specified torque values were reached. The fixture was similar to that used in the initial bending test and was clamped down to the base of the Instron 8872 set up via bolts. To apply torque, the digital torque wrench was attached to the ratchet and breaker bar (**Figure 39**). The torque wrench was set to “peak mode” to record the highest torque value applied. The combined torque wrench, ratchet, and breaker bar were then attached to the bolt in the fixture. Force was manually applied by rotating the ratchet in a clockwise direction until the bolt yielded and failed.

The initial method employed to test torsional loads on the bolts was proven ineffective for the purpose of the present work due to inconsistencies in torque application, so an alternate experimental method was employed. The second, automated, torsion test was implemented at the University of Maine Advanced Structures and Composites Center. Test equipment comprised a custom-made steel fixture and an Instron hydraulic test frame with torque capacity up to 100Nm (**Figure 40**). The custom-made steel fixture was created at Southern Maine Community College and was designed to allow the bolt to be fully threaded in from the top, so that the Instron could attach to the bolt head via a custom hex attachment designed and created at the Advanced Structures and Composite Center.



Figure 39. Breaker bar, 13mm socket, and a half-inch drive socket attached to a digital torque wrench.

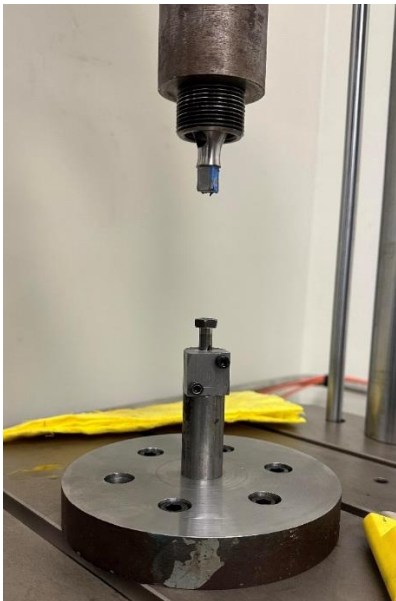


Figure 40. Custom torsion set up at the University of Maine Advanced Structures and Composites Center. On the bottom of the image the custom fixture is shown with a bolt threaded in and secured in place. On the top of the image, custom tooling is shown attached to the loading nose, which was employed to apply torsional loads to the hex head of the bolts.

3 INITIAL DESIGN CONSIDERATIONS

3.1 Introduction

The current work proposed a notched bolt as a fail-safe mechanism for a femoral prosthetic, which entailed a partially threaded bolt modified to have a notched region along its shaft, intended to act as a stress riser (**Figure 41**). The notched bolt would ideally fail under controlled applied loads with multiple modes of failure, such as bending stress and torsional stress.

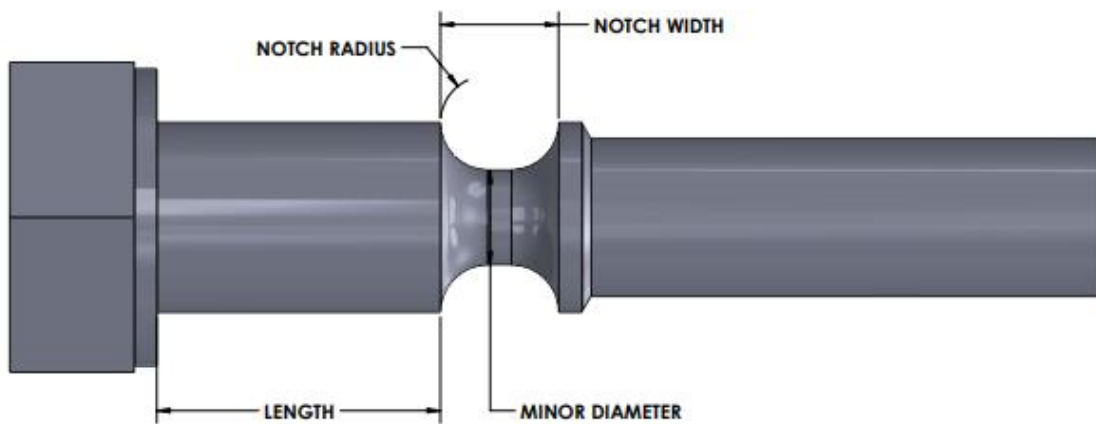


Figure 41. Example of a modified bolt, with labeled regions (threads not shown).

The focus of the presented work was to design, model, and test potential fail-safe components, rather than design a complete attachment system for the external prosthesis to the bone-anchored implant. Implant systems exist as discussed in Section 1.4, but they fail to include an optimized safety mechanism. A fail-safe component is crucial to protect the user's residual limb from bone fractures and tissue damage and must be thoroughly developed prior to the remainder of an attachment system being finalized. Potential ways a notched bolt could fit into an overall safety mechanism is through direct threading into the implant (**Figure 42**) or within the external coupling component, similar to existing devices such as the OPL or IPL systems discussed in Section 1.4. While the former would be the simplest and most readily adopted, the latter would

prevent direct contact between the implant and bolt, allowing for easier removal and replacement in cases of failure. Essential considerations when designing the notched bolt were material of construction, size and geometry, the commercially availability of components, applied loads, and suitability for manual calculations, FEA modeling, and experimental testing.

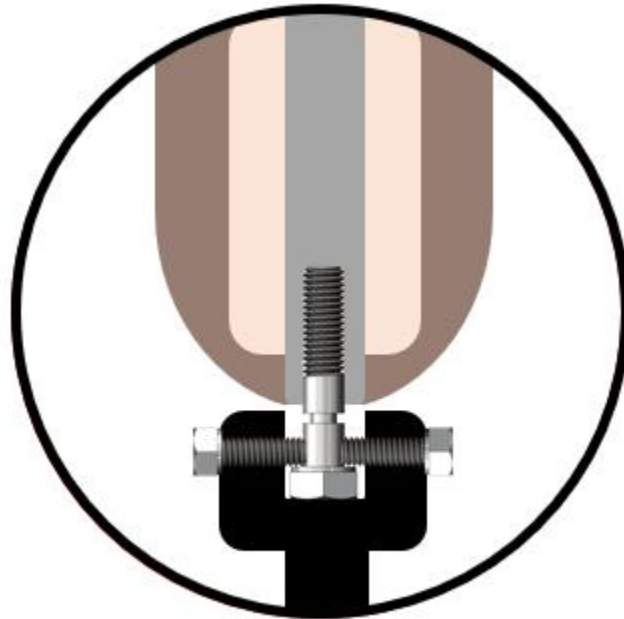


Figure 42. One potential overall coupling device, in which the partially threaded fail-safe bolt would thread directly into the transcutaneous bone-anchored implant.

3.2 Material of Construction

Various materials of construction were considered for potential shear bolts. Materials included, but were not limited to, polypropylene, brass, stainless steel, grade 23 titanium, and grade 5 titanium. Metals comprised the majority of the selected materials, as the goal of the shear bolt was to have the notched region fail prior to plastic yielding. Metals are generally brittle in comparison to plastic materials, which is why the present studies were limited to mostly metals. However, a

plastic (polypropylene) and a more ductile metal (brass) were included for initial comparison. Material properties of interest included yield strength, ultimate tensile strength, Young's modulus, Poisson's ratio, and density. Yield strength is the maximum tensile stress a material can endure before beginning to permanently deform, whereas ultimate tensile strength is the maximum tensile stress a material can withstand before it fails. **Table 9** presents the material properties of considered materials of construction.

Table 9. Material Properties. Ref[93-97].

	Polypropylene	Brass	Stainless Steel	Grade 23 Titanium	Grade 5 Titanium
Yield strength (MPa)	32.5	255	215	790	900
Ultimate tensile strength (MPa)	40	400	505	860	950
Young's modulus (MPa)	1470	106000	197000	113800	113800
Poisson's ratio	0.36	0.32	0.29	0.34	0.34
Density (g/cm³)	0.93	8.73	7.75	4.43	4.43

3.3 Size and Geometry

The size and geometry of the bolts were an essential consideration, as they would affect the overall bolt function. A length range of approximately 25-50 mm and major diameter range of approximately 5-10 mm were chosen based on the envisioned bolt usage. Because the bolt was to have an incorporated notch region to act as a stress riser, the bolt should ideally only be partially threaded, rather than fully. The notch geometry itself was to be varied and analyzed via manual calculations, FEA modeling, and mechanical testing.

3.4 Commercial Availability

To experimentally test bolts with notched regions, bolts must either be manually modified, or custom made via a process such as additive manufacturing. In an attempt to decrease lead time and cost, commercially available bolts were investigated in the general size and materials of interest. **Table 10** below presents the commercially available bolt information, including material, size, cost, threading, system of measurement, and McMaster-Carr part number.

Table 10. Commercially Available Bolts Explored and Their Respective Material, Size, Cost, Threading, System of Measurement, and McMaster-Carr Part Number.

Material	Size	Cost	Threading (partial or full)	System of measurement (metric or standard)	McMaster- Carr part number
Grade 5 titanium	M8 x 1.25mm thread size, 40mm length	\$18.70/piece	Partial	Metric (mm)	94081A792
18-8 stainless steel	M8 x 1.25mm thread size, 40mm length	\$9.17/pack of 10 (\$0.92/piece)	Partial	Metric (mm)	91287A156

Table 10 Continued.

High strength class 10.9 stainless steel	M8 x 1.25mm thread size, 40mm length	\$12.09/pack of 25 (\$0.48/piece)	Partial	Metric (mm)	91310A542
Brass	5/16"-18 thread size, 1½" length	\$9.67/pack of 10 (\$0.97/piece)	Partial	Standard (inches)	92941A587
Nylon	5/16"-18 thread size, 1½" length	\$11.58/pack of 25 (\$2.32/piece)	Partial	Standard (inches)	91244A587
Polyvinyl chloride (PVC)	5/16"-18 thread size, 1½" length	\$3.64/piece	Partial	Standard (inches)	95841A587

Grade 5 titanium was the only grade of titanium available from McMaster-Carr in the bolt geometry of interest. The part's geometry fell within the proposed dimensions, was partially threaded, and has a metric system of measurement. A metric system of measurement was ideal because manual calculations and FEA were performed employing metric units in the present work; the author and collaborators preferred to maintain consistent measurement units. A disadvantage of the grade 5 titanium bolts was the cost per piece. However, experimental costs could be offset by sacrificing less expensive bolts for setup purposes in testing, as long as overall dimensions remained consistent. Two different stainless steel bolts were explored: 18-8 stainless steel and high strength class 10-9 stainless steel. Both had optimal geometry, were partially threaded, and employed a metric system of measurement. The 18-8 stainless steel was slightly less expensive than the high strength class 10-9 stainless steel. However, both were significantly more cost effective than the grade 5 titanium. Brass bolts were explored, but unfortunately were not available in the same size as the titanium or stainless steel options. Polypropylene was not offered in the

proposed geometry by McMaster-Carr, so two alternative plastic materials were investigated: nylon and polyvinyl chloride (PVC). Unfortunately, similar to the brass, the bolt sizing was not the same as the bolts offered in metric measurement systems.

Purchasing commercially available bolts was convenient and more cost effective than the alternative route of custom manufacturing for experimental testing purposes. A lathe was used to easily and effectively modify standard bolts to have a notched region (**Figure 43**).

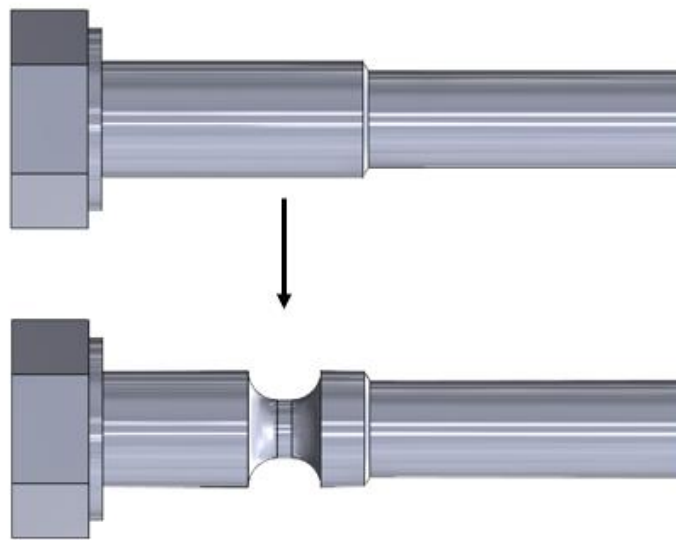


Figure 43. Example of a standard bolt customized to have a notch (threads omitted).

3.5 Critical Applied Forces

Bending and torsion forces were critical forces to consider, as both are experienced by the knee, and by a prosthetic leg attached to a residual femur, on a daily basis. Kutzer et al. investigated loading on the knee joint during daily activities and found that the forces on the knee region could reach up to 46% body weight in a single direction.⁹⁸ Based on the average body weight of 95.8 kilograms reported in the same study, 46% body weight corresponds to a force of up to 432N on

the knee joint during daily activity. Welke et al investigated simulations of resulting loads at the prosthesis interface of transfemoral amputees. The study reported a peak force on the knee during falls of 274 ± 74 percent bodyweight (which corresponds to approximately 1780N). The only FDA-approved device has a reported set bending failure modes at 70 ± 5 Nm (refer to Section 1.6). 70Nm of bending torque on a transfemoral prosthetic device would correspond to approximately 115N (based on the average distance from a person's foot to knee).⁹⁹ Though the stated values are ambiguous and could be affected by a variety of parameters, 432N was employed in initial bending manual calculations as a minimum force the bolts must withstand during daily activities and 1780N was employed in initial bending manual calculations as a force the bolts must fail under.

Torsional forces are not expected to be as high, though still essential to consider and incorporate into a fail-safe mechanism. Taylor et al. investigated forces and moments experienced by osseointegrated endoprostheses for lower extremity amputees. The study found the maximum torsion moment on the tibia during a fall to be 102Nm.⁸² However, the FDA-approved device has a reported factory-set torsion release level at 15 ± 2 Nm (see Section 1.6). As with bending forces, the existing literature is ambiguous and could be affected by numerous parameters, 102 Nm was employed in initial manual calculations to provide a target value for bolt failure due to torsion moments.

3.6 Initial Manual Stress Calculations

To determine which, if any, of the commercially available bolt materials were appropriate for the required shear bolt, manual calculations were completed to compare predicted maximum stress values experienced under the known load conditions to material yield strength. A maximum stress value in excess of the material yield strength for a given bolt geometry would correlate with bolt failure/deformation. In practice, yield strength was used as a reference to analyze the minimum

residual shaft diameter that could be used for each material. It is noted that yield strength rather than ultimate tensile strength was selected as the relevant parameter since any permanent deformation within the shear bolt while in use could lead to unexpected failure at a later point in time and would likely lead to bolt replacement as the geometry of the prosthetic attachment would have been altered.

The objective of the manual calculations was to gain an initial understanding of the appropriate range of notch geometries and materials of bolt construction. A variety of minor diameters (residual diameter of the bolt within the notch) were included in the calculations, ranging from 2.5mm to 6mm. The notch width was set at an arbitrary value of 2mm. Based on the principle of a moment, the larger the distance from the applied load, the greater the moment and therefore stress at the notch would be. Hence, the shaft length (distance under the head of the bolt to the notch) was fixed at the largest value, at 18mm, for a worst-case approach, in the sense that worst case would be bolt deformities or failure due to daily activity forces. **Figure 44** presents the resulting plot of minor diameter versus stress as a result of an applied daily activity bending force of 432N (see Section 3.5). For ease of comparison, the relevant material yield strength values are plotted on **Figure 44** to enable ready determination of the notch geometry below which material yielding is predicted for each of the relevant construction materials. Yield strength values were implemented as a reference to understand if the tested geometries would deform under the applied bending daily activity force of 432N.

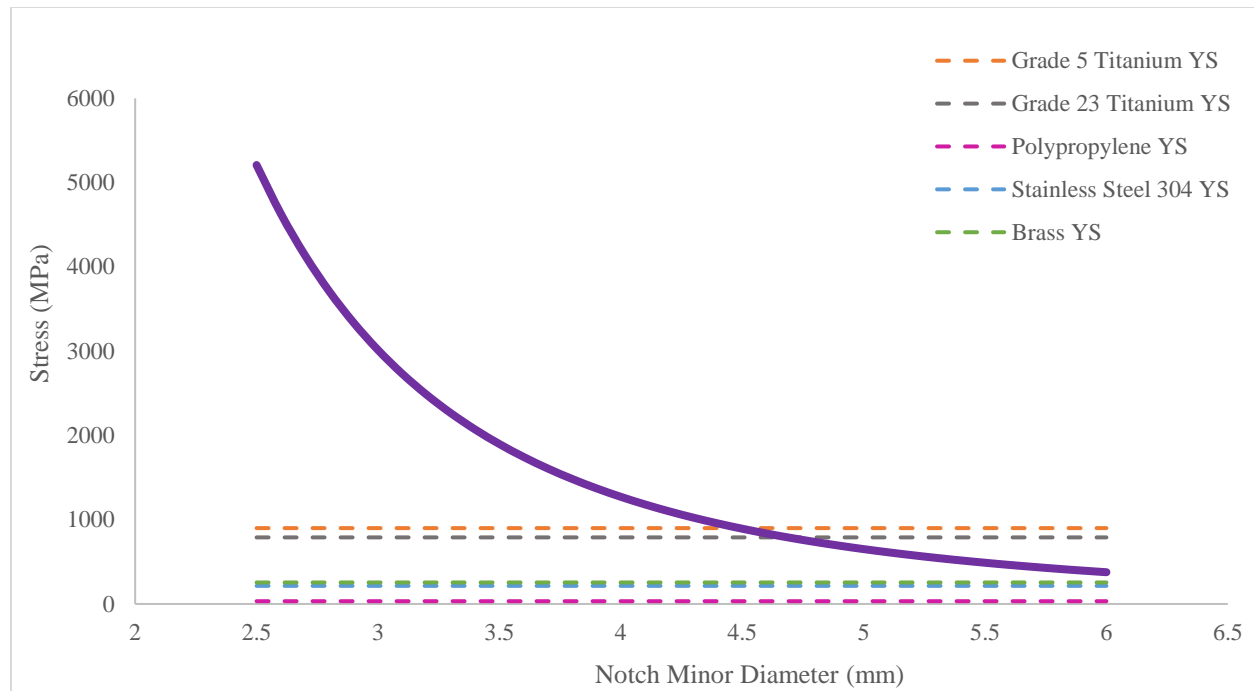


Figure 44. Stress (MPa) at the notched region of a shear bolt as a function of the minor diameter (mm) of the notch (solid curve) as a result of a bending load of 432N. Yield strength of various materials added to aid comparison (dotted lines).

Examination of **Figure 44** reveals that a polypropylene bolt would yield under the applied daily activity bending force of 432N, making it unfit for the proposed application. Analysis of the trends observed in **Figure 44** indicates that the titanium materials provide the greatest flexibility in terms of bolt geometry due to their strength. A material with a smaller yield strength, such as polypropylene, would limit the bolt to a smaller range of notch geometries. Not only did titanium allow for more freedom of design, but it was commercially available in various sized bolts. Therefore, grade 5 titanium was chosen as the first material to model and experimentally test.

In order to determine the approximate bolt/notch geometry required to provide bolt failure under the desired critical applied load, it was necessary to perform a ranging study by varying the distance under the head of the bolt to the notch (termed length), and the residual diameter of the

bolt within the notch (minor diameter). The ranging study was performed manually for lengths of 8 to 21mm and minor diameters of 4 to 7.9mm. **Figure 45** presents the resultant data as a plot of stress at the notch as a function of notch minor diameter as a result of an applied bending peak falling force of 1780N (see Section 3.5). Individual curves at 1mm increments of distance of the notch from the bottom of the bolt head are presented. Grade 5 titanium's ultimate tensile strength was also plotted as a reference value to understand when certain notch geometries may fail, that is, as the stress at the notch reaches the ultimate tensile strength of the material. Ultimate tensile strength was implemented as a reference value to understand if the tested geometries would sufficiently fail under the applied peak falling force of 1780N.

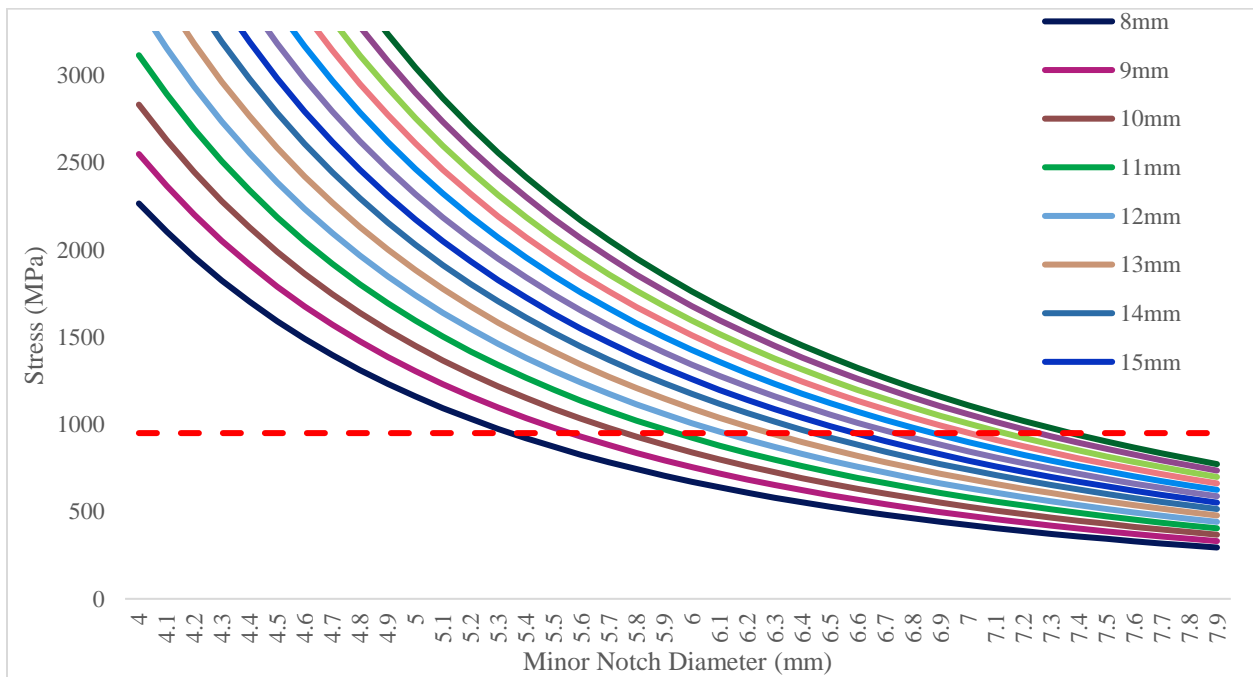


Figure 45. Resultant stress (MPa) at the notch under an applied bending force of 1780N as a function of notch minor diameter (mm) over a range of 8 to 21mm length and 4 to 7.9mm minor diameter, plotted as individual curves at 1mm increments of distance of the notch from the

bottom of the bolt head are presented (solid lines). Grade 5 titanium ultimate tensile strength to aid comparison (red dotted line).

Two major trends are apparent from investigation of **Figure 45**. First, as the notch's distance from the bolt head increases, the calculated stress increases. Second, as the minor diameter of the notch decreases, the calculated stress increases. One main conclusion from the plot is that both the minor diameter and the notch location may be varied to control the applied force at which a given bolt fails.

Figure 44 provides a minimum notch minor diameter due to its display of which materials of construction were able to resist deformation under the applied daily activity bending force of 432N. **Figure 45** provides a maximum notch minor diameter due to its display of which materials of construction sufficiently failed under the applied bending force of 1780N. As a result, an overall approximate minor diameter range of 4.5 to 7.4 mm was determined to model and test for a titanium bolt. An important note is that the experimental tests were not limited to the mentioned minor diameter range, the predictions above were employed only to set initial experimental testing geometries.

To understand the behavior of various modified bolts under torsional forces, it was necessary to perform a ranging study of manual calculations by varying the notch minor diameter and applying a torsion moment of 102 Nm (refer to Section 3.5 above). The ranging study was performed manually over a range of 5 to 5.7mm notch minor diameter due to the arbitrary range initially chosen for bolt modification. **Figure 46** presents the resultant data as a plot of stress at the notch as a function of notch minor diameter as a result of an applied torque moment of 102Nm (see Section 3.5). Grade 5 titanium's von Mises yield strength is also plotted as a reference value to

understand when certain notch geometries may yield, that is, as the stress at the notch reaches the von Mises yield strength.

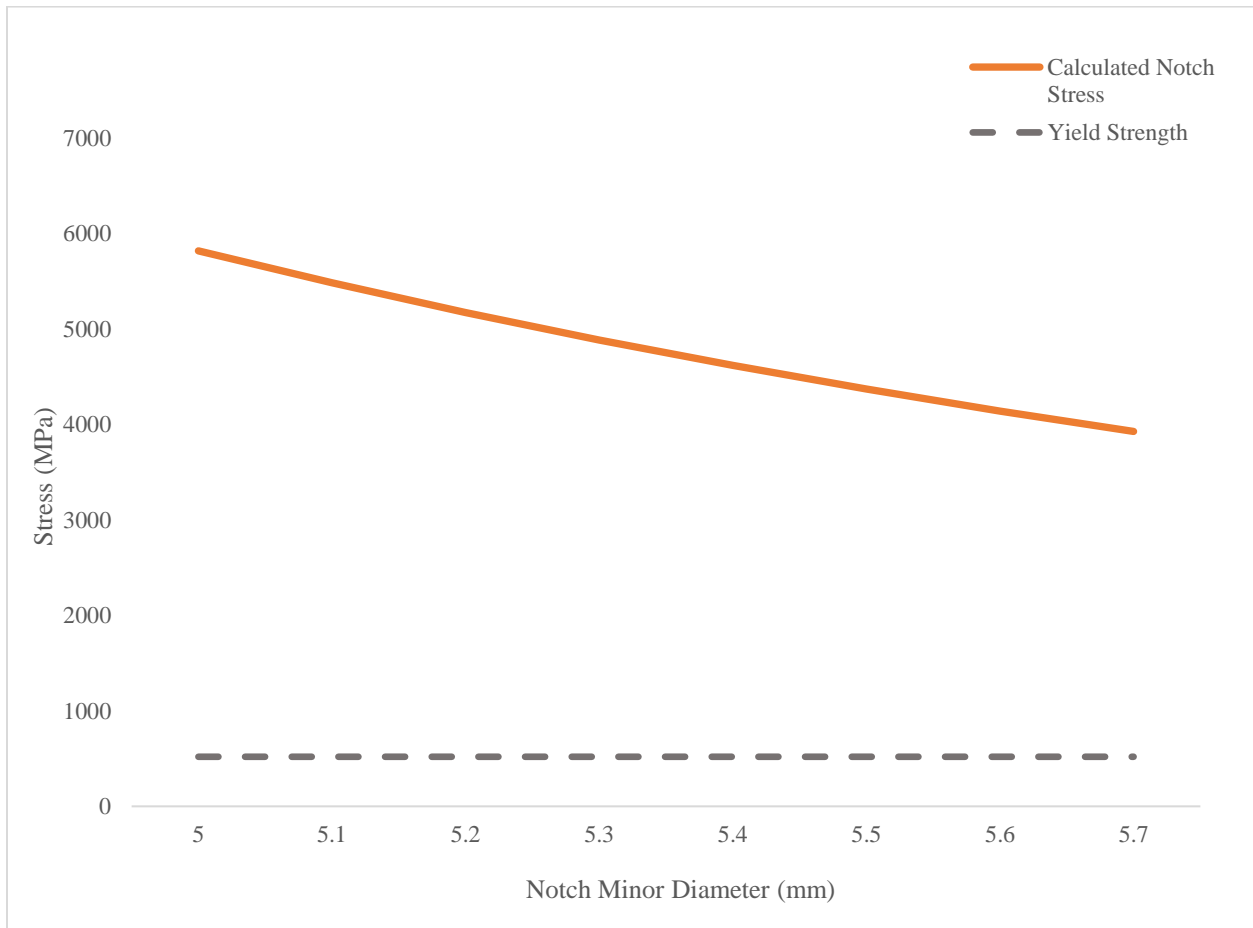


Figure 46. Resultant stress (MPa) at the notch as a function of the notch minor diameter (mm) over a range of 5-5.7mm (solid orange line) as a result of an applied torque moment of 102Nm. Yield strength to aid comparison (dotted gray line).

Analysis of **Figure 46** indicates that failure of bolts with minor diameters ranging from 5-5.7mm minor diameter will occur under less torque moment than the 102Nm employed in the manual calculations. Additionally, a trend is apparent, as the resultant stress decreases as the notch minor diameter increases, likely due to the fact that the larger minor diameters are closer in diameter to the bolt major diameter, ultimately decreasing the effects of the notch acting as a stress riser. The

results show that failure as a result of an applied torque moment of bolts ranging in minor diameters 5-5.7mm will presumably fail, and therefore would all be suitable for experimental testing.

3.7 FEA Modeling Material Property Setup

For the reasons articulated above, grade 5 titanium was chosen as an initial material for experimental testing hence the material properties set in Abaqus were those of titanium. **Table 11** presents the density, Young’s modulus and Poisson’s ratio values employed in the FEA model.

Table 11. Input Titanium Material Properties in Abaqus.

Property	Input Value	Units
Density	4.43 x 10 ⁻⁹	tonne/mm ³
Young’s modulus	110000	MPa
Poisson’s ratio	0.34	-

To simulate plastic deformation, a linear strain-hardening model was employed for the present work (see Section 2.2.2 for additional detail). Ziaja investigated strain-hardening of Ti6Al4V and reported its respective experimental stress-strain curve.¹⁰⁰ The study’s reported initial yield strength and hardening modulus values were implemented, rather than the reported material properties in Section 3.2, into **Equation 3** to solve for yield stress at an arbitrary strain of 2% (typically minimal differences in strain observed beyond 2%). Parameters for **Equation 3** are described in **Table 12**. The values were input as the linear strain-hardening parameters in Abaqus (**Table 13**). Any strain values from 0 to 2% strain were interpolated linearly by Abaqus.

$$S_y = S_{y0} + E_h \epsilon_p$$

Equation 3. Linear strain-hardening model function.

Table 12. Linear Strain-Hardening Parameters.

Parameter	Description	Units
S_y	Yield stress at a given strain	MPa
S_{y^0}	Initial material yield stress	MPa
E_h	Hardening modulus	MPa
ϵ_p	Plastic strain	%

Table 13. Input Values for Abaqus Linear Strain-Hardening Parameters.

Yield Stress (MPa)	Plastic Strain
800	0
825	0.02

4 DETERMINATION OF THE EFFECT OF BOLT GEOMETRY ON FAILURE FORCES UNDER APPLICATION OF A BENDING FORCE

4.1 Introduction

While manual calculations and FEA predictions aim to estimate behaviors of bolts modified to have a notched region, limited studies have been executed on notched bolt geometries made from the proposed materials for the proposed use. Manual calculations and FEA provided an initial range of notch geometries to test bending force on the bolts to understand the effect of various parameters on the stresses at failure which would enable tuning of the bolt geometry to specific failure forces (as specified by the “dangerous” forces determined in excess of daily activities). Experimental bending tests were executed via two different methods to analyze how varying bolt parameters such as material of construction, notch minor diameter, notch location, and notch width affected the bolts’ behavior.

4.2 Materials and Methods

As presented in Section 2.2.3.1, an Instron 8872 machine at the University of Maine Advanced Structures and Composites Center was employed in conjunction with a custom fixture designed to hold the bolt in place while force was applied to the bolt head via a loading nose. The bolts were fully threaded 22mm into the fixture prior to the application of force. An unmodified titanium bolt was used to test the method before any modified bolts were employed. The fixture was observed to yield before the bolt. When a modified titanium bolt was tested, the same observation was documented regarding the fixture. For both experiments, no yielding or damage of the bolts was observed. In addition, it was noted that the loading nose moved along the bolt head towards the shaft and notched region during the testing. Due to the observed yielding of the

fixture as a result of the applied load, and the movement of the loading nose during testing, the initial bending test method was deemed inadequate for the present work. The variability and lack of control in the experimental method led to the conclusion that a new method must be explored and developed for future bending tests.

Consequently, an alternate test method as described in Section 2.2.3.1 was employed at the University of Maine Advanced Manufacturing Center to address the previous failed method. The experimental setup comprised an MTS 810 servo-hydraulic actuator with a 22kip load cell, a custom steel fixture to hold the bolts, a braided cable made of galvanized steel, and a shackle attached to the cable which could be placed around the bolt shaft. Force was applied vertically through pulling the cable in an upward direction. Experimental data were produced in the form of load, displacement, and time in a spreadsheet format for analysis. The alternate bending test method was proven to be successful and suitable for the present testing needs. Specifically, the shackle and cable effectively applied force on the bolt in a vertical direction by pulling upwards on the shaft of the bolt, while the bolt remained threaded into a fixture. A more robust fixture with improved fastening methods prevented the fixture from yielding throughout the testing. The shackle and cable of the MTS 810 servo-hydraulic controlled the load application better than the loading nose employed with the Instron 8872, as they did not have as much freedom to move throughout the tests.

Grade 5 titanium and high strength class 10-9 stainless steel M8 partially threaded bolts, obtained from McMaster-Carr, were employed for the bending tests. The bolts were manually modified with a lathe to have notches that varied in location on the shaft under the head of the bolt (length), minor diameter, and width. Radii were also added to a majority of the notches. **Table 14** presents the dimensions of the manually modified titanium bolts, while **Table 15** presents the

dimensions of the modified stainless steel bolts. For bolts produced in quantities of 2 or more, the bolts were named alphabetically based on their geometry, followed by a number representing the numerical identity within the specified sequence of a given geometry. For example, bolt A was produced in a quantity of two. Therefore, its respective group of bolts were named A1 and A2. The only outliers were the first two modified bolts, 1A and 1B, which did not follow the same alphabetical naming convention.

Table 14. Bending Test Titanium Bolt Geometries.

Bolt	Length (mm)	Minor Diameter (mm)	Notch Width (mm)	QTY	Radius on Notch Edges (mm)
1A	8.7	5	2	1	N/A
1B	8.7	5	2	1	N/A
A	11	4	5	2	2
B	8.7	4	5	2	2
C	11.5	4	5	2	2
D	12	4	5	2	2
E	12	2	5	2	2
F	12	3	5	2	2
G	12	4	5	2	2
H	11	3	6	2	2
I	10	3	7	2	2
J	9	3	8	2	2

Table 15. Bending Test Stainless Steel Bolt Geometries.

Bolt	Length (mm)	Notch Minor Diameter (mm)	Notch Width (mm)	Quantity	Radius on Notch Edges (mm)
L	6	2	5	3	2
M	6	3	5	3	2
N	6	4	5	3	2
O	6	5	5	3	2
P	5	3	6	3	2

Table 15 Continued.

Q	4	3	7	3	2
R	3	3	8	3	2

Figure 47 presents a general diagram of a modified bolt, the labeled dimensions of which will be referenced throughout the following chapters. As per the initial manual calculations, and the FEA predictions, all of the modified bolts were expected to fail at the notched region prior to any yielding at the threads.

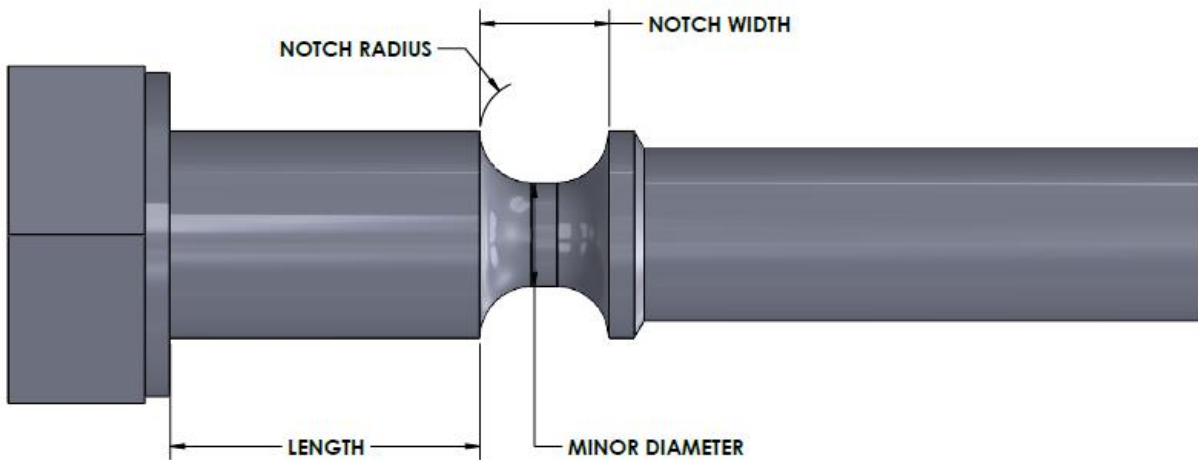


Figure 47. General modified bolt (threads not depicted).

4.3 Results and Discussions

The MTS 810 servo hydraulic system successfully applied force to all of the modified bolts for bending tests via the cable and shackle without any observed yielding of the custom fixture. Initially, an unmodified titanium bolt and an unmodified stainless-steel bolt were tested to ensure the overall system was working as expected. The titanium bolt fractured at its threads, whereas the stainless steel bolt yielded and bent at its threads (**Figure 48**). The unmodified titanium bolt failed

at 3905 N, whereas the unmodified steel bolt reached an onset of deformation under forces in the region of 7430 N. The results confirmed the expectation that the steel bolts would have much higher strength thresholds than the titanium bolts.



Figure 48. Unmodified steel bolt (left) and unmodified titanium bolt (right) after testing.

Bolts 1A and 1B were tested via the MTS method and both sheared at their threads rather than their respective notched region (**Figure 49**). **Figure 50** presents displacement versus force results of all bolts 1A and 1B.



Figure 49. Bolt 1A (left) and Bolt 1B (right) after testing (both titanium bolts).

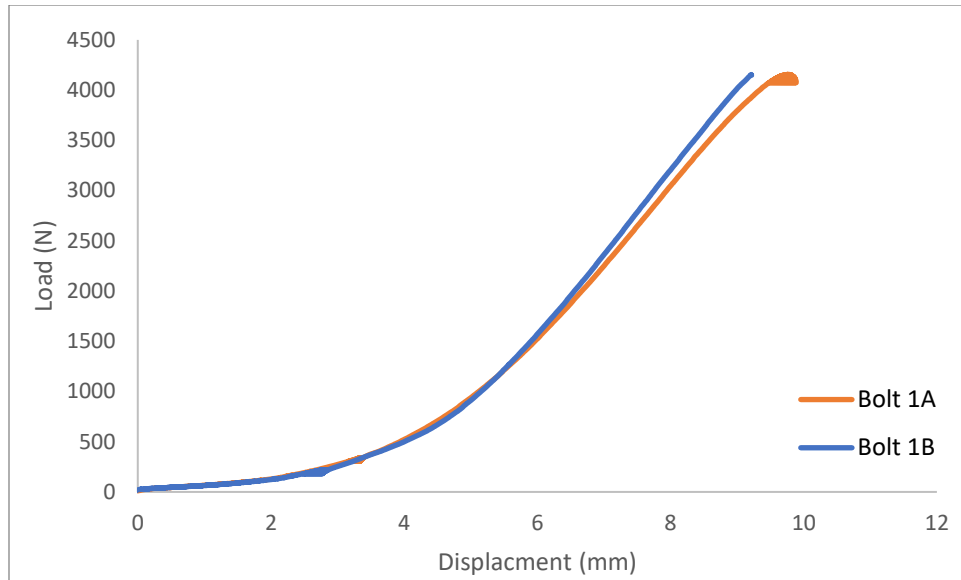


Figure 50. Plot of displacement (mm) versus load (N) of titanium bolts 1A and 1B.

Figure 50 reveals that bolt 1A fractured at 4153.4 N and bolt 1B fractured at 4153.2 N. The failure of bolts 1A and 1B occurred less than 0.2 N apart from each other, indicating excellent reproducibility. Bolt 1A and 1B's recorded displacement values at the time of failure were also similar. The unmodified steel bolt withstood more force than all of the titanium bolts tested, which was expected given its reported ultimate tensile strength value of 1034 MPa, whereas McMaster-Carr reports the titanium bolt's ultimate tensile strength to be 896 MPa. The two modified titanium bolts withstood marginally greater force than the titanium unmodified bolt, although all bolts failed at the threads. The fact that the modified bolts did not fail at the notch, as intended, and as predicted by the manual calculations and FEA, but rather at the threads may have occurred for several reasons. The notch width could have been too small, minimizing the volume of material acting as a stress riser. The location of the notch could have been too close to the location of load application, resulting in too small of an applied moment. Finally, the notch minor diameter could have been too large, resulting in too little stress concentration at the notch. All of the above possibilities were explored further to understand and analyze trends and behaviors of the modified bolts.

Figure 51 presents a plot of the stress versus applied force of the tested modified bolts. It is evident that the failure point of the notched titanium bolts occurred at much greater applied force and stress than was predicted by either manual calculations or the FEA model.

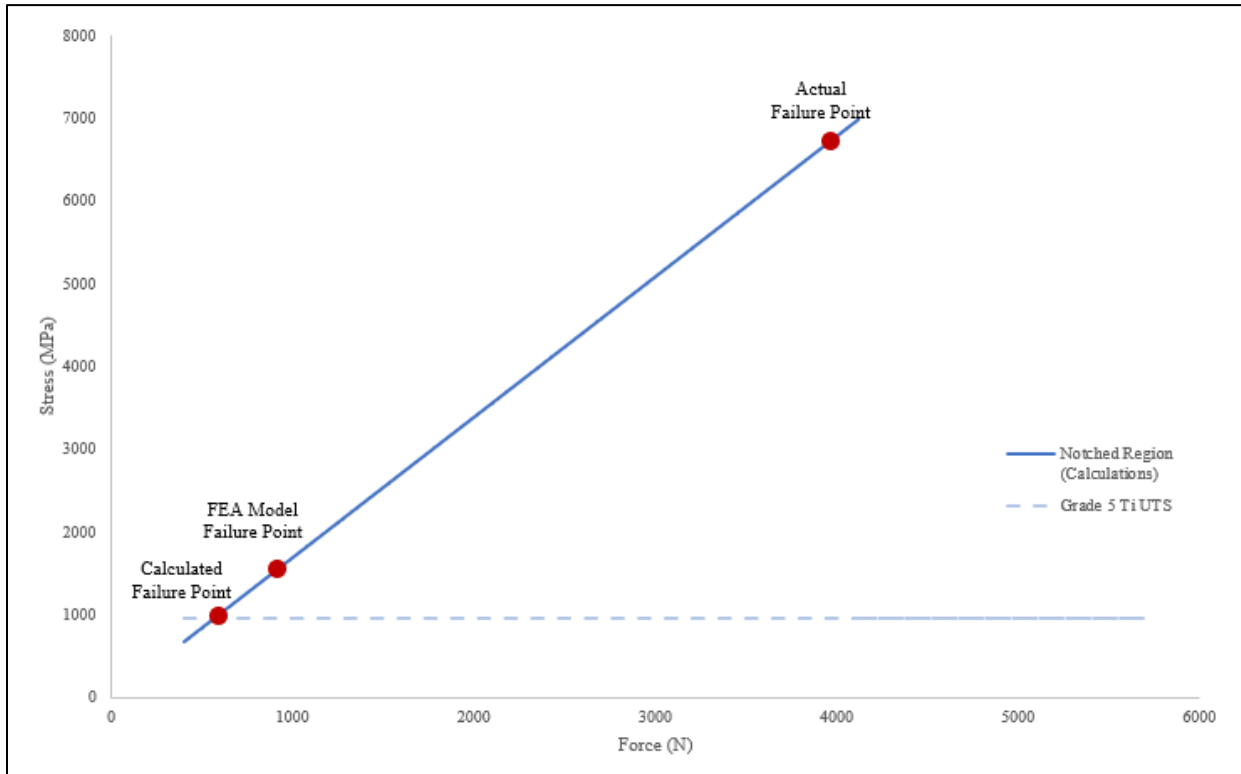


Figure 51. Plot of stress (MPa) versus applied force (N). Manually calculated, FEA modeled, and experimental failure points of the modified titanium bolt geometry are labeled for comparison.

Several factors may contribute to the variation between predicted and applied forces and actual stress values at failure. Specifically, the geometry of the test setup itself varied throughout the experiment as the shackle position on the bolt shaft, and its relative angle, were observed to shift. Critically, it is noted that for the experimental stress and strain values to be accurate, a strain gauge would need to be implemented, which would be costly and beyond the scope and resources available for the present study. To summarize, the measured force at which caused failure of the

bolt is likely accurate, but the calculated stress depicted in **Figure 51** is likely inaccurate due to a variety of reasons such as the experimental setup. Rather than analyzing stress, a more meaningful analysis in future test phases would be to analyze applied load versus displacement of the bolt.

In order to address the fact that the modified bolts did not fail at the notch, but rather at the threads, several modifications were made to the bolt geometries. Specifically, the notch width was increased, the notch location was moved closer to the threads, and the notch minor diameter was decreased. Addition of a radius to each side of the notches was also proposed in an attempt to ensure uniformity at the edges of the notch when machining and encourage stress concentration towards the center of the notch, rather than at the edges. The specifics of the modified bolt geometries are provided, as bolts A-D in **Table 14**.

It is noted that notch width was increased to 5mm from 2mm on all bolts and the notch minor diameter of the new bolts was decreased to 4mm from a previous range of 5.1-5.4mm. Based on the principle of a moment, it was expected that a notch location closer to the threads would fail under smaller forces than a notch further away (i.e., closer to the head of bolt), as such the notch location was moved from 8.7mm below the head of the bolt up to 12mm below the head of the bolt. Radii of 2mm were also added to the corners of the notches. An important note is that bolts B1 and B2 only had one radius on their notch, on the corner closest to the threads. All six other bolts had radii on each edge of their notch.

Experimental testing of bolts A-D revealed that bolts B1 and B2 failed at the threads, whereas bolts A1, A2, C1, C2, D1, and D2 failed in the notch region. **Figure 52** presents an image of a bolt (attached to the test fixture) that had sheared at its notch. **Table 16** presents the peak forces at which the bolts failed, and their respective location of failure. **Figure 53** presents a plot of force versus displacement of bolts A1, C1, and D1.



Figure 52. An example of a bolt that sheared at its notch region.

Table 16. Peak Forces and Locations at Which Bolts A-D Failed.

Bolt	Peak Force (N)	Average Peak Force (N)	Region of Failure
A1	4978	4508.5	Notch
A2	4039		Notch
B1	3833	4093	Threads
B2	4353		Threads
C1	3937	3954.5	Notch
C2	3972		Notch
D1	3906	3678	Notch
D2	3450		Notch

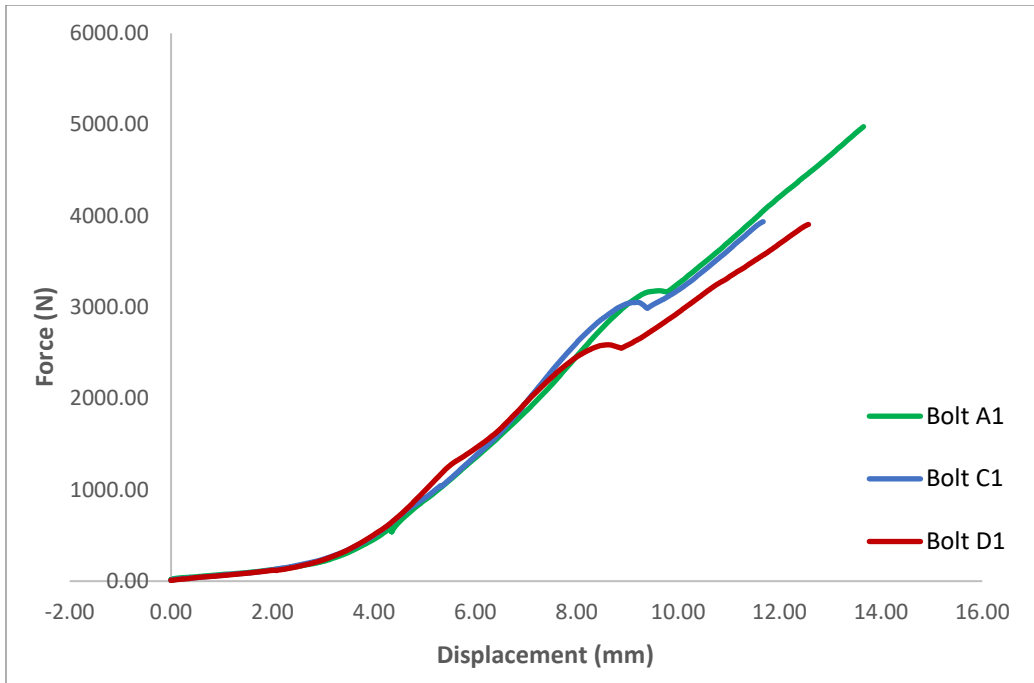


Figure 53. Plot of displacement (mm) versus force (N) of bolts A1 (green line), C1 (blue line), and D1 (red line). As seen in Table 15 above, the results were consistent among bolts of the same geometry for bolts A, C, and D. To maintain simplicity, only one of each bolt geometry is depicted.

Analysis of **Figure 53** shows a trend with the bolts that sheared at the notched region (Bolts A, C and D). The bolts with notches closest to the threads failed under the least amount of force, whereas the bolts with notches closest to the head of the bolt failed under the largest amount of force. That is, the larger the length value (i.e., the closer to the threads), the greater the force required for the bolt to shear. The observed trend agrees with basic moment principle: that is, as length increases from the applied load to the notch, the moment increases and a smaller load is required to cause failure.

Though the MTS method successfully applied force, caused failure amongst all tested bolts, and the data followed the expected trend in terms of the effect of moment, some concerns

were noted during testing. Specifically, plastic yielding of the bolts was observed for an extended period prior to failure. An example of plastic yielding visibly apparent in a bolt is shown below in **Figure 54**. As seen in **Figure 53**, the load-displacement slope is relatively small (less steep) and shows a large amount of displacement under the applied load prior to fracture. A potential contribution to the initial increase in displacement and gradual slope observed in the plotted results is the elongation of the cable. The slopes of the linear elastic region (initial region) in the experimental plots are not as large as expected or in comparison to the FEA predictions, which could possibly be a result of stretching of the braided cable throughout the experiments. Additionally, the onset of the linear region of the plots were delayed. It is hypothesized that the cable may have had initial slack to eliminate, which would result in a delay in the onset of the linear region of the force-displacement plots, and could have stretched throughout the tests, which would decrease the apparent slope of the linear elastic region of the plot. Both possibilities would significantly affect the experimental results and therefore required investigation.



Figure 54. Display of plastic yielding in bolt during testing.

While some yielding is expected due to the nature of the bolt material employed (titanium), other experimental factors may have contributed. Additional factors that must be considered are

related to the overall test method, and include slack uptake in the cable, movement of the shackle along the shaft of the bolt, and movement of the fixture. Indeed, it was observed that as the plastic yielding occurred in the bolt, the shackle visibly shifted along the shaft of the bolt as the cable remained perpendicular to the base of the MTS throughout the tests. To avoid shackle movement, the force would have to be applied perpendicularly to the bolt consistently throughout the experimental runs. To do so, the cable would need to be connected to a loading head that had torsional movement as it applied force.

To understand the total elongation and initial slack of the cable present during the bending tests, a cable deflection test was performed in which load was applied directly to the base of the MTS setup via the braided cable without any bolt. It was intended that such data would provide a means of accounting for the effect of cable slack and elongation on force-displacement measurements of bolts. A load of 9200 N was gradually applied in a vertically by pulling in an upwards direction away from the base. The load, displacement, and time were recorded for analysis. **Figure 55** presents the resultant load-displacement curve for the cable test.

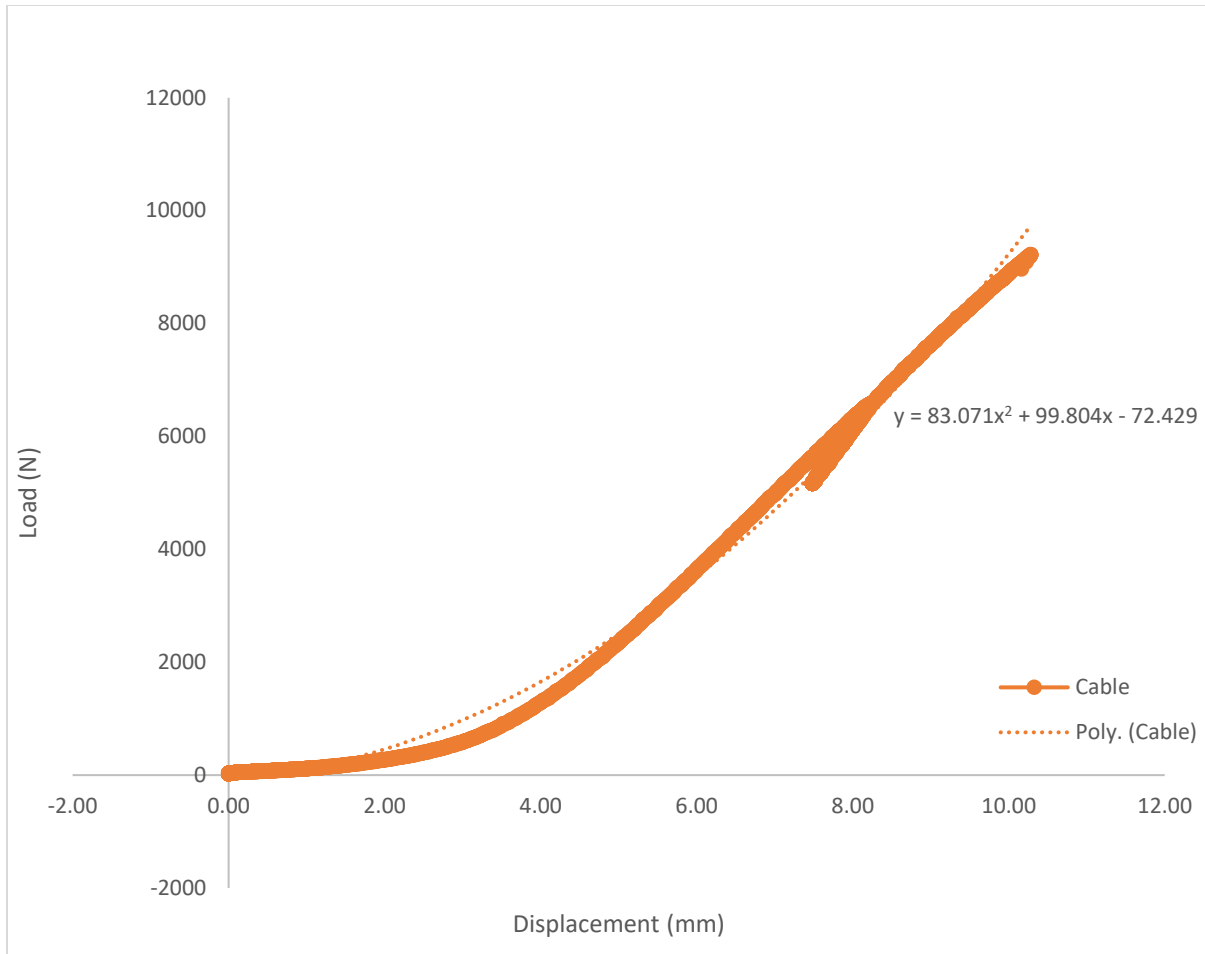


Figure 55. Resulting plot of the cable elongation and slack test displayed as displacement (mm) versus applied load (N) (solid line). Curve fit polynomial (dashed line).

Analysis of **Figure 55** indicates that the region from approximately 0 mm to 3 mm corresponds to a large amount of displacement as a result of a small, applied load. From approximately 4 mm to 10 mm however the slope increases greatly with an approximately linear dependence of displacement upon applied load observed. The region of large displacement resulting from a comparatively small applied force (i.e., from 0 mm to ~3 mm) is likely due to the elimination of slack in the cable. The linear response region (i.e., from ~4 mm to 10 mm), is presumably due to the large force applied to the taut cable and elongation in the cable.

In order to provide a means for subtracting the effect of cable slack uptake and elongation on experimental bolt data, a polynomial curve fit of the load-displacement curve of the cable results was performed to produce a formula, where x and y represent the displacement and load, respectively (see **Equation 4**). Though the curve fit is not ideal, it was deemed sufficient for its purpose and as a proof of concept. The polynomial formula enabled decent normalization of the experimental data via subtraction.

$$y = 83.071x^2 + 99.804x - 72.429$$

Equation 4. Curve fit polynomial formula representing the cable elongation data, where x and y correspond to the displacement and load, respectively.

In practice, **Equation 5** was employed by inputting a defined force value and producing a calculated cable displacement value. The resultant cable displacement was then subtracted from the experimental displacement values to produce a value that represents the bolt displacement for any given experiment considering cable slack and elongation. **Figure 56** presents an example of a data set plotted before and after the cable adjustment procedure was performed. The difference in slopes between the initial plot and adjusted plot indicated there may have been presence of cable elongation in the experimental tests.

$$x = \frac{-99804 + \sqrt{99804^2 - 332284(-72429 - 1000y)}}{166142}$$

Equation 5. Rearranged curve fit polynomial formula representing the cable elongation data.

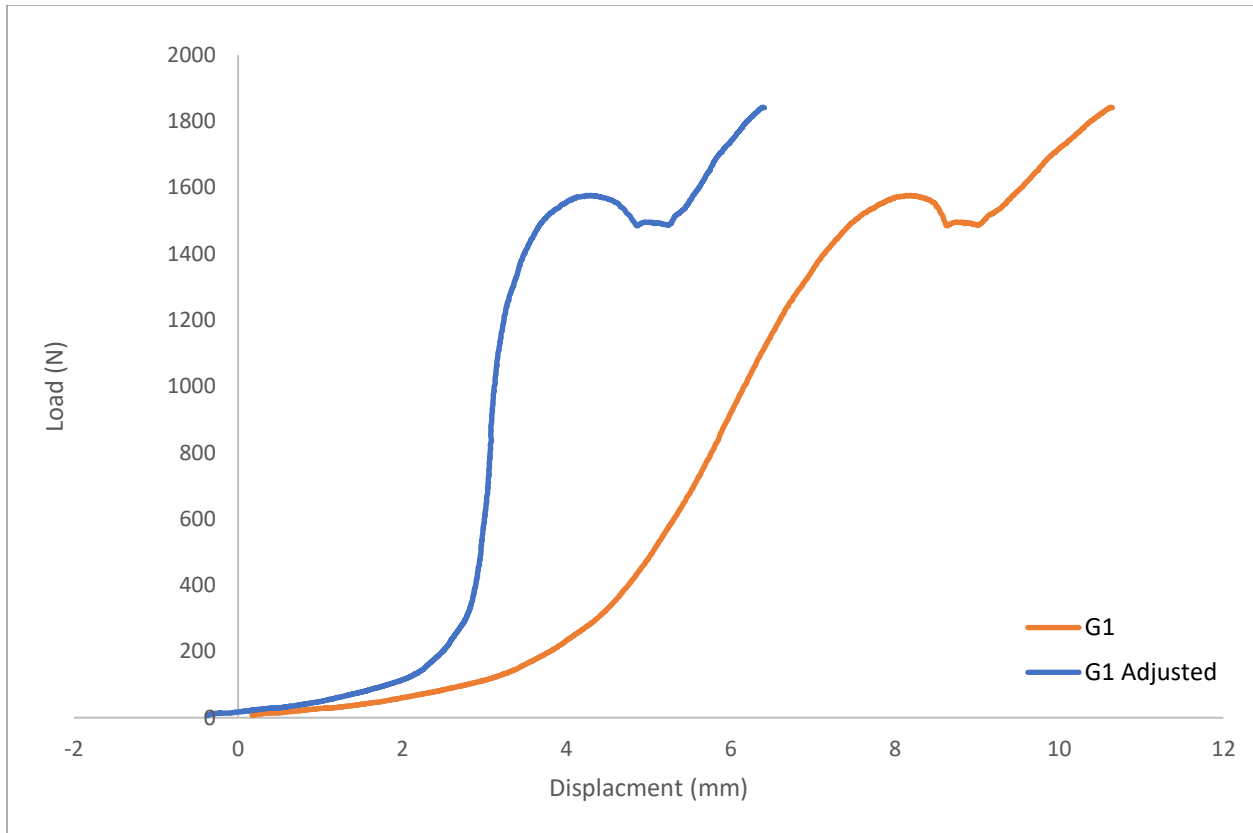


Figure 56. An example plot of displacement (mm) versus load (N) before and after cable displacement adjustment. G1 raw experimental data (orange line) versus Bolt G1 data with cable slack and elongation data subtracted (blue line).

The cable extension experiment and a subsequent analysis allowed for a more accurate representation of the bolt data. By subtracting the cable extension values from the experimental data, the force at fracture and displacement at fracture were more accurately evaluated.

The experimental applied forces required to fracture the bolts were too high for use as a prosthetic shear bolt, and as such geometric changes to the bolt were necessary. Specifically, the next phase of tests investigated a decreased notch minor diameter and separately, an increased notch width, both of which were predicted to decrease the required applied force to induce bolt fracture. To this end, bolts E, F, and G were machined to analyze the effect of varied notch minor diameter (2mm,

3mm, and 4mm, respectively), while bolts F, H, I, and J were designed to analyze the effect of varied notch width (5mm, 6mm, 7mm, and 8mm, respectively). When the notch minor diameter was varied, the location and notch width were kept consistent. Similarly, when the notch width was varied, the location and notch minor diameter were maintained as fixed parameters. All notches were placed as close to the threads as feasible, while leaving 1 mm of space between the end of the notch and the start of the threads. The experimental results were adjusted based on the cable elongation test, outlined above, to better represent the bolt displacement versus applied load curves.

The MTS method was successfully employed to apply force to all twelve titanium modified bolts until fracture occurred. The results were consistent among bolts of the same geometry. It is not simple to average the load-displacement plots due to the potential for varying force and time stamps across several experimental data sets, so only one data set of each bolt geometry is depicted in the presented plots and tables. All the bolts failed at their notched regions. **Figure 57** presents plots for displacement versus load for bolts tested to analyze notch width, that is F, I, H, and J. Force values at fracture are reported in **Table 17**.

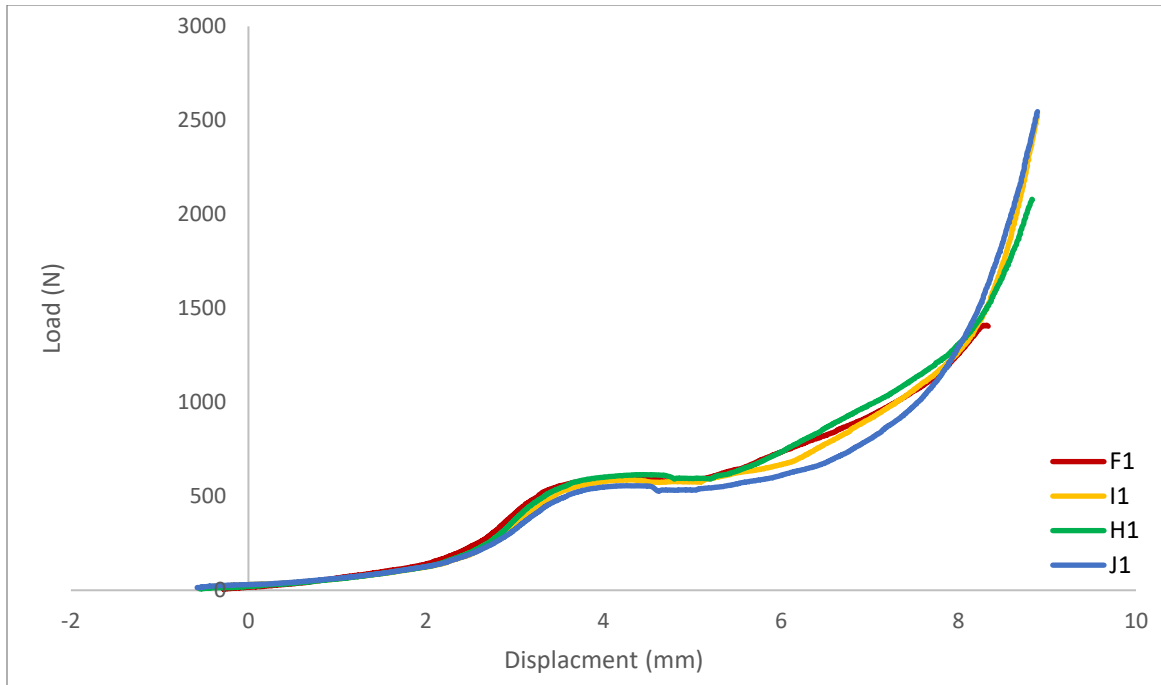


Figure 57. Plot of displacement versus load for bolts F1, I1, H1, and J1. F1 (notch width of 5mm) shown in red, H1 (notch width of 6mm) shown in green, I1 (notch width of 7mm) shown in yellow, and J1 (notch width of 8mm) shown in blue.

Examination of **Figure 57** reveals that all four bolts fractured at a comparable displacement (only a difference of 0.67mm), and that the force at fracture increased monotonically with notch width. It is hypothesized that the increase in fracture force with notch width may be attributed to the material’s plasticity, as a larger notch volume correlated to a larger elastic region.

Table 17. Reported Failure Force Values for Bolts F1, H1, I1, and J1 and Their Respective Averages.

Bolt	Notch Width (mm)	Failure Force (N)	Average Failure Force (N)
F1	5	1404	1492

Table 17 Continued.

F2	5	1580	
H1	6	2070	2026
H2	6	1982	
I1	7	2470	2569
I2	7	2668	
J1	8	2544	2962
J2	8	3380	

Plots of displacement versus load as predicted by FEA for bolts F, H, I and J (varied notch widths of 5mm, 6mm, 7mm, and 8mm, respectively) were plotted below in **Figures 58, 59, 60, and 61.**

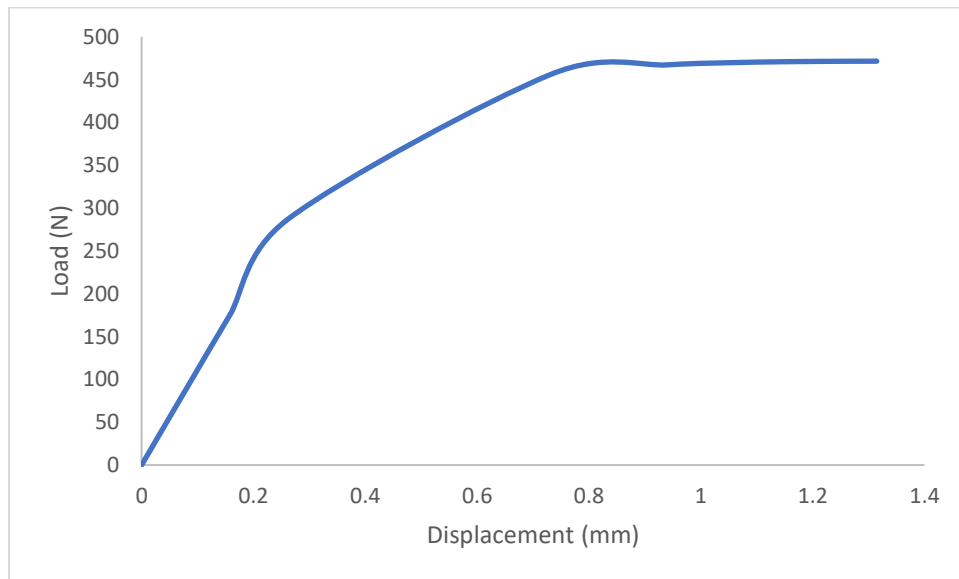


Figure 58. FEA plot of displacement (mm) versus load (N) for bolt F (notch width of 5mm).

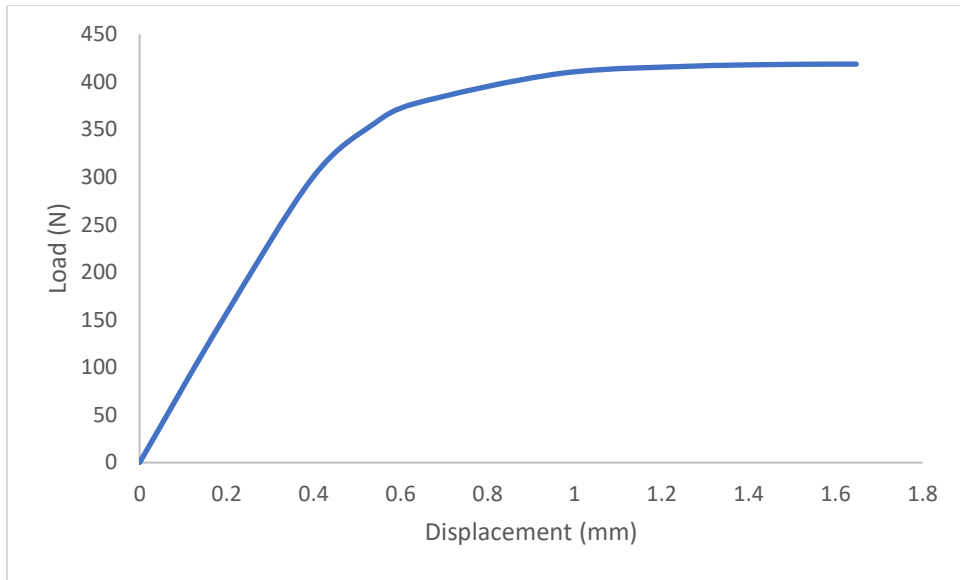


Figure 59. FEA plot of displacement (mm) versus load (N) for bolt H (notch width of 6mm).

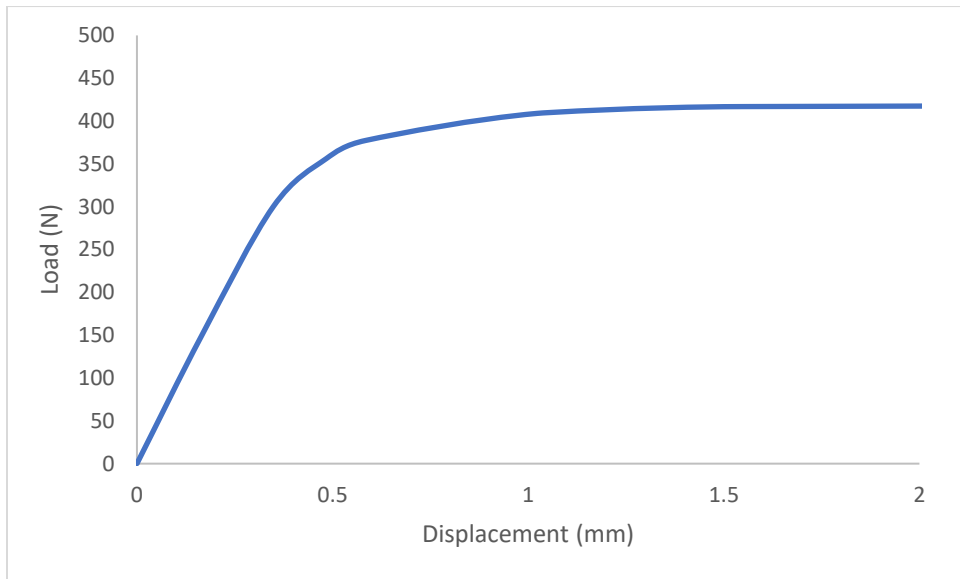


Figure 60. FEA plot of displacement (mm) versus load (N) for bolt I (notch width of 7mm).

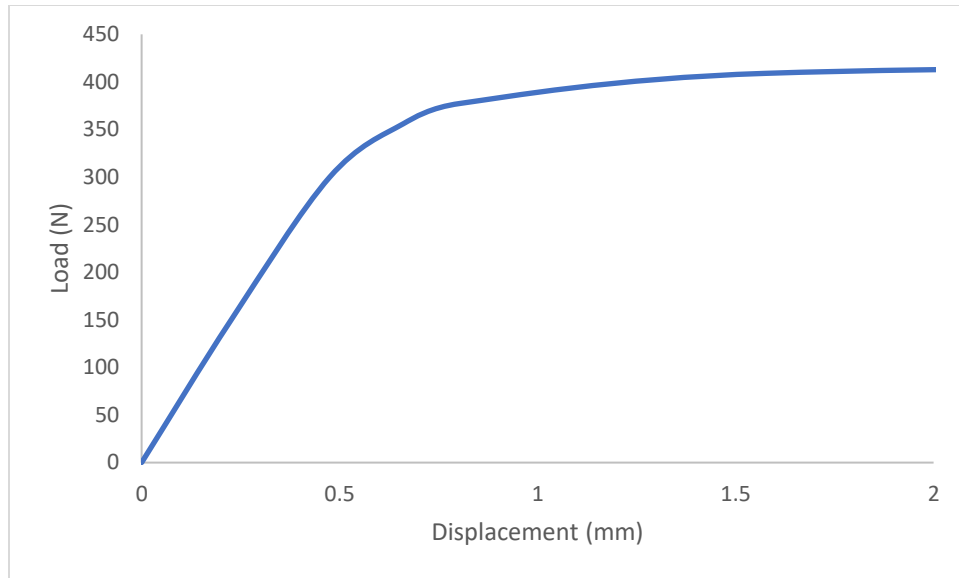


Figure 61. FEA plot of displacement (mm) versus load (N) for bolt J (notch width of 8mm).

Figures 58-61 do not present a definite trend comparative to their respective experimental results. However, there is a general trend observed across all figures, which entails a steep initial slope (representing the linear elastic region) and a switch to a more gradual slope once plastic yielding has begun. The near horizontal lines indicate a continuous plastic region, which will continue to deform/rotate as modeled with the linear-hardening model. **Figures 58 and 59** (bolts F and H, respectively) display incomplete FEA modeling due to the computation crashing. The model failure is exemplified by the difference in displacement shown in **Figures 60 and 61** (bolts I and J, respectively). A potential cause of analyses crashing could be due to excessive deformation of mesh elements near the notch. Further investigation would be necessary to resolve the issue for large deformations.

Figure 62 presents a plot of displacement versus load for the bolts E1, F1, and G1, that is, bolts with minor diameters of 2mm, 3mm, and 4mm, respectively. It is evident from examination of **Figure 62** that as the notch minor diameter increased the force at fracture showed no apparent

trend. The displacement at failure showed a consistently decreasing trend with increasing minor diameter. The experimental results were adjusted based on the cable test results to better represent the bolt displacement versus load. Force values for the tested bolts are recorded in **Table 18**.

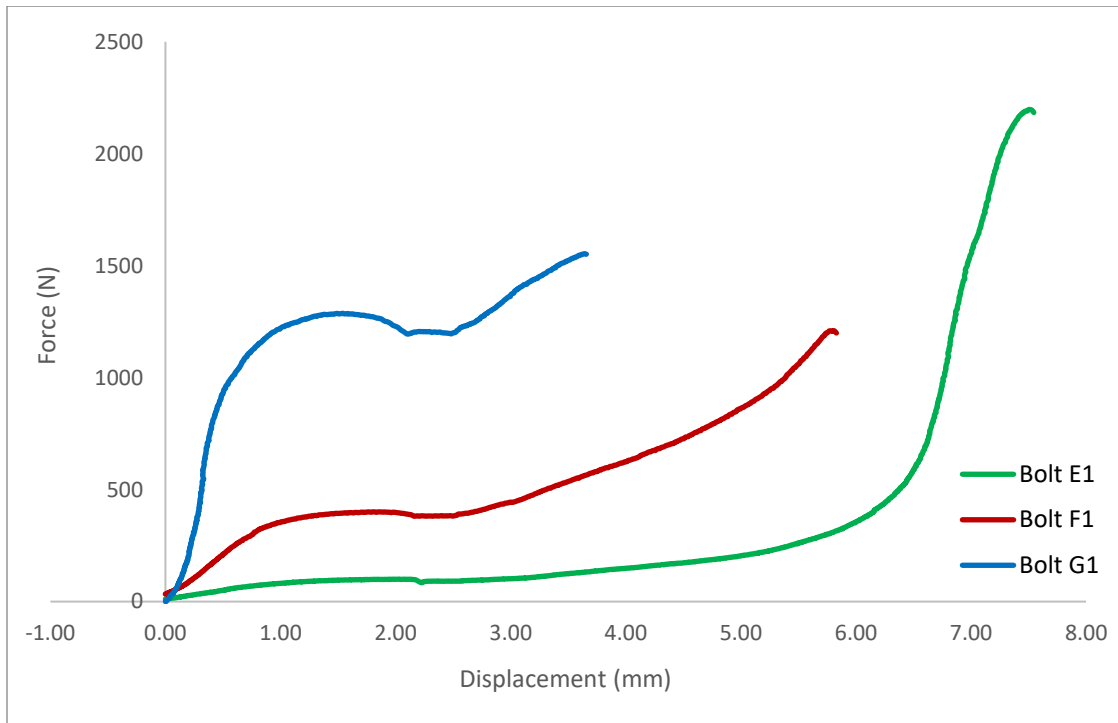


Figure 62. Plot of displacement (mm) versus force (N) for bolts E1, F1, and G1. E1 (minor diameter of 2mm) shown in green, F1 (minor diameter of 3mm) shown in red, and G1 (minor diameter of 4mm) shown in blue.

The lack of a definitive trend in force at fracture observed prevents ready interpretation of the data presented in **Figure 62**. The observed trend of decreasing displacement at failure with increasing notch diameter may suggest that the greater the residual material in the notch the less plasticity the bolt exhibits and hence the less displacement required to induce failure. Unfortunately, the added notch region may be allowing for more plastic yielding in the bolt than expected or wanted.

Table 18. Reported Failure Force Values for Bolts E1, F1, and G1 and Their Respective Averages.

Bolt	Minor Diameter (mm)	Failure Force (N)	Average Failure Force (N)
E1	2	2284	2267
E2		2250	
F1	3	1404	1492
F2		1580	
G1	4	1841	2253
G2		2665	

The FEA plots for bolts E and G and their respective experimental data (varied notch minor diameters of 2mm and 4mm, respectively) as a result of applied bending forces were plotted below in **Figures 63 and 64**. An FEA plot for bolt F (minor diameter of 3mm) is depicted above in **Figure 58**.

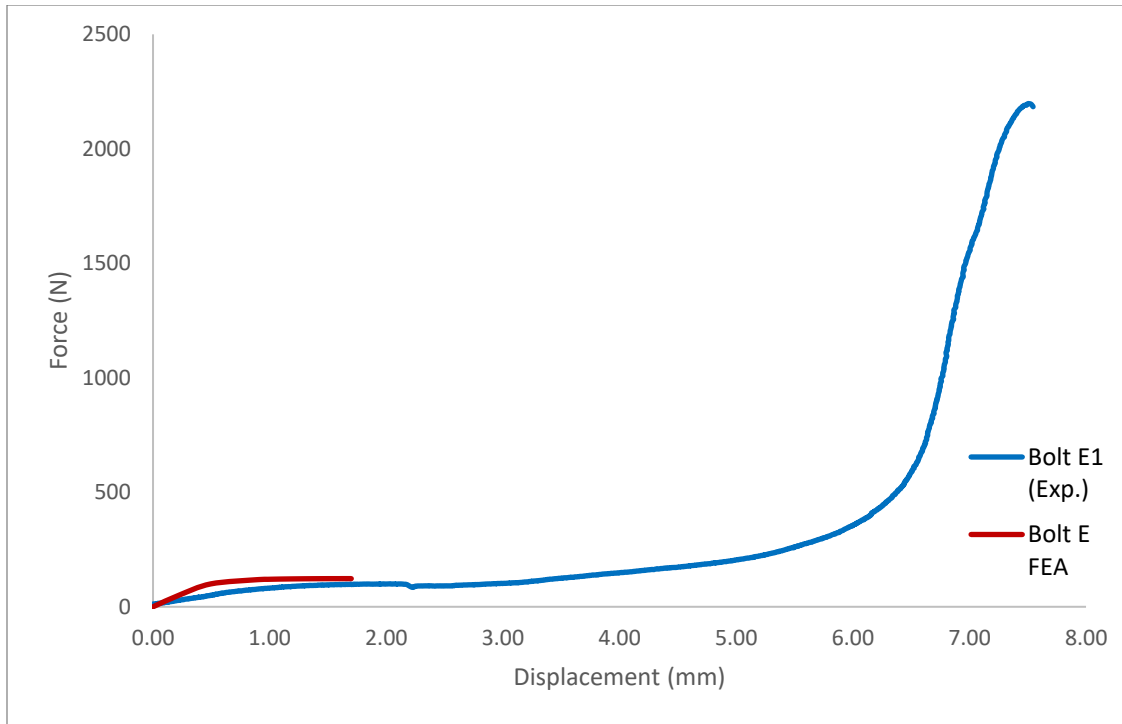


Figure 63. Plot of displacement (mm) versus load (N) as a result of bending force on bolt E (minor diameter of 2mm). Experimental data is shown in blue, whereas FEA data is shown in red.

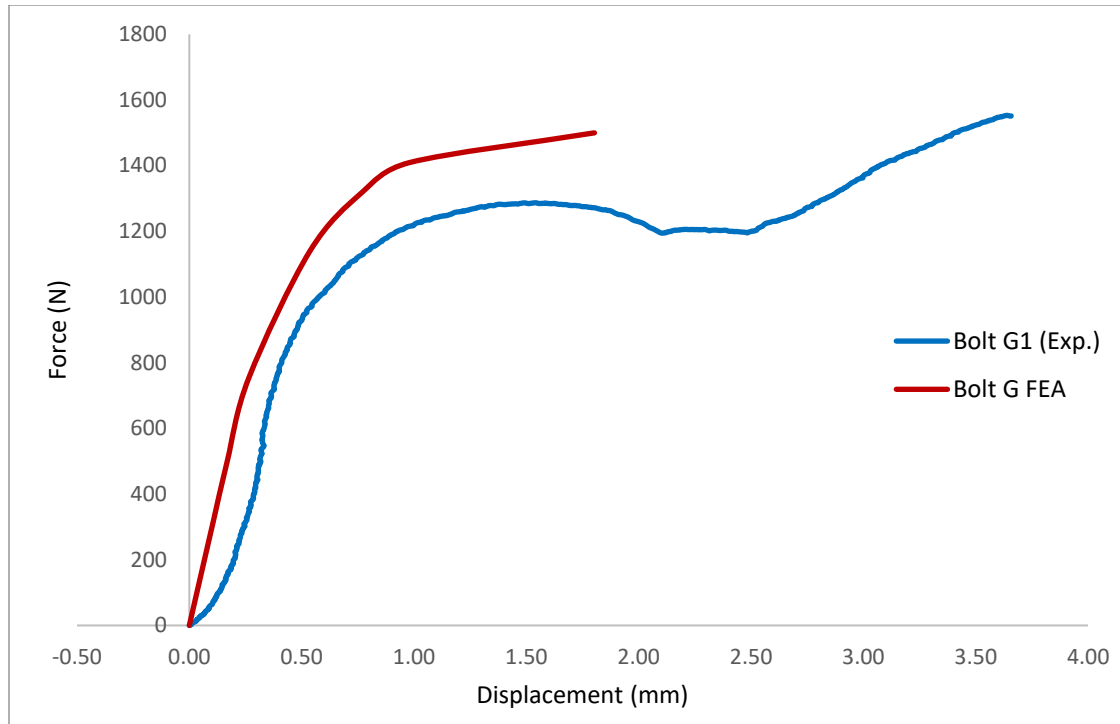


Figure 64. Plot of displacement (mm) versus load (N) as a result of bending force on bolt G (minor diameter of 4mm). Experimental data is shown in blue, whereas FEA data is shown in red.

Analysis of **Figures 63 and 64** shows that the FEA model appears to match the experimental force versus displacement curves very well up until the point at which the model predicts failure. A potential cause of failure in the model may be due to excessive deformation of mesh elements near the notch; further investigation would be required to resolve the issue. It is noted that the experimental data continues to displacement values of from, 3.5-6mm and forces of 2000N greater than the predicted failure point.

As noted above, the FEA model fit the experimental data very well at low applied forces/displacements but predicted fracture at much lower forces and displacements than observed experimentally. The MTS method had a variety of factors that were not as easily controlled as in

the FEA models, so it was expected that the two would not agree precisely. Additionally, the linear hardening model used for the FEA was not as accurate as a model such as Johnson-Cook. However, models such as Johnson-Cook are much more complex and difficult to control. For the purpose of the bolt testing, the linear hardening model was deemed to be sufficient.

Due to the amount of plasticity observed in the titanium bolt testing, a high strength steel with greater brittleness, based on its known material properties, was explored to determine the force at fracture and relative displacements in similar bolt geometries. Plasticity should be avoided in order to achieve a more immediate failure under controlled conditions. Though the ultimate tensile and yield strength values would be greater than titanium's, it was anticipated that a more brittle material may lead to fracture prior to excessive plastic yielding, which would be ideal for the bolt's purpose of quick release of a prosthetic device under controlled conditions. Consequently, bolts L, M, N, O, P, Q, and R were tested under bending loads employing the same MTS 810 servo hydraulic method as for the titanium bolts. The exact bolt dimensions are presented in **Table 19**. The experimental results were adjusted based on the cable test results to better represent the bolt displacement versus load data.

Table 19. Bending Test Stainless Steel Bolt Geometries.

Bolt	Length (mm)	Notch Minor Diameter (mm)	Notch Width (mm)	Quantity	Radius on Notch Edges (mm)
L	6	2	5	3	2
M	6	3	5	3	2
N	6	4	5	3	2
O	6	5	5	3	2
P	5	3	6	3	2
Q	4	3	7	3	2
R	3	3	8	3	2

Figure 65 presents the experimental results of bolts M, P, Q, and R (notch widths of 5mm, 6mm, 7mm, and 8mm, respectively). Bolts M, P, Q, and R had identical geometries to those of titanium bolts F-J in order to have an exact comparison of the impact on the force at fracture and the displacement of the two materials of construction. The data is corrected for cable slack and extension. **Table 20** presents the forces at fracture for bolts M, P, Q, and R, and their respective averages.

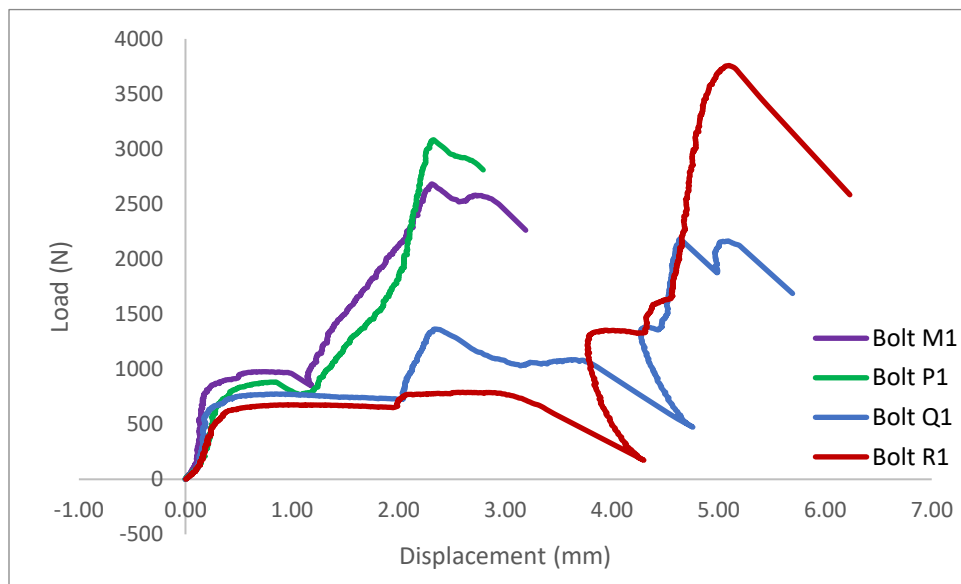


Figure 65. Plot of displacement (mm) versus load (N) for bolts M1, P1, Q1, and R1. M1 (notch width of 5mm) shown in purple, P1 (notch width of 6mm) shown in green, Q1 (notch width of 7mm) shown in blue, and R1 (notch width of 8mm) shown in red.

Table 20. High Strength Steel Results with Varied Notch Width.

Bolt	Notch Width (mm)	Failure Force (N)	Average Failure Force (N)
M1	5	2537	2703
M2		3029	
M3		2544	

Table 20 Continued.

P1	6	3104	2911
P2		3252	
P3		2376	
Q1	7	2016	2284
Q2		2014	
Q3		2823	
R1	8	2868	2682
R2		2891	
R3		2288	

Analysis of **Figure 65** indicates no clear trend in force at fracture or displacement as a function of notch width for the steel bolts, while there were trends apparent in the titanium studies employing bolts of the same geometries. Further studies would be necessary to confirm the presence or absence of trends as it relates to the notches material of construction and notch geometry.

It should be noted that for two of the steel bolt bending tests, specifically, Q1 and R3, the shackle shifted into the notch during testing. Small amounts of shackle movement had been documented in previous testing, but not to the extent of moving into the notched region. No definitive reasoning for the extreme movement can be given, however it is noted that the large amount of load applied compared to previous experimental runs may have been a factor. Additionally, it should be noted that the plotted results display backtracking of displacement, which could be due to the implementation of the cable data and the respective data adjustments or movement of the shackle throughout experimental testing.

Figure 66 displays the experimental results of bolts L, M, N, and O (minor diameters of 2mm, 3mm, 4mm, and 5mm, respectively). The purpose of the four modified bolts was to analyze

the effect of varied notch minor diameter on modified high strength steel bolts. Because the results were consistent among bolts of the same geometry and averaging the load-displacement curves is complex, only one of each bolt geometry is depicted in the figures below. Additionally, the bolts were purposely the exact same geometries as in the titanium modified bolt experimental tests for an accurate comparison of the two materials of construction. **Table 21** presents the forces at fracture for bolts L-O and their respective averages.

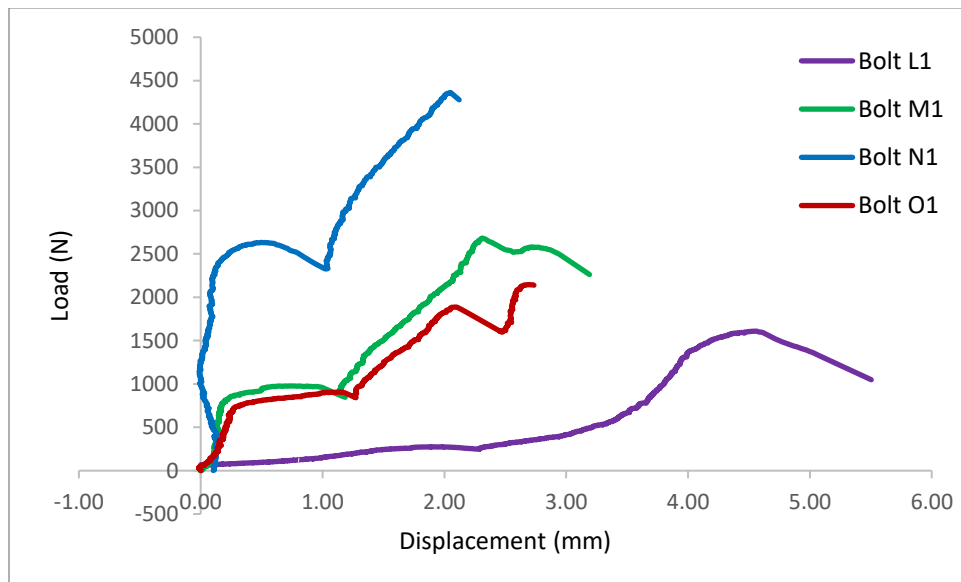


Figure 66. Plot of displacement (mm) versus load (N) for bolts L1, M1, N1, and O1. L1 (minor diameter of 2mm) shown in purple, M1 (minor diameter of 3mm) shown in green, N1 (minor diameter of 4mm) shown in blue, and O1 (minor diameter of 5mm) shown in red.

Table 21. Force Values when Notch Minor Diameter was Varied.

Bolt	Notch Minor Diameter (mm)	Failure Force (N)	Average Failure Force (N)
L1	2	1327	1465
L2		1543	
L3		1525	
M1	3	2537	2703

Table 21 Continued.

M2		3029	
M3		2544	
N1	4	4677	4873
N2		5205	
N3		4738	
O1		2283	
O2	5	3077	2520
O3		2201	

Analysis of **Figure 66** indicates that bolts L-N display a trend of increasing failure force with increasing minor diameter (i.e., the notch with the smallest minor diameter, L, withstood the least force). Bolt O was an exception and did not match the trend of the other bolt geometries. An additional observation of **Figure 66** is that the bolts with smaller notch diameters were generally seen to show more plastic yielding, similar to in the titanium tests. The greater extent of plasticity is indicated by a more gradual slope. However, plasticity was generally less apparent in the steel data as in the modified titanium bolts due to the high strength steel being a more brittle material. As documented in previous sections (**Table 9**), Young’s modulus for steel is much higher than for titanium. A higher Young’s modulus value correlates to a more brittle material, which is likely to show less plasticity past the yield point. It is important to note that, for the current work, it was determined unnecessary to model the steel bolts in FEA. The high strength steel was implemented to test the concept of employing a more brittle material for a shear bolt. However, future FEA models could be expanded to include material beyond titanium, such as high strength steel.

4.4 Conclusions Regarding Shear Bolt Failure Under Bending Conditions

The initial bending experiments employing titanium modified bolts indicated that titanium was too ductile of a material for the bolts proposed use. An increase in notch width was shown to

withstand greater forces. It was hypothesized that the increase in fracture force with notch width may have been attributed to the material's plasticity, as a larger notch volume leads to a larger elastic region. The increase in fracture force could have also indicated that the stress was not concentrated in a small region, but over a larger region. The observed trend of decreasing displacement at failure with increasing notch diameter may have suggested that the greater the residual material in the notch the less plasticity the bolt exhibits and hence the less displacement required to induce failure. The high strength steel bending tests showed plasticity, but not to the same extent as the titanium bolts. The steel bolts indicated no trend with regard to notch width but showed a trend of increasing failure force (fracture force) with increasing minor diameter.

Overall, it was concluded that a more brittle material, such as a high strength steel, reduces plastic yielding in the modified bolts. Results also indicated that a higher strength material will withstand greater forces and require a larger load for failure to occur. However, the high strength steel still displayed plasticity and required significantly large forces to fracture. For future bending tests, additional brittle materials should be evaluated, such as a ceramic. Additionally, to initiate failure sooner, a crack propagation method should be considered. In the case of employing a brittle material with a high ultimate strength, such as high strength steel, a geometrical modification to the notch could be implemented such as switching from a curved notch to a triangular notch, or the addition of a divet to the existing curved notch (i.e., a small notch on the existing notch), that would propagate failure at a lesser force value. However, fatigue would need to be considered and analyzed if crack propagation was to be explored.

5 DETERMINATION OF THE EFFECT OF BOLT GEOMETRY ON FAILURE FORCES UNDER APPLICATION OF A TORSIONAL FORCE

5.1 Introduction

Failure under torsion of a safety mechanism (a shear bolt in the present work) is essential in prosthetic applications. Existing methods have factory-set maximum torsion levels of $15\pm 2\text{Nm}$. Experimental torsion tests were executed via two different methods to analyze how varying bolt parameters such as material of construction, notch minor diameter, notch location, and notch width affected the bolts' behavior. Both unmodified and modified titanium bolts were employed, and experimental results were compared to manual calculations and FEA predictions to determine the parameters of greatest influence.

5.2 Materials and Methods

An initial setup comprising a Durofix Digital Angle Torque Adapter, a 13mm socket, a half-inch drive ratchet, a breaker bar, a clamp, and a custom steel fixture were employed at the University of Maine Advanced Structures and Composites Center. The fixture was fastened to the base of an Instron 8872 machine via six M10 bolts, and the modified experimental bolts were fully threaded 22mm into the fixture. To apply torque, a socket was applied to the digital torque wrench, which was attached to the ratchet and breaker bar, and then the assembly was attached to the bolt in the fixture. Force was manually applied by rotating the ratchet in a clockwise direction until the bolt yielded and failed. The maximum torque applied was recorded by the digital torque adapter. Two unmodified titanium bolts were tested initially, but the torsion values at which they failed were inconsistent and unreliable. The Digital Angle Torque Adapter, 13mm socket, ratchet, and the

breaker bar were difficult to keep together during the tests, and the test method was found to be extremely difficult to control without an automated machine.

A second torsion testing method was developed to address the shortcomings of the initial protocol. The new testing system comprised an Instron hydraulic test frame with torque capacity up to 100Nm and a custom-made steel fixture for the modified bolts. A custom attachment was also created for connection of the Instron loading nose to the hex bolt head. The bolts were fully threaded 22mm into the fixture and the loading nose applied torque via twisting the head of the bolt. Experimental data was produced in the form of torque, rotary displacement, and time. The new method was proven successful and effective for the present work.

Six Grade 5 titanium M8 bolts were obtained from McMaster-Carr and manually modified with a lathe to have notches that varied in notch minor diameter. **Table 22** reports the dimensions of the modified bolts employed in the experimental torsion tests. It is noted that the bolt geometries were named alphabetically based on their geometry, followed by a number representing the numerical identity within the specified sequence of a given geometry. For example, bolt S was produced in a quantity of two. Therefore, the bolts in its respective group were named S1 and S2. The results predicted by initial manual calculations were that the bolts with smaller notch minor diameters would require less force to fail than the bolts with larger notch minor diameters.

Table 22. Titanium Bolt Modifications for Torsion Tests.

Bolt	Length (mm)	Notch Minor Diameter (mm)	Notch Width (mm)	QTY	Radius on Notch Corner (mm)
S	12	2	5	2	2
T	12	3	5	2	2
U	12	4	5	2	2

5.3 Results and Discussions

The Instron hydraulic test frame effectively applied torsion to the hex heads of bolts S, T, and U and caused failure at the notches, rather than the threads (as seen in the early bending tests). An additional benefit to the new test method was an increased number of data points for analysis versus the single maximum force value obtained from the initial torsion testing method.

Figures 67, 68, and 69, present plots of bolt head rotation versus applied torque for bolts S, T, and U, respectively. An important note is that all plots were translated in both axes to start at the origin to address the presence of initial slack in the custom tooling.

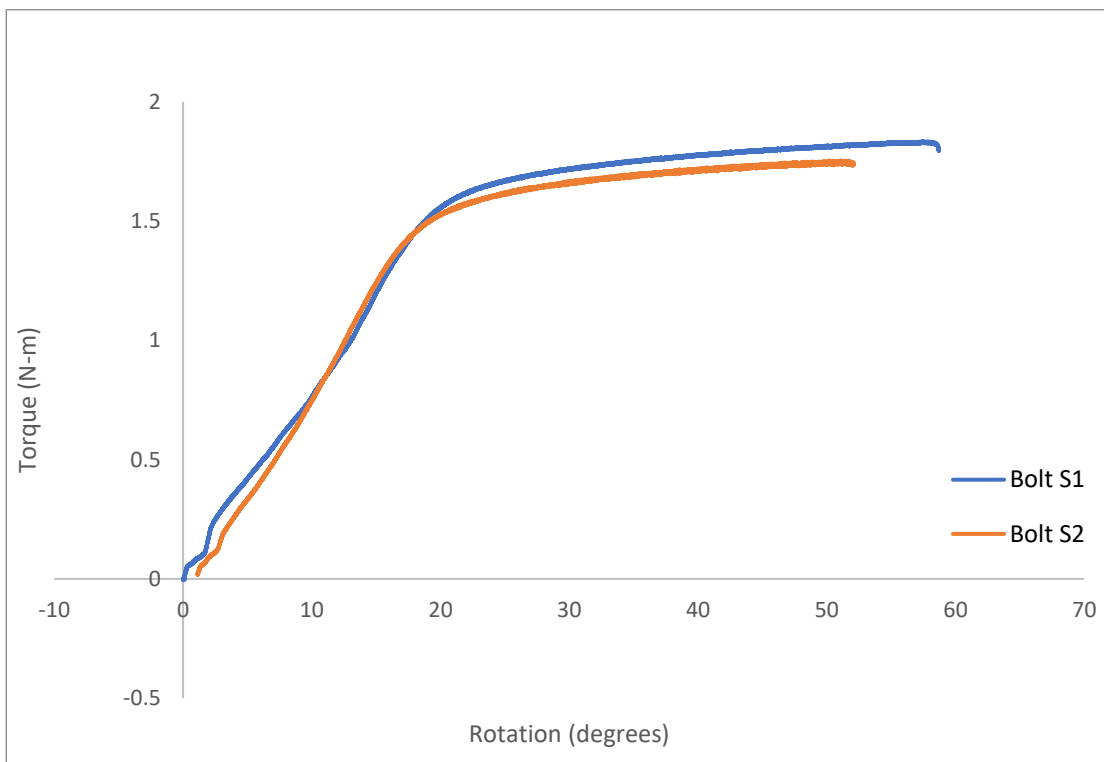


Figure 67. Plot of rotation versus torque for bolts S1 and S2 (minor diameters of 2mm). S1 is shown in blue and S2 is shown in orange.

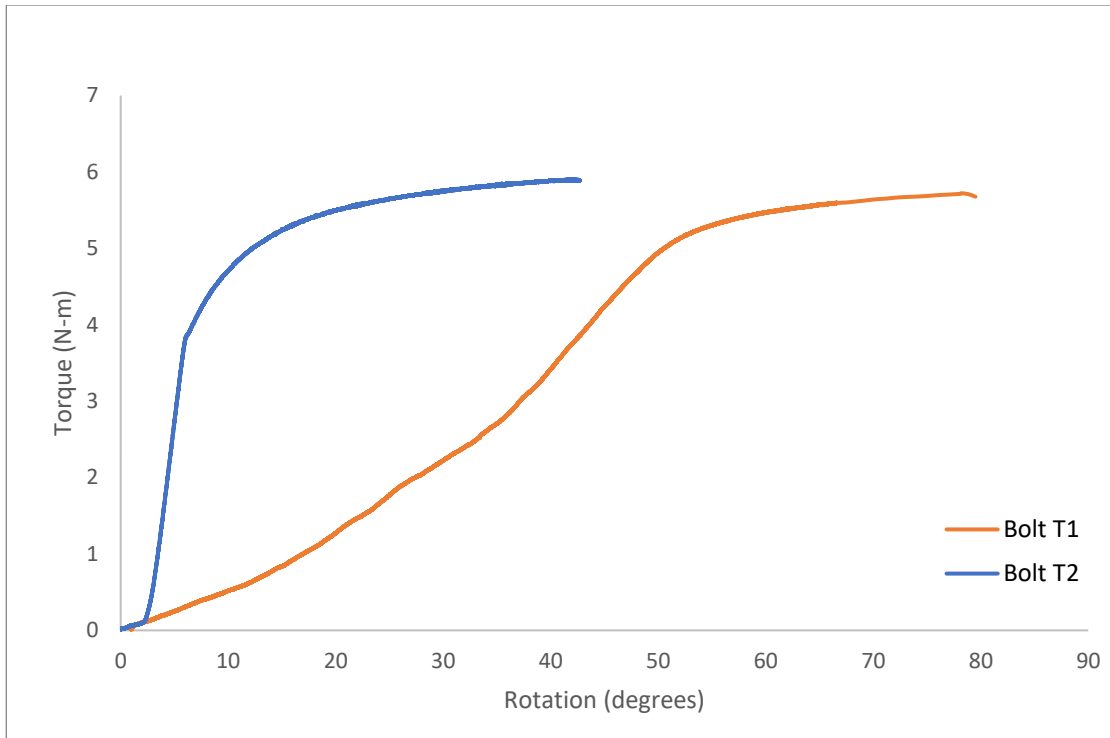


Figure 68. Plot of rotation versus torque for bolts T1 and T2 (minor diameters of 3mm). T1 is shown in orange and T2 is shown in blue.

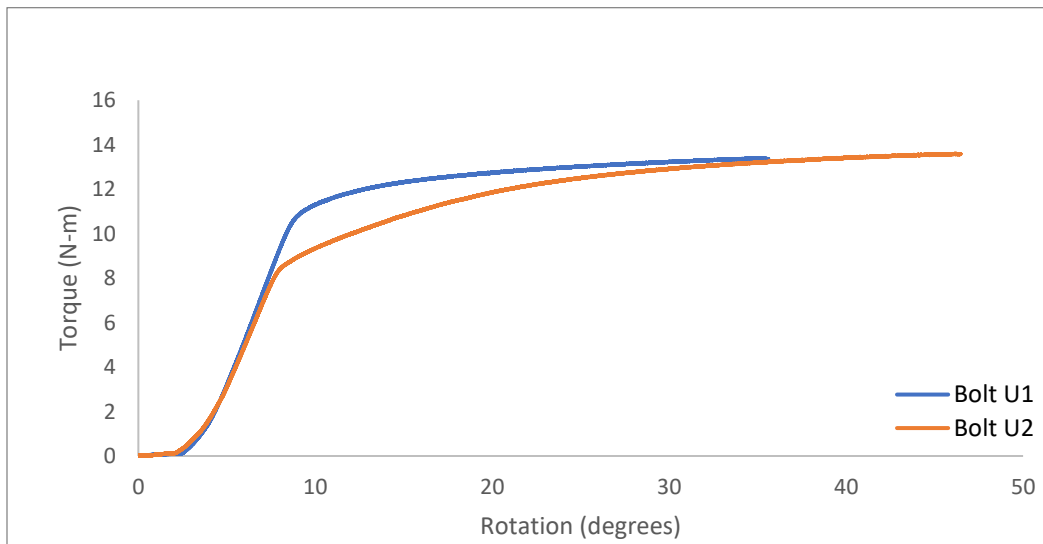


Figure 69. Plot of rotation versus torque for bolts U1 and U2 (minor diameters of 4mm). U1 is shown in blue and U2 is shown in orange.

FEA plots for bolts S, T, and U (varied notch minor diameters of 2mm, 3mm, and 4mm, respectively) are presented in **Figures 70, 71 and 72**.

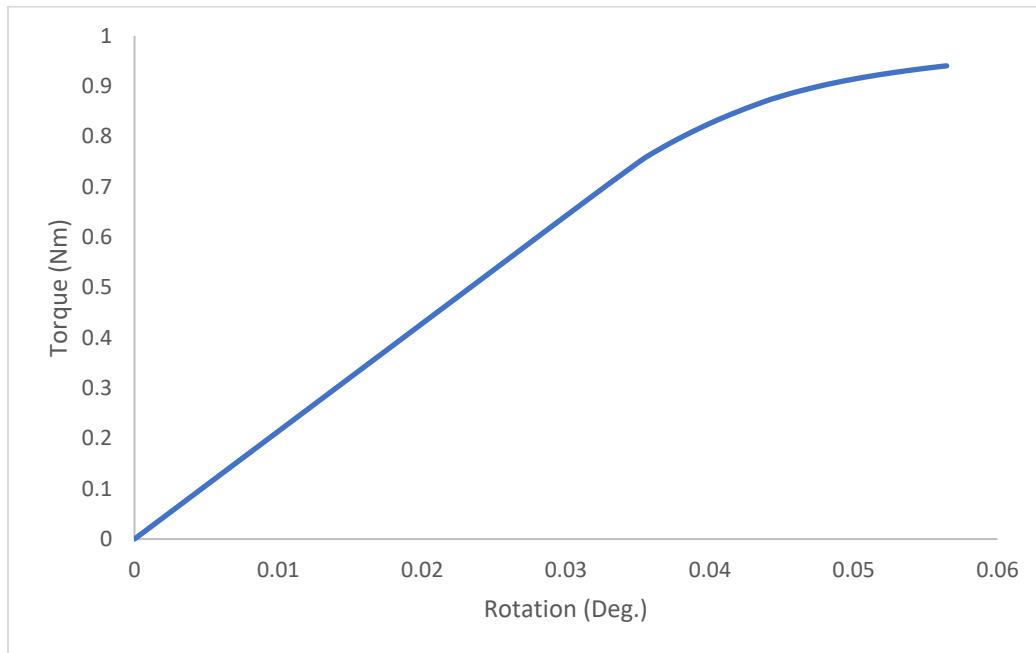


Figure 70. FEA plot as rotation versus torque for bolt S (minor diameter of 2mm).

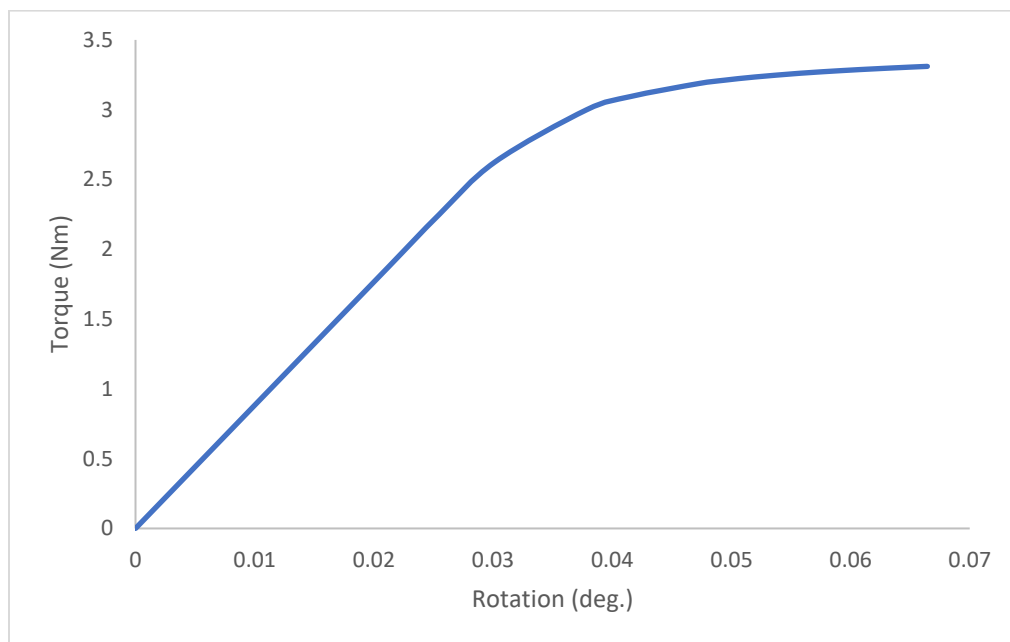


Figure 71. FEA plot as rotation versus torque for bolt T (minor diameter of 3mm).

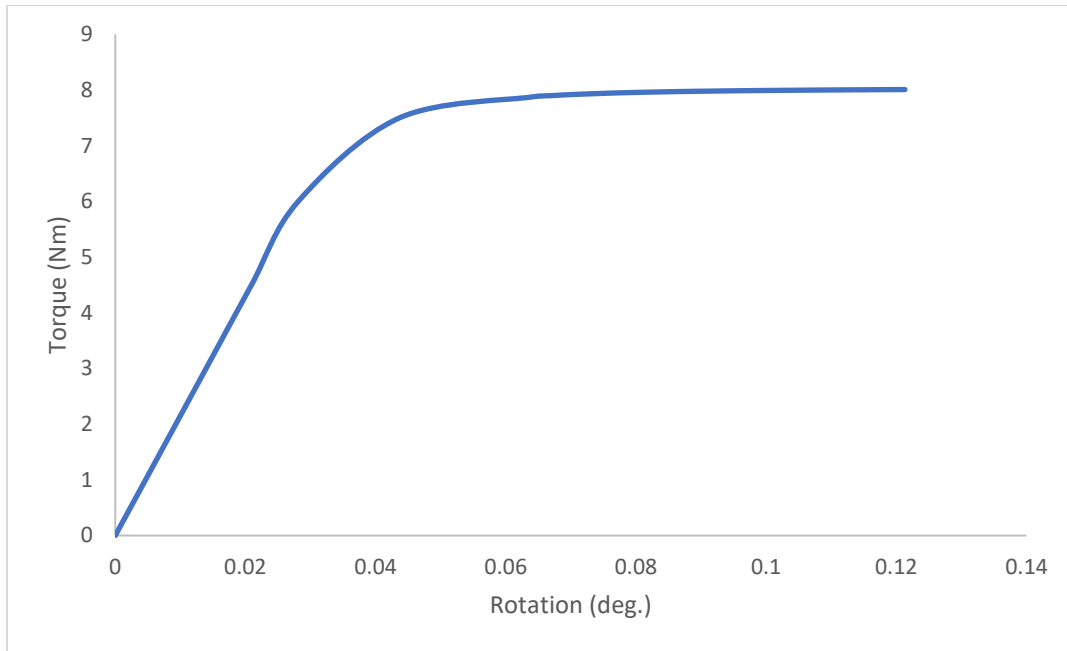


Figure 72. FEA plot as rotation versus torque for bolt U (minor diameter of 4mm).

Analysis of **Figures 67-69** reveals that there is generally good reproducibility in the test method, except for bolts T1 and T2. Bolts S and U were consistent among each of their two respective bolts. The bolts with smaller minor diameters (i.e., bolts S1 and S2) withstood the least amount of torque. Bolts U1 and U2 reached the desired maximum torque value of $15\pm 2\text{Nm}$. Because the region of desired torque was reached, no further exploration of the dominant geometric values were performed. However, it is noted that future work would likely require a different material of construction to meet the bending requirements for failure/release which would mean repeating and potentially extending the torsion study. Though the FEA results plotted in **Figures 70-72** display much smaller displacement values and therefore do not accurately represent the experimental rotation observed in **Figures 67-69**, they show similar trends with regard to fracture torque values

reached. Further analysis would be needed to understand the limited rotation observed in the FEA model.

5.4 Conclusions Regarding Shear Bolt Failure Under Torsion Conditions

Failure under torsion of a safety mechanism (a shear bolt in the present work) is essential in prosthetic applications. Experimental torsion tests were executed via employment of an Instron hydraulic test frame, a custom steel fixture, and custom tooling, to analyze how varying bolt notch minor diameter affected the bolts' behavior when torsion forces were applied. For preliminary tests, there was satisfactory reproducibility in the test method. The desired torque failure values were reached, as such no further exploration of the impact of bolt geometry was undertaken. However, further studies would likely include a different material of construction to address the bending challenges, which would require additional torsion studies. The FEA plots did not represent the experimental data in terms of rotation but did however produce torque values that were in close proximity to the experimental torque failure results. Additional investigation would be required to understand underestimation of the FEA model with regard to the overall rotation.

6 Conclusions and Future Work

6.1 Conclusions

Common attachment mechanisms for external prosthetic components to a residual limb, that is, sockets, pose numerous challenges. Issues include skin irritation, discomfort, socket fit issues, and immobility. Transcutaneous implants have great potential as a connection method for external prosthetic components to a residual limb, especially with the porous metal developments of the UMaine foam metals research group that address the previous issues of infections with existing solid transcutaneous implants. Only one such system is FDA-approved but is inadequate due to its corresponding high infection rates and suboptimal fail-safe mechanism. Hence, the present work was undertaken to develop an optimized fail-safe mechanism to be incorporated into a porous metal transcutaneous implant system.

Transcutaneous porous metal implants are a promising solution to the challenges resulting from solid transcutaneous implants for attachment to prosthetic devices. However, a thoroughly engineered fail-safe mechanism is essential to protect the user's residual limb and surrounding tissues. Existing fail-safe devices do not provide complete release, which is an extreme risk for the user. The proposed mechanism of a shear bolt would allow for a full breakaway as a result of dangerous loads and could in theory predictably fail under any applied load. A combination of manual calculations, FEA modeling, and mechanical testing were employed to evaluate the effect of a variety of shear bolt parameters on the forces at failure. Manual calculations and FEA modeling were employed to predict shear bolt geometries which would lead to failure under specific load conditions. Mechanical testing was subsequently employed to verify the calculations and model predictions. Bending force and torsional force experimental test methods were established and provided data regarding the force-displacement performance of modified bolts'

notch geometry. Generally, notches placed closer to the threads of the bolts withstood less force. Both titanium and high strength steel were tested. Titanium displayed much greater levels of plasticity than the high strength steel showed, although the latter withstood larger loads. Overall, shear bolts of steel were found to be more brittle and closer to a material of interest for the purpose of the present work.

The bending experiments of titanium bolts indicated that titanium was too ductile a material for the proposed use of the shear bolts. Greater notch widths were shown to withstand greater forces, which may have been attributed to the material's plasticity. The observed trend of decreasing displacement at failure with increasing notch diameter may have suggested that the greater the residual material in the notch the less plasticity the bolt exhibits and hence the less displacement required to induce failure. There was no definite trend observed with regard to the notch width of the steel bolts. However, an increase in minor diameter was observed to correlate to an increase in failure force (fracture force). The high strength steel bending tests showed plasticity, but not to the same extent as the titanium bolts. However, the steel bolts withstood significantly greater forces than the titanium bolts, which is problematic for the use of a shear bolt as a safety method for prosthetic detachment. The torsion forces required to cause the titanium bolts to fail reached the desired range of $15\pm 2\text{Nm}$, so no further exploration was performed in the present work.

FEA modeling was employed for both bending tests and torsion tests. The FEA plots did not correlate well with the experimental data, other than at low displacements. Some models displayed incomplete plots, potentially due to computational crashes as a result of excessive deformation of mesh elements near the notch. The FEA plots of torsion did not represent the experimental data in terms of rotation but did produce torque values that were in close proximity

to the experimental results. Additionally, a consistent trend was shown across all torsion FEA plots, displaying an initial steep slope followed by a drastic change to a much more gradual slope once plasticity had started to occur.

Though a fail-safe mechanism was not finalized, an improved understanding of the performance and governing parameters of a notched shear bolt was established. Effective experimental testing methods were developed and employed in both bending and torsion tests, and ways for additional improvements were identified for future testing. The bending forces required to shear the various tested bolts were significantly higher than required for the desired application. The desired torsion failure forces however were met. Additional materials will likely need to be explored to address the need for a shear bolt that fails under both controlled bending forces and controlled torsion forces, which would entail expanded studies for both bending and torsion.

6.2 Future Work

Future studies are warranted prior to the present work being implemented as a fail-safe mechanism for attachment of a prosthetic to a residual limb. The torsional forces at failure were within the desired failure range, but the bending forces at failure were deemed too large, and therefore additional work would be required to achieve a shear bolt capable of controlled failure as a result of either bending forces or torsional forces. Only bending and torsion were considered in the present work; future studies should consider fatigue testing. In addition to fatigue testing, crack propagation should also be considered as a way to cause failure of a high strength material under smaller loads. One potential design that could be analyzed is a triangular notch, rather than a curved notch presented in the current work. A triangular notch could possibly lead to fracture under smaller loads and eliminate observed plasticity. The bending and torsion tests should also be expanded to a test a greater variation of brittle materials such as ceramics, or potentially

composites. It is noted that the experimental bending force test method had multiple variables that may have affected the results. Therefore, the method should be developed further. Specifically, a means to attach the cable to the bolt to enable application of consistently perpendicular force would be beneficial. Overall, valuable data was produced in the present work regarding numerous notched bolts' geometries, and the effect of various materials of construction. Further, experimental test methods for bending forces and torsion forces were developed. It is considered therefore that a significant portion of the work necessary to develop an effective fail-safe mechanism capable of complete release of a prosthetic from a residual limb up application of force in excess of daily activity has been accomplished.

BIBLIOGRAPHY

1. Prosthesis. *National Cancer Institute*. Accessible at: <https://www.cancer.gov/publications/dictionaries/cancer-terms/def/prosthesis> (Accessed 7 December 2021).
2. Paudel, B. *et al.* Two faces of major lower limb amputations. *Univ Med J (KUMJ)*, 3(3):212-6. (2005).
3. Prosthetic vs. Prosthesis: The Correct Usage. Amputee Coalition. Accessible at: <https://www.amputee-coalition.org/resources/prosthetic-vs-prosthesis/> (Accessed 25 July 2023).
4. Daley, J. This 3000-year-old Wooden Toe Shows Early Artistry of Prosthetics. *Smithsonian Magazine*. (2017). Accessible at: <https://www.smithsonianmag.com/smart-news/study-reveals-secrets-ancient-cairo-toe-180963783/> (Accessed 26 July 2023).
5. Seymour, R. *Prosthetics and Orthotics*, 1(4-5). Lippincott Williams and Wilkins. (2002).
6. Our History. Hanger. Accessible at: <https://hanger.com/history/Pages/Timeline.aspx> (Accessed 25 July 2023).
7. Patellar Tendon Tear. OrthoInfo. Accessible at: <https://orthoinfo.aaos.org/en/diseases--conditions/patellar-tendon-tear/#:~:text=The%20patellar%20tendon%20attaches%20the,muscles%20by%20the%20quadriceps%20tendon.> (Accessed 26 July 2023).
8. Quadrilateral Socket. Beast Prosthetics. Accessible at: <https://www.beastprosthetics.co.uk/prosthetic-solutions/lower-limb-solutions/sockets-and-suspension-methods/above-knee/quadrilateral-socket/#:~:text=The%20quadrilateral%20socket%20is%20a,and%20securely%20within%20the%20socket.> (Accessed 26 July 2023).
9. Fred R.T. Nelson MD, FAAOS & Carolyn Taliaferro Blauvelt. *A Manual of Orthopedic Terminology* (Eighth Edition). Elsevier. (2015).
10. Piezer, E. Veterans Administration Prosthetics Center Research Report. VA. Accessible at: <https://www.rehab.research.va.gov/jour/73/10/1/146.pdf> (Accessed 26 July 2023).
11. Ottobock 3S80 Sport Prosthesis. Progressive Orthotics & Prosthetics. Accessible at: <https://www.progoandp.com/ottobock-3s80/> (Accessed 26 July 2023).
12. Ziegler-Graham, K. *et al.* Estimating the Prevalence of Limb Loss in the United States: 2005 to 2050. *Archives of Physical Medicine and Rehabilitation*, 89(3):422-9. (2008).
13. Owings, M. & Kozak, LJ. Ambulatory and Inpatient Procedures in the United States, 1996. *Vital Health Stat 13*, (139):1-119. (1998).

14. Magee, R. Amputation through the ages: the oldest major surgical operation. *Aust N Z J Surg*, 68(9):675-8. (1998).
15. Olaolorun, D.A. Amputations in general practice. *Niger Postgrad Med J*, 8(3):133-5. (2001).
16. McGimpsey, G. & Bradford, T.C. Limb Prosthetics Services and Devices. *Bioengineering Institute Center for Neuroprosthetics Worcester Polytechnic Institution*. (2017).
17. Balk, E.M. *et al.* Lower limb prostheses: measurement instruments, comparison of component effects by subgroups, and long-term outcomes. Comparative effectiveness review: number 213. *U.S. Department of Health and Human Services*. (2018).
18. Klenow, T. & Schulz, J. Adjustable-Volume Prosthetic Sockets: Market Overview and Value Propositions. *Canadian Prosthetics & Orthotics Journal*. (2021).
19. Pezzin, L.E. *et al.* Use and satisfaction with prosthetic limb devices and related services. *Arch Phys Med Rehabil*. (2004).
20. Paterno, L. *et al.* Sockets for limb prosthesis: a review of existing technologies and open challenges. *IEEE Transactions on Biomedical Engineering*, 23;65(9). (2018).
21. Identifying and Managing Skin Issues with Lower-Limb Prosthetic Use. Amputee Coalition. (2011). Accessible at: <https://www.amputee-coalition.org/resources/managing-skin-issues/> (Accessed 26 July 2023).
22. Meulenbelt, H.E. *et al.* Determinants of skin problems of the stump in lower-limb amputees. *Arch. Phys. Med. Rehabil.*, 90(1):74-81. (2009).
23. Janchai, S. *et al.* Comparison of removable rigid dressing and elastic bandage in reducing the residual limb volume of below knee amputees. *J. Med. Assoc. Thai*. **91**, 20 (2008).
24. Fernie, G. R. & Holliday, P. J. Volume fluctuations in the residual limbs of lower limb amputees. *Arch. Phys. Med. Rehabil*. **63**, 162–165 (1982).
25. Sanders, J. E. & Fatone, S. Residual limb volume change: Systematic review of measurement and management. *J. Rehabil. Res. Dev*. **48**, 949–986 (2011).
26. Lilja, M., & Öberg, T. Proper time for definitive transtibial prosthetic fitting. *JPO: Journal of Prosthetics and Orthotics* **9**(2), 90–95 (1997).
27. What is Vascular Disease? Foundation to Advance Vascular Cures. Accessible at: <https://www.vascularcures.org/patients/what-is-vascular-disease#:~:text=Vascular%20disease%20occurs%20when%20an,can%20%E2%80%9Cp resent%E2%80%9D%20themselves%20anywhere.> (Accessed 26 July 2023).
28. Paterno, L. *et al.* Residual limb volume fluctuations in transfemoral amputees. *Scientific Reports*, 11. (2021).

29. Prosthetic FAQs for the New Amputee. Amputee Coalition. Accessible at: <https://www.amputee-coalition.org/resources/prosthetic-faqs-for-the-new-amputee/> (Accessed 25 July 2023).
30. Suspension Sleeves. Gillette Children's. Accessible at: <https://www.gillettechildrens.org/your-visit/patient-education/suspension-sleeves#:~:text=Suspension%20sleeves%20help%20hold%20the,the%20prosthesis%20onto%20the%20limb.> (Accessed 26 July 2023).
31. Sanders, J.E. *et al.* How does adding and removing liquid from socket bladders affect residual limb fluid volume? *J Rehabil Res Dev.*, 50(6):845-60. (2013).
32. Caspers, C.A. Hypobarically-controlled artificial limb for amputees. United States Patent 5549709. (1996).
33. Engstrom, B. Therapy for amputees. *Elsevier Health Sciences.* (1999).
34. Bramley, J.L. *et al.* Changes in Tissue Composition and Load Response After Transtibial Amputation Indicate Biomechanical Adaptation. *Ann Biomed Eng.*, 49(12):3176-3188. (2021).
35. The use of biocomponent fabrics for bonding polypropylene sockets in prostheses. Digital Resource Foundation for the Orthotics & Prosthetics Community. Accessible at: http://www.oandplibrary.org/poi/1985_03_145.asp#:~:text=Polypropylene%20is%20well%20known%20for,to%20bond%20to%20other%20materials. (Accessed 26 July 2023).
36. Van der Stelt, M. *et al.* Pioneering low-cost 3D-printed transtibial prosthetics to serve a rural population in Sierra Leone – an observational cohort study. *The Lancet discovery science*, vol. 35. (2021).
37. Resan, K.K. *et al.* Design and Manufacturing of Prosthetic Below Knee Socket by Modular Socket System. *Journal of Engineering and Sustainable Development*, 20(2). (2016).
38. What is Laminating? Plastics International. Accessible at: <https://www.plasticsintl.com/blog/what-is-laminating/> (Accessed 26 July 2023).
39. Normann, E. *et al.* Modular socket system versus traditionally laminated socket: a cost analysis. *Prosthetics and Orthotics International*, vol. 35. (2017).
40. Klenow, T. & Schulz, J. Adjustable-Volume Prosthetic Sockets: Market Overview and Value Propositions. *Canadian Prosthetics & Orthotics Journal.* (2021).
41. Greenwald, R.M. *et al.* Volume management: Smart Variable Geometry Socket (SVGS) technology for lower-limb prostheses. *J Prosthet Orthot.*, 15(3):107–112. (2003).
42. Ogawa, A. *et al.* Design of lower limb prosthesis with contact pressure adjustment by MR fluid. *Annu Int Conf IEEE Eng Med Biol Soc*, 330-3. (2008).

43. Jinaga, R. *et al.* The Synthesis of Organic Oils Blended Magnetorheological Fluids with the Field-Dependent Material Characterization. *Int J Mol Sci.*, 20(22):5766. (2019).
44. Pin-Site Infections. International Center for Limb Lengthening. Accessible at: <https://www.limblength.org/patient-info/after-surgery/pin-site-infections/#:~:text=Pin%2Dsite%20infections%20are%20the,to%20a%20more%20significant%20infection.> (26 July 2023).
45. Prosthetic Liners: A Conversation with Our Prosthetists. Medical Center Orthotics & Prosthetics. Accessible at: <https://mcoopro.com/blog/prosthetic-liners/#:~:text=How%20are%20prosthetic%20liners%20made,a%20variety%20of%20suspension%20options.> (Accessed 25 July 2023).
46. Types of Prosthetic Knees. Hanger Clinic. Accessible at: <https://www.scheckandsiress.com/patient-information/care-and-use-of-your-device/knee-prosthesis-liner-pin-lock/> (Accessed 26 July 2023).
47. Limb Loss Below the Knee. Hanger Clinic. Accessible at: <https://www.scheckandsiress.com/patient-information/care-and-use-of-your-device/below-knee-prosthesis/> (Accessed 25 July 2023).
48. Limb Loss Below the Knee. Hanger Clinic. Accessible at: <https://www.scheckandsiress.com/patient-information/care-and-use-of-your-device/below-knee-prosthesis/> (Accessed 26 July 2023).
49. ESP FlexiSleeve Suspension Sleeve. MMAR Medical Group, Inc. Wholesale Distribution. Accessible at: <https://www.mmarmedical.com/ESP-FlexiSleeve-Suspension-Sleeve-p/ks-esp-0-b-ks-esp-5-t.htm> (Accessed 26 July 2023).
50. Osseointegration Limb Replacement. HSS. Accessible at: https://www.hss.edu/condition-list_osseointegration.asp (Accessed 25 July 2023).
51. Hoellwarth, J.S. *et al.* The Clinical History and Basic Science Origins of Transcutaneous Osseointegration for Amputees. *Adv. Orthop.* (2022).
52. Hugate, R. Transcutaneous implant for skeletal attachment of external prosthetic devices. United States Patent US10390975B2. (2019).
53. Bachus, K.N. & Borchert, J.D. Releasible attachment system for a prosthetic limb. United States Patent US8246693B2. (2012).
54. Bachus, K. *et al.* Releasible attachment system for a prosthetic limb. United States Patent US20120310371A1. (2012)
55. FDA Approves Prosthetic Implant for Above-the-Knee Amputations. FDA. (2020). Accessible at: <https://www.fda.gov/news-events/press-announcements/fda-approves-prosthetic-implant-above-knee-amputations> (Accessed 26 July 2023).

56. Patient Labeling. OPRA Implant System and OPRA Rotasafe. Integrum. Accessible at: https://www.accessdata.fda.gov/cdrh_docs/pdf8/H080004c.pdf (Accessed 26 July 2023).
57. Humanitarian Use Device. University of Virginia. Accessible at: [https://research.virginia.edu/irb-hsr/humanitarian-use-device#:~:text=An%20HDE%20is%20a%20type,Humanitarian%20Use%20Devices%20\(HUD\).](https://research.virginia.edu/irb-hsr/humanitarian-use-device#:~:text=An%20HDE%20is%20a%20type,Humanitarian%20Use%20Devices%20(HUD).) (Accessed 26 July 2023).
58. Transfemoral (above-knee) Amputations. Integrum. Accessible at: <https://integrum.se/what-we-do/our-products-future-solutions/opra-implant-system/transfemoral-above-knee-amputations/> (Accessed 26 July 2023).
59. OPRA Implant System Instructions for Use. Integrum. Accessible at: https://www.accessdata.fda.gov/cdrh_docs/pdf8/H080004S002C.pdf (Accessed 26 July 2023).
60. Sullivan, J. et al. Rehabilitation of the trans-femoral amputee with an osseointegrated prosthesis: the United Kingdom experience. *Prosthetics and Orthotics International*, 27, 114-120. (2003).
61. Transfemoral (above-knee) Amputations. Integrum. Accessible at: <https://integrum.se/what-we-do/our-products-future-solutions/opra-implant-system/transfemoral-above-knee-amputations/> (Accessed 26 July 2023).
62. Mooney, V. *et al.* Percutaneous implant devices. *Ann. Biomed Eng.*, 5(1):34-46. (1977).
63. Tillander, J. *et al.* Osseointegrated titanium implants for limb prostheses attachments: infectious complications. *Clin Orthop Relat Res*, 468(10):2781-8. (2010).
64. Li, Y. & Fellander-Tsai, L. The bone anchored prostheses for amputees – Historical development, current status, and future aspects. *Biomaterials*. (2021).
65. Osseointegration Prosthetic Limb Patient Information. Osseointegration Group of Australia. Accessible at: <https://amputeeimplantdevices.com/wp-content/uploads/2014/03/OGAAP-OPL-Brochure.pdf> (Accessed 26 July 2023).
66. Spongiosa. ICRPaedia. (2010). Accessible at: <http://icrpaedia.org/Spongiosa#:~:text=Term%20referring%20to%20the%20combined,the%20axial%20and%20appendicular%20skeleton.> (Accessed 26 July 2023).
67. The ESKA endo-stem adapted exo-prosthesis care concept according to Dr. Grundei. Accessible at: <https://eskaorthopaedic.de/en/home-en/> (Accessed 26 July 2023).
68. Bobyn, J. D. *et al.* The Optimum Pore Size for the Fixation of Porous-Surfaced Metal Implants by the Ingrowth of Bone. *Clin. Orthop. Relat. Res*, No. 150, 263–270. (1980).
69. Bobyn, J. D. *et al.* Characteristics of Bone Ingrowth and Interface Mechanics of a New Porous Tantalum Biomaterial. *J. Bone Joint Surg. Br.*, 81 (5), 907–914. (1999).

70. Hong, S.B. *et al.* A New Ti-5Ag Alloy for Customized Prostheses by Three-Dimensional Printing (3DP). *J. Dent. Res.*, 80, 860–863. (2001).
71. Albrektsson, T *et al.* Osseointegrated Titanium Implants. Requirements for Ensuring a Long-Lasting, Direct Bone-to-Implant Anchorage in Man. *Acta Orthop. Scand.*, 52 (2), 155–170. (1981).
72. Spivack, Kyle J., "Highly Porous Foam Materials for Uses in Reconstructive Orthopedic Surgery and Transcutaneous Implant Applications" (2015).
73. Spivack, K.J. *et al.* Soft tissue in-growth of porous, three-dimensionally printed, transcutaneous implants of varying material and pore geometry. United States Patent US20180021139A1. (2018).
74. Meller, A. De. Produit Métallique Pour L'obtention D'objets Laminés, Moulés Ou Autres, et Procédés Pour Sa Fabrication, French Patent 615,147, 1926 (1925).e. *French Pat. Lit.* (1925).
75. J. A. Bjorksten. *et al.* Foamed metal low density core material for sandwich construction, Wright Air Development Center. (1953).
76. McFadden, C. Inspired by Nature but as Tough as Iron: What is Metal Foam Used For? Interesting Engineering. (2020). Accessible at: <https://interestingengineering.com/inspired-by-nature-but-as-tough-as-iron-what-is-metal-foam-used-for#:~:text=On%20the%20whole%2C%20metal%20foams,copper%2C%20zinc%2C%20or%20lead.&text=Metal%20foams%20have%20some%20very,for%20material%20scientists%2C%20amongst%20others.> (Accessed 26 July 2023).
77. Banhart, J. Manufacturing Routes for Metallic Foams. *JOM*, 52(12):22-27. (2000).
78. Parveez, B. *et al.* Microstructure and Mechanical Properties of Metal Foams Fabricated via Melt Foaming and Powder Metallurgy Technique: A Review. *Materials (Basel)*, 15(15):5302. (2022).
79. Dabrowski, B. *et al.* Highly Porous Titanium Scaffolds for Orthopaedic Applications. *J. Biomed. Mater. Res. B. Appl. Biomater.*, 95 (1), 53–61. (2010).
80. Medlin, D.J. *et al.* "Metallurgical Characterization of a Porous Tantalum Biomaterial (Trabecular Metal) for Orthopaedic Implant Applications." *Medical Device Materials: Proceedings of the Materials & Processes for Medical Devices Conference* 394-398. (2004).
81. W. C. Miller *et al.*, "The prevalence and risk factors of falling and fear of falling among lower extremity amputees", *Arch. Phys. Med. Rehabil.*, vol. 82, no. 8, pp. 1031-1037, Aug. 2001.

82. Taylor, C.E. *et al.* Estimated forces and moments experienced by osseointegrated endoprostheses for lower extremity amputees. *Gait Posture*, 80:49-55. (2020).
83. Engineering Fundamentals Refresh: Strength vs. Stiffness vs. Hardness. Fictiv. (2023) Accessible at: <https://www.fictiv.com/articles/engineering-fundamentals-refresh-strength-vs-stiffness-vs-hardness#:~:text=It's%20the%20maximum%20tensile%20stress,at%20which%20total%20failure%20occurs.> (Accessed 26 July 2023).
84. Stress Concentration Factor (Kt). Corrosionpedia. (2020). Accessible at: [https://www.corrosionpedia.com/definition/1035/stress-concentration-factor-kt#:~:text=A%20stress%20concentration%20factor%20\(Kt\)%20is%20a%20dimensionless%20factor%20that,compared%20to%20a%20reference%20stress.](https://www.corrosionpedia.com/definition/1035/stress-concentration-factor-kt#:~:text=A%20stress%20concentration%20factor%20(Kt)%20is%20a%20dimensionless%20factor%20that,compared%20to%20a%20reference%20stress.) (Accessed 26 July 2023).
85. Norton, R.L. *Machine Design* (Fifth Edition), Appendix C. (2013).
86. Maximum Shear Stress Criterion. Efunda. Accessible at: https://www.efunda.com/formulae/solid_mechanics/failure_criteria/failure_criteria_ductile.cfm#:~:text=The%20von%20Mises%20criterion%20states,stress%20C%20s3%20%3D%200. (Accessed 26 July 2023).
87. Failure Criteria for Yielding. Centre de Mise en Forme des Matériaux. (2008). Accessible at: https://andriandriyana.files.wordpress.com/2008/03/yield_criteria.pdf (Accessed 26 July 2023).
88. Collins, J.A. *et al.* *Mechanical Design of Machine Elements and Machines* (Second Edition), pg. 218. (2009).
89. What is FEA? Simscale. Accessible at: <https://www.simscale.com/docs/simwiki/fea-finite-element-analysis/what-is-fea-finite-element-analysis/> (Accessed 26 July 2023).
90. Vel, S. & Maalouf, S. MEE456 ABAQUS Tutorials. (2022).
91. Density. Britannica. (2023). Accessible at: <https://www.britannica.com/science/density> (Accessed 26 July 2023).
92. Titanium Hex Head Screw. McMaster-Carr. Accessible at: <https://www.mcmaster.com/94081A792/> (Accessed 26 July 2023).
93. Titanium Ti-6Al-4V (Grade 5), Annealed. ASM Aerospace Specification Metals Inc. Accessible at: <https://asm.matweb.com/search/SpecificMaterial.asp?bassnum=mtp641> (Accessed 26 July 2023).
94. Titanium Ti-6Al-4V ELI (Grade 23), Annealed. Matweb. Accessible at: https://www.matweb.com/search/datasheet_print.aspx?matguid=c4297fb8f1094da189732c224e3be1ed (Accessed 26 July 2023).

95. Overview of materials for Polypropylene, Molded. Matweb. Accessible at:
<https://www.matweb.com/search/DataSheet.aspx?MatGUID=08fb0f47ef7e454fbf7092517b2264b2&ckck=1> (Accessed 26 July 2023).
96. Overview of materials for Brass. Matweb. Accessible at:
https://www.matweb.com/search/datasheet_print.aspx?matguid=d3bd4617903543ada92f4c101c2a20e5 (Accessed 26 July 2023).
97. 304 Stainless Steel. Matweb. Accessible at:
<https://matweb.com/search/DataSheet.aspx?MatGUID=abc4415b0f8b490387e3c922237098da&ckck=1> (Accessed 26 July 2023).
98. Kutzner, I. *et al.* Loading of the knee joint during activities of daily living measured in vivo in five subjects. *J Biomech.*, 43(11):2164-73. (2010).
99. Anthropometry. Common dimensions. *Ergoweb*. Accessible at:
<https://ergoweb.com/anthropometry/#:~:text=Elbow%20height%20average%3A%2041%20in,Knee%20height%3A%2024%20in.&text=A%20range%20is%20often%20used%20to%20accommodate%20both%20tall%20and%20short%20people>. (Accessed 25 July 2023).
100. Ziaja, W. Finite element modelling of the fracture behaviour of surface treated Ti-6Al-4V alloy. *Computational Materials Science and Engineering*, 1(1):53-60. (2009).

BIOGRAPHY OF THE AUTHOR

Emma F. Sperry was born in Portland, Maine, on November 30, 1999. Raised in Westbrook, Maine, she attended Westbrook High School and graduated in 2018. She subsequently attended the University of Maine, where she earned a Bachelor's degree in Biomedical Engineering, which was conferred upon graduation in May of 2022. Emma pursued a Master's of Science in Biomedical Engineering through a 4+1 program at the University of Maine. Emma is currently employed by ARCH Additive as an Additive Manufacturing Project Engineer and intends to continue working after completion of her Master's degree. In her spare time, Emma enjoys hiking, skiing, yoga, traveling, and spending time with family and friends. She is a candidate for a Master of Science degree in Biomedical Engineering from the University of Maine in August of 2023.